Global Biogeochemical Cycles

RESEARCH ARTICLE
10.1029/2025GB009033

Special Collection:
EMIT: The Earth Surface Mineral Dust Source Investigation

Global Model Estimates of Atmospheric Al, Ca, Fe, Si, and Ti From Dust and Non-Dust Aerosols Informed by EMIT Surface Mineralogy and Evaluated Against Observations

Natalie M. Mahowald[1], Longlei Li[1], María Gonçalves Ageitos[2,3], Ronald L. Miller[4], Carlos Pérez García-Pando[2,5], Paul Ginoux[6], Vincenzo Obiso[2], Philip G. Brodrick[7], Roger N. Clark[8], Karine Desboeufs[9], Robert O. Green[7], Gregory S. Okin[10], David R. Thompson[7], Sagar Rathod[11], Esteban Gazel[1], Adrian Hornby[1], Emile Journet[12], Maria Grazia Alaimo[13], Célia Alves[14], Andres Alastuey[15], Paulo Artaxo[16], Alex R. Baker[17], Francisco Barraza[18], Silvia Becagli[19], Clifton S. Buck[20], Giulia Calzolai[21], Shankararaman Chellam[22], Ying Chen[23], Patrick Y. Chuang[24], David D. Cohen[25], Cristina Colombi[26], Evangelia Diapouli[27], Gaetano Dongarra[13], Konstantinos Eleftheriadis[27], Johann P. Engelbrecht[28], Corinne Galy-Lacaux[29], Cassandra Gaston[30], Dario Gomez[31], Yenny González Ramos[32,33], Jenny Hand[34], Roy M. Harrison[35], Barak Herut[36,37], Philip K. Hopke[38,39], Zsofia Kertesz[40], Katriina Kyllönen[41], Fabrice Lambert[42,43], Willam M. Landing[44], Remi Losno[45], Franco Lucarelli[21,46], Willy Maenhaut[47], Christopher Marsay[48], Hitoshi Matsui[49,50], Randall V. Martin[51], Yasser Morera-Gómez[52], Adina Paytan[53], Joseph Prospero[30], Sergio Rodríguez[32,54], Geraldine Sarthou[55], Rachel Shelley[17], Ronald L. Siefert[56], Patricia Smichowski[31], and Daniela Varrica[13]

[1]Department of Earth and Atmospheric Sciences, Cornell University, Ithaca, NY, USA, [2]Barcelona Supercomputing Center, Barcelona, Spain, [3]Department of Project and Construction Engineering, Universitat Politècnica de Catalunya – BarcelonaTech, Terrassa, Spain, [4]NASA Goddard Institute for Space Studies, New York, NY, USA, [5]ICREA, Catalan Institution for Research and Advances Studies, Barcelona, Spain, [6]NOAA/OAR Geophysical Fluid Dynamics Laboratory, Princeton, NJ, USA, [7]Jet Propulsion Laboratory, California Institute of Technology, Pasadena, CA, USA, [8]Planetary Science Institute, Tucson, AZ, USA, [9]CNRS, LISA, Université Paris Cité and Université Paris Est Creteil, Paris, France, [10]University of California Los Angeles, Los Angeles, CA, USA, [11]La Follette School of Public Affairs, University of Wisconsin-Madison, Madison, WI, USA, [12]CNRS, LISA, Université Paris Est Creteil and Université Paris Cité, Créteil, France, [13]Dipartimento di Scienze della Terra e del Mare, University of Palermo, Palermo, Italy, [14]Department of Environment, Centre for Environmental and Marine Studies (CESAM), University of Aveiro, Aveiro, Portugal, [15]Institute of Environmental Assessment and Water Research (IDAEA-CSIC), Barcelona, Spain, [16]Instituto de Fisica, Universidade de Sao Paulo, Sao Paulo, Brazil, [17]School of Environmental Sciences, University of East Anglia, Norwich, UK, [18]Saw Science, Invercargill, New Zealand, [19]Department of Chemistry "Ugo Schiff", University of Florence, Sesto Fiorentino, Italy, [20]Skidaway Institute of Oceanography, University of Georgia, Savannah, GA, USA, [21]National Institute for Nuclear Physics (INFN) - Florence Division, Sesto Fiorentino, Italy, [22]Department of Civil & Environmental Engineering and Department of Chemical Engineering, Texas A&M University, College Station, TX, USA, [23]Department of Environmental Science and Engineering, Fudan University, Shanghai, China, [24]Earth & Planetary Sciences Department, University of California Santa Cruz, Santa Cruz, CA, USA, [25]Centre for Accelerator Science, Australian Nuclear Science and Technology Organisation, Lucas Heights, NSW, Australia, [26]Environmental Monitoring Sector, Arpa Lombardia, Milan, Italy, [27]Environmental Radioactivity & Aerosol Technology for Atmospheric & Climate Impact Lab, INRaSTES, N.C.S.R. Demokritos, Attiki, Greece, [28]Desert Research Institute (DRI), Reno, NV, USA, [29]CNRS, IRD, LAERO, University of Toulouse, Toulouse, France, [30]Rosenstiel School of Marine, Atmospheric, and Earth Science, University of Miami, Miami, FL, USA, [31]Comision Nacional de Energia Atomica, Gerencia Química, Buenos Aires, Argentina, [32]Izaña Atmospheric Research Center (IARC), Agencia Estatal de Meteorología (AEMET), Santa Cruz de Tenerife, Spain, [33]Scientific Department, CIMEL, Paris, France, [34]Cooperative Institute for Research in the Atmosphere, Colorado State University, Fort Collins, CO, USA, [35]School of Geography, Earth and Environmental Sciences, University of Birmingham, Birmingham, UK, [36]Israel Oceanographic & Limnological Research, Haifa, Israel, [37]Faculty of Marine Sciences, Ruppin Academic Center, Michmoret, Israel, [38]Institute for a Sustainable Environment, Clarkson University, Potsdam, NY, USA, [39]Department of Environmental Medicine and Public Health Sciences, University of Rochester School of Medicine and Dentistry, Rochester, NY, USA, [40]HUN-REN Institute for Nuclear Research (ATOMKI), Debrecen, Hungary, [41]Finnish Meteorological Institute, Helsinki, Finland, [42]Geography Institute, Pontificia Universidad Catolica de Chile, Santiago, Chile, [43]Center for Climate and Resilience Research, Santiago, Chile, [44]Department of Earth, Ocean, and Atmospheric Science, Florida State University, Tallahassee, FL, USA, [45]Institut de Physique du Globe de Paris, CNRS, Université Paris Cité, Paris, France, [46]Physics and Astronomy Department, University of Florence, Sesto Fiorentino, Italy, [47]Department of Chemistry, Ghent University, Gent, Belgium, [48]School of Marine Science and Policy, University of Delaware, Newark, DE, USA, [49]Graduate School of Environmental Studies, Nagoya University, Nagoya, Japan, [50]Institute for Space–Earth

Key Points:

- Earth Surface Mineral Dust Source Investigation mineralogical distributions are used for the dust source elemental distribution
- Non-dust sources are included for natural and anthropogenic sources
- Observations of Al, Ca, Fe, Si, and Ti are compiled for land-based stations and cruise data and compared to modeled values

Supporting Information:

Supporting Information may be found in the online version of this article.

Correspondence to:
N. M. Mahowald,
mahowald@cornell.edu

Citation:
Mahowald, N. M., Li, L., Gonçalves Ageitos, M., Miller, R. L., Pérez García-Pando, C., Ginoux, P., et al. (2026). Global model estimates of atmospheric Al, Ca, Fe, Si, and Ti from dust and non-dust aerosols informed by EMIT surface mineralogy and evaluated against observations. *Global Biogeochemical Cycles*, *40*, e2025GB009033. https://doi.org/10.1029/2025GB009033

Received 15 DEC 2025
Accepted 22 APR 2026

Author Contributions:
Conceptualization: Natalie M. Mahowald
Data curation: Karine Desboeufs, Robert O. Green, Gregory S. Okin, David R. Thompson, Sagar Rathod, Esteban Gazel, Adrian Hornby,

Emile Journet, Maria Grazia Alaimo, Célia Alves, Andres Alastuey, Paulo Artaxo, Alex R. Baker, Francisco Barraza, Silvia Becagli, Clifton S. Buck, Giulia Calzolai, Shankararaman Chellam, Ying Chen, Patrick Y. Chuang, David D. Cohen, Cristina Colombi, Evangelia Diapouli, Gaetano Dongarra, Konstantinos Eleftheriadis, Johann P. Engelbrecht, Corinne Galy-Lacaux, Cassandra Gaston, Dario Gomez, Yenny González Ramos, Jenny Hand, Roy M. Harrison, Barak Herut, Philip K. Hopke, Zsofia Kertesz, Katriina Kyllönen, Willam M. Landing, Remi Losno, Franco Lucarelli, Willy Maenhaut, Christopher Marsay, Hitoshi Matsui, Randall V. Martin, Yasser Morera-Gómez, Adina Paytan, Joseph Prospero, Sergio Rodríguez, Geraldine Sarthou, Rachel Shelley, Ronald L. Siefert, Patricia Smichowski

Formal analysis: Natalie M. Mahowald, María Gonçalves Ageitos, Ronald L. Miller, Carlos Pérez García-Pando, Paul Ginoux, Vincenzo Obiso, Philip G. Brodrick, Roger N. Clark

Methodology: Natalie M. Mahowald

Software: Natalie M. Mahowald, Longlei Li

Supervision: Natalie M. Mahowald

Visualization: Natalie M. Mahowald

Writing – original draft: Natalie M. Mahowald

Writing – review & editing: Longlei Li, María Gonçalves Ageitos, Ronald L. Miller, Carlos Pérez García-Pando, Paul Ginoux, Vincenzo Obiso, Philip G. Brodrick, Roger N. Clark, Karine Desboeufs, Robert O. Green, Gregory S. Okin, David R. Thompson, Sagar Rathod, Esteban Gazel, Adrian Hornby, Emile Journet, Maria Grazia Alaimo, Célia Alves, Andres Alastuey, Paulo Artaxo, Alex R. Baker, Francisco Barraza, Silvia Becagli, Clifton S. Buck, Giulia Calzolai, Shankararaman Chellam, Ying Chen, Patrick Y. Chuang, David D. Cohen, Cristina Colombi, Evangelia Diapouli, Gaetano Dongarra, Konstantinos Eleftheriadis, Johann P. Engelbrecht, Corinne Galy-Lacaux, Cassandra Gaston, Dario Gomez, Yenny González Ramos, Jenny Hand, Roy M. Harrison, Barak Herut, Philip K. Hopke, Zsofia Kertesz, Katriina Kyllönen, Willam M. Landing, Remi Losno, Franco Lucarelli, Willy Maenhaut, Christopher Marsay, Hitoshi Matsui, Randall V. Martin, Yasser Morera-Gómez, Adina Paytan, Joseph Prospero, Sergio Rodríguez, Geraldine Sarthou, Rachel Shelley, Ronald L. Siefert, Patricia Smichowski

Environmental Research, Nagoya University, Nagoya, Japan, [51]Energy, Environmental and Chemical Engineering, Washington University, St. Louis, MO, USA, [52]Universidad de Navarra, Instituto de Biodiversidad y Medioambiente BIOMA, Pamplona, Spain, [53]Earth and Planetary Science, University of California, Santa Cruz, CA, USA, [54]Consejo Superior de Investigaciones Científicas, IPNA CSIC, Tenerife, Spain, [55]CNRS, IRD, Ifremer, LEMAR, University of Brest, Plouzané, France, [56]Chemistry Department, United States Naval Academy, Annapolis, MD, USA

Abstract Atmospheric deposition of micro-nutrients like Fe has been shown to be important for ocean biogeochemistry. The largest source of atmospheric Fe and other elements (e.g., Ca, Al, Si, and Ti) is desert dust, although there are significant non-dust sources in some regions (e.g., combustion, sea salts, volcanoes). However, past estimates of these elements have been substantially uncertain due to limited information about the composition of the desert source regions. Here we use elemental distributions estimated from new Earth Surface Mineral Dust Source Investigation (EMIT) observations, which provide mineralogical composition at the surface of the Earth based on imaging spectroscopy measurements from the International Space Station. We focus on total elemental amounts, not on the soluble fraction. We add in other sources of these elements (anthropogenic and natural) and compare to a compilation of available surface concentration data from stations over land and from shipborne observations. The combined observational and model synthesis provides new information about the distribution and deposition of these elements. Our results suggest that the modeled distribution is similar to available observations, but discrepancies still exist in both natural desert dust regions as well as regions dominated by anthropogenic sources. Comparisons between the model estimated Ca/Al ratios and observations in some dust dominated regions suggest an underestimate of Ca/Al ratios. Global budgets for Ca, Al, Fe, Si, and Ti suggest that desert dust remains the dominant source, although volcanic and anthropogenic contributions are important in some regions. Changes in elemental distributions since preindustrial times were also estimated.

Plain Language Summary We provide estimates of the atmospheric concentrations and deposition of aluminum, calcium, iron, silicon, and titanium using models and compiled observations from land and ship-based studies. These estimates provide improved information about the distribution and allow future studies to consider the possible impacts of atmospheric transport of these elements.

1. Introduction

Atmospheric deposition of biogeochemically relevant elements on land and ocean ecosystems can provide important nutrients and enhance growth or be toxic and inhibit ecosystem functions (Chapin et al., 1986; Likens et al., 1996; Paytan et al., 2009; Rodríguez et al., 2023; Schlesinger, 1997). Human emissions of fossil fuel derived particles, as well as the anthropogenic modifications to aerosols such as from wildfire or arid regions (Hamilton et al., 2018; Kok et al., 2023; Mahowald et al., 2018; Van Marle et al., 2017), have substantially altered atmospheric aerosol inputs to land and ocean ecosystems, potentially modifying biogeochemistry and carbon uptake in these systems (Duce et al., 2008; Jickells & Moore, 2015; Jickells et al., 2005; Mahowald, 2011; Mahowald et al., 2011). Most of the earlier studies on atmospheric deposition and their impact have focused on nitrogen, iron, or phosphorus (e.g., Chien et al., 2016; Duce et al., 2008; Jickells et al., 2005; Mahowald et al., 2008; Vet et al., 2014), although other elements are also likely to be important for ocean and land biogeochemistry (e.g., Baker et al., 2006; Jickells & Moore, 2015; Lu et al., 2024; Mackey et al., 2012; Mahowald et al., 2017, 2018).

Desert dust is the most abundant component of atmospheric aerosols by mass and provides many important elements to land and ocean ecosystems (Mahowald et al., 2017, 2018). The major elements in desert dust are aluminum (Al), calcium (Ca), iron (Fe), silicon (Si), and titanium (Ti), each combined with oxygen and hydrogen in the mineral form, although the quantity of these varies slightly in different arid or desert regions depending on the mineralogy in the source regions (Desboeufs et al., 2005; Formenti et al., 2008; Rodríguez et al., 2020; Zhang et al., 2015).

Atmospheric Fe deposition to the open ocean is likely important both for phytoplankton growth in Fe-limited regions (Boyd et al., 2007, 2017; Martin, 1990) as well as the higher Fe requirements for nitrogen-fixing organisms (Capone et al., 1997; C. M. Moore et al., 2013; K. Moore et al., 2006; Tagliabue et al., 2017), and because

of this, atmospheric Fe deposition to the oceans has been extensively studied (Duce et al., 1991; Hamilton et al., 2021; Ito et al., 2019; Mahowald et al., 2009; Matsui et al., 2018; Myriokefalitakis et al., 2018; Opazo et al., 2025).

Besides Fe, the other dominant elements in dust (Al, Ca, Si, and Ti) may also play an important biogeochemical role once they are deposited. Al is one of the dominant elements in dust composition comprising about 7%–8% by mass (Zhang et al., 2015). In the ocean, Al plays a potentially important role in diatom opal remineralization, linking it to Si availability for diatoms (Mahowald et al., 2018; Orians & Bruland, 1986; van Hulten et al., 2014). Ca plays important roles in ocean biogeochemistry as a main sink for the carbonate ion, as well as a nutrient for ocean biota although atmospheric deposition from land to ocean is likely smaller than riverine inputs (Fantle & Tipper, 2014). Si is important for ocean biogeochemistry, as many important ocean organisms (e.g., diatoms) require it in substantial amounts to form shells and other structural materials (Tréguer et al., 2021), and atmospheric deposition is estimated to represent about 10% of the new inputs from riverine sources (Schlesinger, 1997; Tréguer et al., 2021). Ti in the ocean is thought to have limited biotic interactions (Orians et al., 1990) and has been used to help interpret paleorecords (e.g., Murray et al., 1993). On land, both Ca and Al play important roles in buffering soil pH (Fantle & Tipper, 2014; Schlesinger, 1997), although in most soils atmospheric deposition is unlikely to be important compared to local bedrock or soil sources (Fantle & Tipper, 2014; Schlesinger, 1997). Ca in the atmosphere can play an important buffering role, modifying the aerosol pH (Baker et al., 2021).

The abundance of each element varies in different soils, creating differences in atmospheric dust composition which can be used as a geochemical tracer of different dust sources (Grousset & Biscaye, 2005). These variations in composition also change the biogeochemical, radiative, and chemical properties of the dust that are important to consider in modeling studies (Hand et al., 2004; Journet et al., 2008; Okin et al., 2004; Scanza et al., 2015). Previously, soil mineralogy and elemental composition estimates used Food and Agriculture Organization (FAO) soil type maps, combined with approximately 1,000 soil samples (Claquin et al., 1999; Journet et al., 2014). Alternatively, studies have used elemental soil concentrations to create maps of dust source composition (Zhang et al., 2015). This approach extrapolates a few data points, mostly from non-arid agricultural regions, to millions of grid cells thousands of kilometers away in semi-arid and arid regions, which then causes substantial uncertainties in the resulting mineral and elemental composition estimates (Li et al., 2021; Okin et al., 2004; Scanza et al., 2015; Wong et al., 2021). One of the novel contributions of this research is that we take advantage of new mineralogy maps provided from the Earth Surface Mineral Dust Source Investigation (EMIT) (Green et al., 2023). This space-borne mission has measured surface mineralogy in arid and semi-arid regions across the globe at 60 m pixels which are combined and aggregated into 0.5° × 0.5° grid boxes (Okin et al., 2023).

The atmospheric deposition of non-ferrous elements, when considered, has previously only focused on dust deposition, ignoring other non-dust sources of these elements (e.g., Measures & Vink, 2000; van Hulten et al., 2014; Zhang et al., 2015). Globally-averaged estimates suggest important anthropogenic and natural sources (e.g., combustion, sea salts, volcanoes), which may differ at the regional level (Mahowald et al., 2018; Nriagu, 1989; Nriagu & Pacyna, 1988; Pacyna & Pacyna, 2001; Schlesinger, 1997). While in some contexts the soluble fraction is more important, here we focus on the total elemental amounts, since there are much more data and knowledge of these fractions (Mahowald et al., 2018).

In this paper we simulated the atmospheric emissions, transport, and deposition of total (not only soluble) Al, Ca, Fe, Si, and Ti, the dominant elements in dust, using the new EMIT-derived soil mineralogy data set, but also including sources from anthropogenic and other natural sources. From this comprehensive approach, we can better understand both where and when the non-dust sources are important, as well as how these elements are likely to have changed since preindustrial times. In Section 2, we introduce the models and data used in the paper. Section 3 compares our results against available observations for the distribution of the elements. We then show global budgets and estimate the change in deposition of these elements since preindustrial times to highlight the land and ocean ecosystems where the impact of human perturbations to these elements could be the largest on their biogeochemistry. Finally, we present our summary and conclusions.

2. Methods

2.1. Atmospheric Modeling

Elemental aerosol concentration simulations were conducted using the appropriate parameterizations within the Community Atmosphere Model, version 6 (CAM6) and the atmospheric component of the Community Earth System Model (CESM2) coordinated at the National Center for Atmospheric Research (NCAR) (Hurrell et al., 2013; Liu et al., 2011; Scanza et al., 2015). The model calculates three-dimensional transport by nudging toward MERRA2 winds (Gelaro et al., 2017) and wet and dry deposition for gases and aerosols. Simulations were conducted at approximately 1° × 1° horizontal resolution with 56 vertical layers for 4 years, with the last three years (2013–2015) used for the analysis (Computational and Information Systems Laboratory, 2019). These simulations are very similar to those used for previous aerosol studies (e.g., Lu et al., 2024; Mahowald, Li, Vira, et al., 2025).

The default model includes prognostic dust, sea salts, black carbon, organic carbon, and sulfate aerosols using a modal aerosol scheme (Li et al., 2021; Liu et al., 2011, 2016). In order to improve the simulation of coarse mode particles, the coarse model size parameters were returned to the values in the CAM5, and there was an improvement to the dry deposition scheme (Li et al., 2022). Fossil fuel emissions of sulfate, organic carbon and black carbon follow the Climate Model Intercomparison Project 6 emission scenarios for present day for 2010 (Gidden et al., 2019). All aerosols are subject to dry and wet deposition (Liu et a., 2011; 2016).

2.2. Desert Dust Elemental Distributions at the Sources

Desert dust or mineral aerosols are entrained into the atmosphere in dry, sparsely vegetated regions subject to strong winds. The Dust Entrainment and Deposition scheme (Zender et al., 2003) is used with the updated Brittle Fragmentation Theory (Kok et al., 2014) and improved incorporation of aspherical particles for optics and deposition (Huang et al., 2021; Kok et al., 2017; Li et al., 2022). Eight different minerals were simulated for dust, and the elemental contribution from each mineral, as estimated in Menut et al. (2020), is used to estimate the Al, Ca, Fe, Si, and Ti elemental emissions and distributions (Table S1 in Supporting Information S1). The global annual dust emission in our simulation is approximately 2,900 Tg yr^{-1}, with a global mean dust optical depth in the visible band (0.44–0.63 μm) of ~0.03.

This model version is identical to the one used in Li et al., 2022, except for the changes in the EMIT soil mask, described below, and the model performs for the dust, very similar to previous versions in terms of comparisons to aerosol optical depth, surface dust concentrations and deposition (Figure S1 in Supporting Information S1). Note that it is often difficult for dust models to simulate all three: optical depth, concentrations and deposition accurately (Huneeus et al., 2011), and here we emphasize the dust tuning that accurately describes the deposition since we are interested in biogeochemistry impacts of the deposition.

NASA's EMIT mission provides estimates of soil mass fraction at 0.5° × 0.5° spatial resolution for the minerals chlorite, calcite, dolomite, goethite, gypsum, hematite, illite/muscovite, kaolinite, montmorillonite, and vermiculite (Brodrick et al., 2025; Green et al., 2020). EMIT uses the spectral radiance measured from the International Space Station's orbit (Thompson et al., 2024) to estimate surface reflectance spectra (Coleman et al., 2024; Green, 2022). Minerals are identified from reflectance features using the linear feature matching algorithm Tetracorder at the instrument's native 60-m spatial sampling (Clark et al., 2003, 2024). EMIT scenes are mosaiced together by selecting cloud-free measurements with the minimum solar zenith angle from between August 2022 and October 2024. Locations with less than 65% bare soil are excluded, along with areas with consolidated mineralogy (e.g., rock formations), and all pixels within each half-degree grid cell are averaged together to identify the mass fraction. The EMIT mineral maps do not acquire data poleward of ±52° latitude and these regions instead use data from previous mineral mass fraction estimates (Claquin et al., 1999; Journet et al., 2014). While EMIT maps represent remote sensing measurements, they do include errors. For example, Ca (predominately from calcite) may be underreported by the EMIT data due to detection issues (Clark et al., 2024). The diagnostic absorption for carbonates is at 2.3 microns and the absorption coefficient in that spectral region interferes with the corresponding absorption coefficients for phyllosilicates, including muscovite and illite. Thus the presence of significant muscovite and illite can mask the carbonate absorptions, leading to carbonate non-detections or lower detections. A second effect has to do with the derived reflectance calibration in the EMIT data. Some, but not all, scenes have an artifact near 2.3 microns that can affect detection of minerals with 2.3

micron absorptions, including calcite, dolomite, chlorites, and serpentines, again leading to either non or lower detections (Clark et al., 2024). Ongoing work is attempting to remove these issues from the EMIT product.

EMIT does not directly observe quartz and feldspar. These abundance maps are produced using the calibrated VSWIR reflectance spectra interpreted through a Hapke-style model of the soil surface coupled with the Tetracorder spectral-matching algorithm (Clark et al., 2024). Size-resolved mineral mass fractions in aerosols at emission are estimated based on Brittle Fragmentation Theory (Kok, 2011) after partitioning the EMIT mineral bulk abundances into clay (≤2 μm) and silt (2–50 μm) fractions based on empirical relationships that incorporate soil texture data, Food and Agriculture Organization (FAO) soil classifications, and additional observational constraints (Claquin et al., 1999; Journet et al., 2014). For this study iron oxides are assumed to be evenly distributed across particle sizes, although there is evidence that there may be more iron oxides in smaller sizes (Panta et al., 2023). Iron oxides consist of hematite and goethite following Li et al. (2022). There is limited availability of optical properties for chlorite and vermiculite, and there is very little in the inventories, and thus these two minerals are combined into the kaolinite for this study.

2.3. Other Aerosol Sources of Al, Ca, Fe, Si, and Ti

The model was modified to allow the addition of several new aerosol sources using the speciated dust version (Li et al., 2021, 2024), that are simulated separately and added together to get the resulting distribution and deposition. The additional sources of aerosols (such as industrial ash and primary biogenic particles) use the same chemical and optical properties as bulk dust (e.g., density, shape and complex refractive index).

Industrial emissions include metallic aerosol particles (e.g., industrial ash) from combustion, and we base our emissions here on the detailed study of mineralogy from combustion focused on Fe (Rathod et al., 2020). That study provides spatial distributions of the fine and coarse estimates of Fe from coal, wood, oil, gasoline, diesel, smelting, wood fuels and fires for Fe (Rathod et al., 2020). The ratios of Al, Ca, Si, and Ti to Fe are estimated from literature sources and used to simulate the combustion contribution to these elements (Table S2 in Supporting Information S1). Road dust emissions estimated from the GAIN model are added to the model using the ECLIPSEV6_CLE base case (Klimont et al., 2017; Philip et al., 2017). Emissions from cement production due to combustion (of whatever fuel is used) are included here, but not from fugitive emissions from cement plants (Rathod et al., 2020). Biomass burning emissions are included using emissions of black carbon multiplied by literature derived ratios (Table S3 in Supporting Information S1). We are missing possible braking emissions.

Previous estimates show natural primary biogenic particles as sources of these elements (Mahowald et al., 2018; Rauch & Pacyna, 2009). Primary biogenic particles are accidently or deliberately released from ecosystems either as whole particles, such as bacteria, pollen, or spores, or as entrained leaf or insect pieces (Burrows et al., 2009; Despres et al., 2012; Heald & Spracklen, 2009; Jaenicke, 2005; Mahowald et al., 2008) and here we use an identical approach as in Mahowald, Li, Vira, et al. (2025). Assumptions about size are likely to be very important for the resulting distribution and impacts. For example, studies show that P budgets are quite different if 5 different size bins or 1 size bin are included in models (Brahney et al., 2015). Bacteria sources are included from a monthly climatology (Burrows et al., 2009). Fungal spore emissions are calculated offline on observed leaf area index, temperature, and a source parameterization (Heald & Spracklen, 2009; Janssen et al., 2020). An additional terrestrial biogenic source is estimated based on leaf area index following Mahowald et al. (2008). Elemental composition of primary biogenic materials is estimated from the limited literature (Table S3 in Supporting Information S1).

Sea spray contains trace quantities of metals (Marsay et al., 2022; Rauch & Pacyna, 2009). Based on the available literature, the fraction of each element from these sources is multiplied by the sea salt source in the model (Table S3 in Supporting Information S1). Note that it is possible that these studies include the impact of marine primary biogenic material and thus no additional marine primary biogenic particles are included.

Studies have shown that volcanoes can be an important contributor to trace elements in aerosols, through eruptive activities and degassing (Mahowald et al., 2018; Rauch & Pacyna, 2009). While most metals are likely to come from eruptive activities, there is no climatological database of ash currently available (Hornby et al., 2023; Rauch & Pacyna, 2009), thus we use a non-eruptive source spatial distribution for sulfur (S) for this study (Spiro et al., 1992), with a constant source across the time periods. For volcanic sources, the concentration of trace elements is commonly expressed using their ratio to S. The amount of Fe emission for this study is tuned to be

close to that in Rauch & Pacyna, 2009 at a global level, and the ratios of the elements are used to deduce the emissions of other elements. We summarize recently measured concentrations of the elements from volcanic ash (Table S4 in Supporting Information S1). The amount of different elements is sensitive to the size fraction (Tomašek et al., 2025) as well as the type of volcano (Hornby et al., 2023): the variability due to the type of volcano and composition appears stronger than the size differences (López-Darias et al., 2025; Tomašek et al., 2025). The size is especially important for the Si content, as there is a strong size segregation for Si, so we reduce the Si in the PM_{10} size fraction assumed here, but otherwise use the Hornby et al., 2023 estimates. We note that this approach does not rely on a direct physical conversion factor between sulfur emissions and ash, but instead uses observed elemental-to-sulfur ratios and global constraints to approximate emissions. This introduces substantial uncertainty, which if volcanoes are important, should be refined in the future.

The total emissions from all sources is listed in Table S5 in Supporting Information S1 and discussed in more detail in Section 3.2. The surface concentration fraction that is in the $PM_{2.5}$ size fraction is shown for each source and each element in Table S5 in Supporting Information S1, the remaining fraction largely represents coarse-mode ($PM_{2.5}$-PM_{10}) aerosol, as the model primarily resolves particles within the PM_{10} range.

2.4. Atmospheric Surface Concentration Observations

Elemental in situ concentration measurements are routinely made in several global networks, and these are combined with field studies and cruises to create a global distribution of the different aerosols in atmospheric surface concentrations as part of the COARSEMAP/AEROMAP effort (Lu et al., 2024; Wiedinmyer et al., 2017; Wong et al., 2021). Data from land-based stations are collected by announcing the effort publicly (Wiedinmyer et al., 2017), searching the literature for sources, individually contacting authors, as well as downloading publicly-available data (e.g., https://cbas-data.nilu.no/; https://www.spartan-network.org/; https://www.epa.gov/outdoor-air-quality-data). Since one of our goals is to constrain atmospheric deposition to oceans, we also include cruise data (e.g., https://www.geotraces.org/; Baker et al., 2013). We focus here on total elemental amounts, not on the soluble fraction, for which there is much less data.

For land-based data, we focus on the climatological annual means for 1986–2023 which are calculated for all values at each station that are above the detection limits. At some stations or times, concentrations can be below the detection limit, and excluding these data or time periods could bias our average values. We focus only on the stations that have more than 50% of the data above the detection limit. For those included stations, if the values were reported as below the detection limit, we include in the average one-third of the minimum detection limit. The reported detection limits should provide an upper limit of aerosol mass and allow us to include sites whose observations are otherwise too low to include, while reducing the potential biasing of our compilation toward higher values (Data Set S1). Studies have suggested errors of up to 30% in coarse mode detection of Al and Si, with smaller errors in $PM_{2.5}$ (Hyslop et al., 2015; Liu et al., 2025; Lucarelli et al., 2018).

The largest variability in surface concentration aerosol distributions at the global scale is the spatial distribution of the annual mean (Mahowald, Li, Vira, et al., 2025), so we focus on understanding and reproducing the climatological mean surface concentration spatial distribution in the PM_{10}, and consider the $PM_{2.5}$ aerosol in the supplement. Variability within 1 year at the same land-based station, between different years at the same station, spatial variability within one model grid box due to the coarse spatial resolution, measurement uncertainties and differences in measurement methods, all contribute to uncertainty in these comparisons (Mahowald, Li, Vira, et al., 2025). Although episodic events may lead to larger deviations, we estimate that at land-based stations model values within a factor of 3 of the observed values should be considered within the uncertainties (Mahowald, Li, Vira, et al., 2025). This is much less than spatial distributions which vary over 4–5 orders of magnitude. Comparisons are made to the surface layer in the model (bottom ~50 m), and thus the results are sensitive to errors in the boundary layer processes in the models.

In dust dominated regions (as defined by the model as dust is more than 50% of the total) we look at the relative amount of different elements compared to Al to evaluate the composition of the dust. For these comparisons, the errors from spatial and temporal variability become less important, and we assume the largest errors are due to measurement errors. Because Al content in dust is relatively constant, it is usually used as the standard, although Al and Si may have 30% errors due to measurement methods as discussed above. Propagating these errors in the denominator and numerator produces error bars of a factor of 2, which are used for the comparisons for different

elements over Al. Notice that our definition of dust dominated may be biased due to errors in the sources or transport of aerosols.

For the ocean-based data, we include all measurements across all time periods, although these are limited. Since many measurements represent just one daily or weekly average, these are more likely to be subject to the large temporal variability and less representative of the annual mean. Previous studies have estimated that the uncertainty in model (annual average) versus single observation is close to one order of magnitude, and we use that here for comparisons (Mahowald et al., 2008).

Annual average and climatological monthly mean values for the station data are provided in the associated Zenodo database (Mahowald, Li, Vira, et al., 2025), as well as in Data Set S1. Compiled cruise data are provided in Data Set S2. Information about location and the relevant citations are included in these data sets.

2.5. Model/Data Comparisons

We focus this study on the PM_{10} component, as that is the relevant size fraction for biogeochemistry (since most of the mass is in the larger size fractions; Mahowald et al., 2011), and $PM_{2.5}$ data are shown in the supplement. Comparisons are made at the global and regional level between the annual averages in the model versus the observations, to see how the model performs in simulating large spatial gradients, using the regions defined in Figure S2 in Supporting Information S1 (similar to Mahowald, Li, Vira, et al. (2025)). Because in some regions there are too many data, obscuring individual points, we average the observations to a $2° \times 2°$ grid to better discern differences between model values and observations. The grid used is sampled using every other model grid point.

Statistical comparisons include the correlation coefficients (Kendall ranked correlation), slope of the observations versus the model with uncertainty, root mean squared differences between model and observations, average observational values, average model values (at the observational sites), the fraction of comparisons when the model and observations are within the uncertainty bounds discussed in Section 2.4, and the number of observations. These statistics are included in supplemental tables discussed in the text.

2.6. Preindustrial Versus Present Day Estimates

The descriptions above are for the present day (model is for 2013–2015; observations are 1980s–2025). To estimate preindustrial values, we assume that all the anthropogenic sources are zero, and non-dust natural sources are the same as present day (e.g., volcanoes, sea salts and primary biogenic particles). As these sources tend to be smaller, these assumptions are unlikely to significantly impact our results. For preindustrial dust sources, we use the paleodata from Kok et al. (2023) which indicates that dust has changed about 55% since preindustrial times. We force a change in the emissions at each grid box in each region so that the mean will be consistent with the paleodata.

3. Results and Discussion

Since this research represents the first study of multiple sources, not just of dust, but also of Al, Ca, Si, and Ti, we start with an evaluation of the atmospheric concentrations resulting from the assumptions described in Section 2. For Fe, this is less important, as it was previously evaluated (e.g., Hamilton et al., 2019; Mahowald et al., 2009), and we use those examples to contextualize the new results from this study.

3.1. Model/Data Comparisons

3.1.1. Aluminum (Al)

The spatial distribution of the modeled PM_{10} surface concentrations of Al has the maximum in the dust belt, across North Africa and into the Middle East and Central Asia (Figure 1; regions are defined in Figure S2 in Supporting Information S1). This feature is as expected and will be true of all the elements in this paper (fraction shown explicitly in Figure 2) since Al, Ca, Fe, Si, and Ti all are major constituents of desert dust, which is the most abundant aerosol by mass. Land-based station data are limited for Al in PM_{10} (Figure 1a), particularly in the desert regions, and they broadly agree with the model across four orders of magnitude. Some of the highest concentrations are in eastern Asia near Shanghai (Figure 1), where there may be significant non-desert dust sources, such

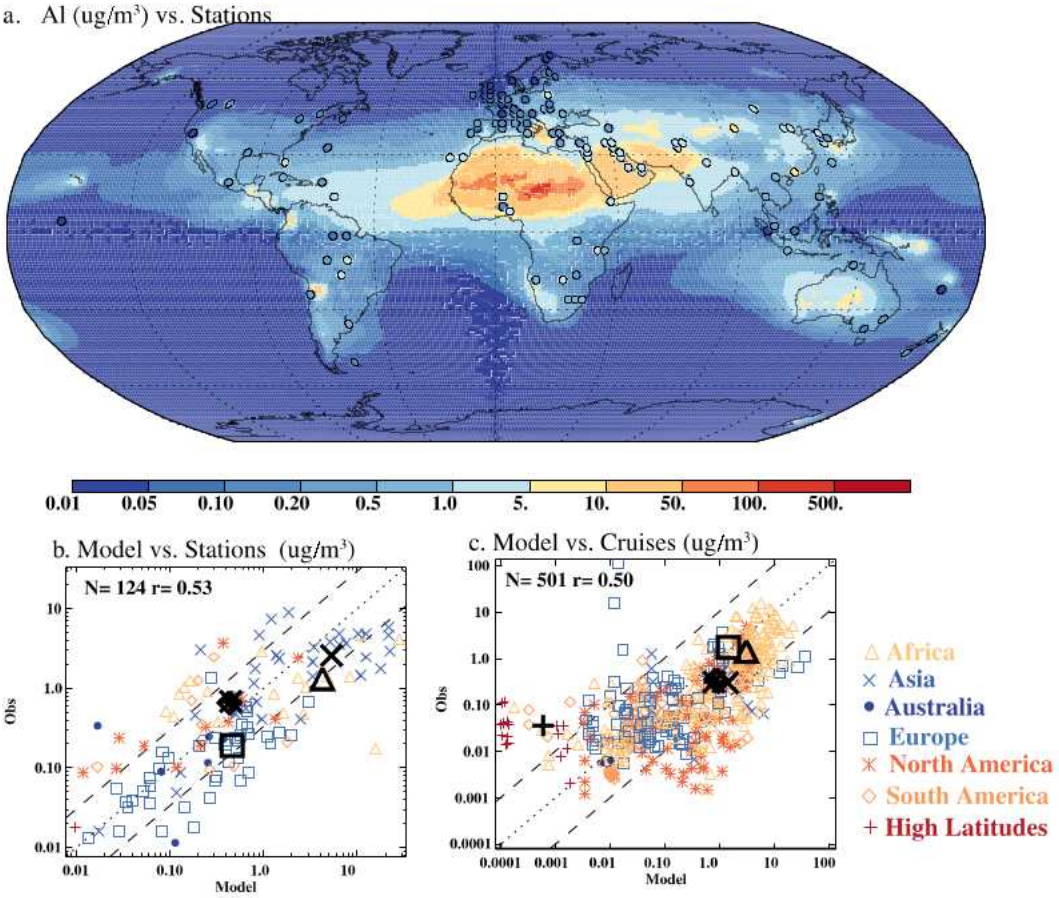

Figure 1. Al surface concentrations in the PM_{10} size fraction. Modeled values in μg/m^3 are shown in the background in (a) while the circles represent the observational measurements from land-based stations using the same color bar. A comparison of the model (*x*-axis) to the observations (*y*-axis) is shown for the station-based land data (b) and the cruise data (c). The spatial comparison between the model and cruise data is shown in Figure S4a in Supporting Information S1. For clarity, all the observations are gridded to 2° × 2° cells. In the scatter plots, the color and symbols indicate the regions, the bold black symbols are the average across each region (indicated by the symbol), the dotted line is the 1:1 line and the dashed lines are the factor of 3 for land-based measurements (b) and 10 for ocean cruise data (c) uncertainty estimates. More statistics are shown in Table S6 in Supporting Information S1. The regions are defined in Figure S2 in Supporting Information S1. More detailed views of the regions are shown in Figure S6 in Supporting Information S1. *N* and *r* represent the number of observations and correlation coefficient, respectively.

as agricultural, construction, or road dust. The model tends to overpredict Al over Africa and Asia which may be due to an overprediction of dust or a mistake in the seasonality (Formenti et al., 2014) in the model in those regions (e.g., Aboagye-Okyere et al., 2025), although the regional averages are just within the uncertainty bounds. However, we do not see this overprediction consistently across all the dust-derived elements (below) nor in the dust specific comparisons (Figure S1 in Supporting Information S1), so it could also be an error in the amount of Al in the dust, or due to other emissions, since our observations of Al are in regions where non-dust sources also contribute (Figure 2). In addition, it could be due to an underestimate in assessment of the Si and Al in the coarse particles when measured with techniques based on the detection of emitted X-rays such as Particle Induced X-ray Emission (PIXE) and X-Ray Fluorescence (XRF) (Lucarelli et al., 2018); this effect is due to the self-absorption of the low-energy X-rays inside the particle and may cause an underestimation of the order of 20% if not properly corrected (Formenti et al., 2010). Note that it is difficult to match the aerosol optical depth, deposition records and surface concentrations close to dust source regions at the same time as is the case in most dust models (Albani et al., 2014; Huneeus et al., 2011), perhaps because of errors due to not accurately including larger dust particles (Li et al., 2026). Because we are most interested in biogeochemical effects, the match in dust deposition (Figure S1c in Supporting Information S1) is most important.

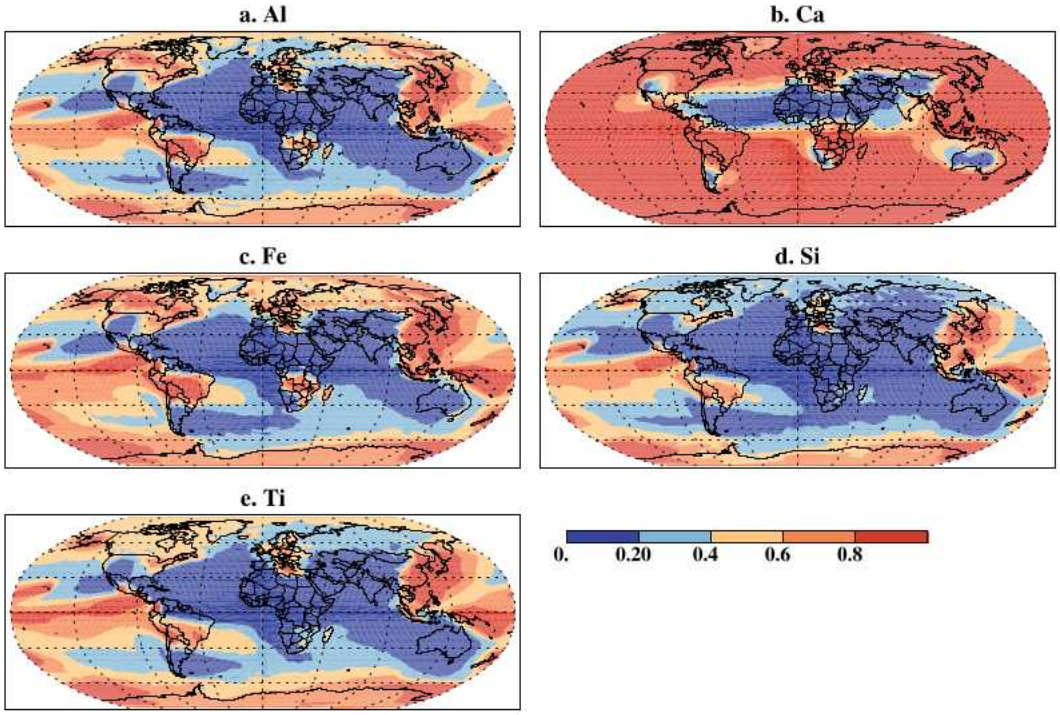

Figure 2. Non-dust fraction for each of the elements. Model based estimates of the annual average concentration contribution from non-dust sources for (a) Al, (b) Ca, (c) Fe, (d) Si, and (e) Ti.

The dominant dust sources of Al are the minerals Illite and Kaolinite (Figure S7 in Supporting Information S1). Non-dust Al sources dominate away from the main dust sources areas (Figure 2), and the dominant sources spatially are volcanoes over most of the oceans, fires and coal burning over some land regions (Figure S8 in Supporting Information S1; budgets will be discussed in Section 3.2). The simulation of Al in the non-dust dominated regions like North America and Europe, with abundant anthropogenic aerosol sources (Figure 2), suggests that the non-dust sources of Al are roughly correct (North America) or slightly too high (Europe) (Figures 1a and 1b). The $PM_{2.5}$ simulations of Al are better across most regions, except for Europe (Figures S2a and S2b in Supporting Information S1), and these smaller sizes will tend to be more dominated by anthropogenic emissions. The percent of the observations and model comparisons that are outside of the uncertainty bounds of 3× (Section 2.4) is 47% and 28% for PM_{10} and $PM_{2.5}$ (Tables S6 and S7 in Supporting Information S1), respectively; for PM_{10} these are larger than expected if we consider these 1-sigma bounds, suggesting improved emission estimates for PM_{10} are needed.

The cruise data for Al in the PM_{10} size fraction show more correspondence with the average from the observations than the land station data, except in high latitudes (Figure S4a in Supporting Information S1 and Figure 1c). Notice that there are very high values from cruise observations close to Iceland, consistent with an episodic volcanic source that we are not simulating (Alex Baker, personal communication, 7 March 2024; Achterberg et al., 2021). There are much less cruise data for the $PM_{2.5}$ size fraction, and they show that the regional averages are within the uncertainty bounds, although the model overpredicted observations at many sites. (Figures S5a and S5b; Table S9 in Supporting Information S1).

3.1.2. Calcium (Ca)

For Ca, the maximum modeled concentrations are again in desert regions, and are verified to a limited extent by PM_{10} land-based observations (Figures 3a and 3b). The model does better simulating Ca than Al across Asia, Africa, and Europe, but not South America where the modeled values are too high, and North America where the modeled values tend to be too low (Figure 3b vs. Figure 1b). In non-dust dominated regions, such as parts of Europe or North America which have good data coverage (Figures 2d and 3a), the model is similar to available observations, suggesting that the non-dust sources in the model are reasonably represented within observational

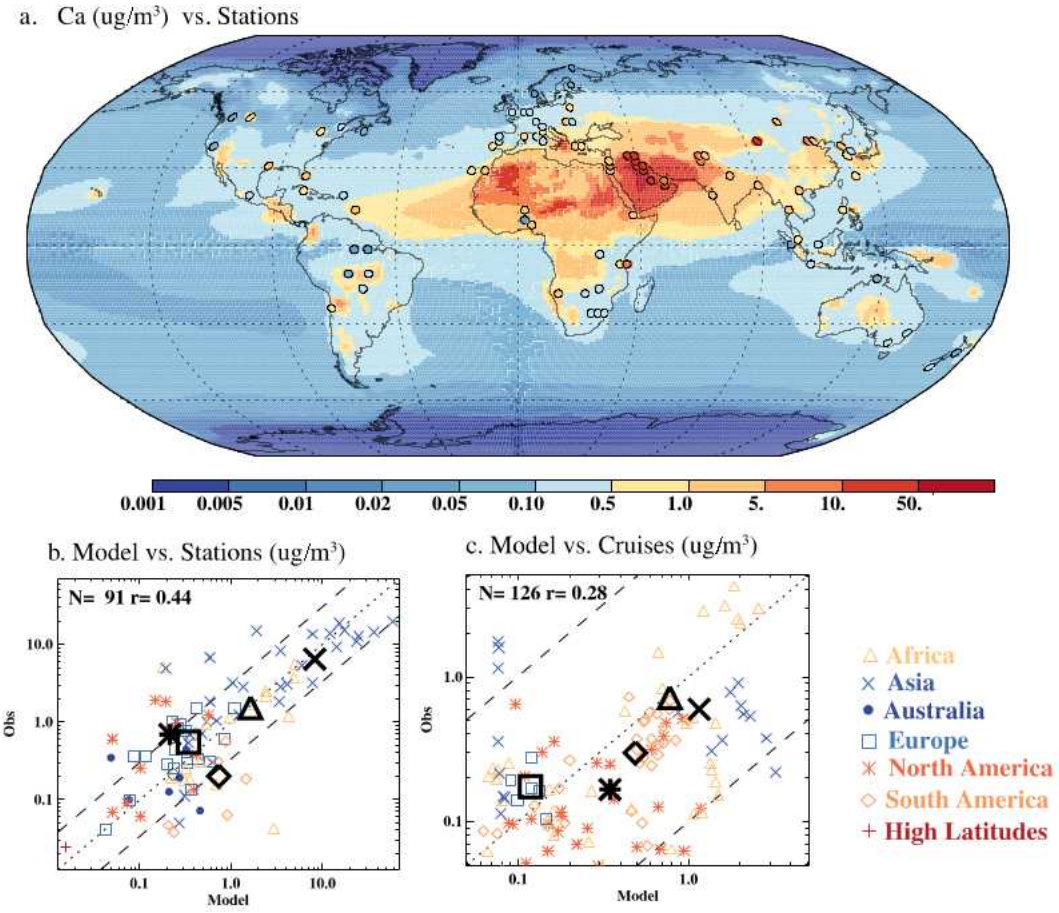

Figure 3. Same as Figure 1 but for Ca surface concentrations in the PM_{10} size fraction. Modeled values in μg/m^3 are shown in the background in (a), while the circles represent the observational measurements from land-based stations using the same color bar. A comparison of the model (*x*-axis) to the observations (*y*-axis) is shown for the station-based data (b) and the cruise data (c). The spatial comparison between the model and cruise data is shown in Figure S4b in Supporting Information S1. For clarity, all the observations are gridded to 2° × 2° cells. In the scatter plots, the color and symbols indicate the regions, the bold black symbols are the average across each region (indicated by the symbol), the dotted line is the 1:1 line and the dashed lines are the factor of 3 for land-based measurements (b) and 10 for ocean cruise data (c) uncertainty estimates. More statistics are shown in Table S6 in Supporting Information S1. More detailed views of the regions are shown in Figure S9 in Supporting Information S1. *N* and *r* represent the number of observations and correlation coefficient, respectively.

uncertainty. The dominant dust source comes from Calcite (Figure S11 in Supporting Information S1) while non-dust sources of Ca are modeled to be sea salts over the oceans, and volcanoes, fires and coal over some land regions (Figure S12 in Supporting Information S1). Sources such as dust from agriculture or construction are not included in the model. Globally 43% and 47% of the observational/model comparison were outside the 3× uncertainty bounds (Tables S6 and S7 in Supporting Information S1) for PM_{10} and $PM_{2.5}$, respectively: so the model does better for predicting Ca in PM_{10} than for $PM_{2.5}$ in contrast to the results for Al. Model results for $PM_{2.5}$ across South America are especially high, but results in the other regions are within the uncertainties, although the model produces values that are a little high for Africa and North America (Figures S3c and S3d in Supporting Information S1).

If we focus on the ratios of Ca/Al in dust dominated regions (Figure 4a), we see that the model is underpredicting the ratio of Ca/Al. This is likely due to the under-detection of calcite in the EMIT methods (see methods; Clark et al., 2024), although some of it could be due to under-detection of Al in the PM10 atmospheric concentrations (see methods; Lucarelli et al., 2018; Hyslop et al., 2015; Liu et al., 2025). The underprediction by the model is the

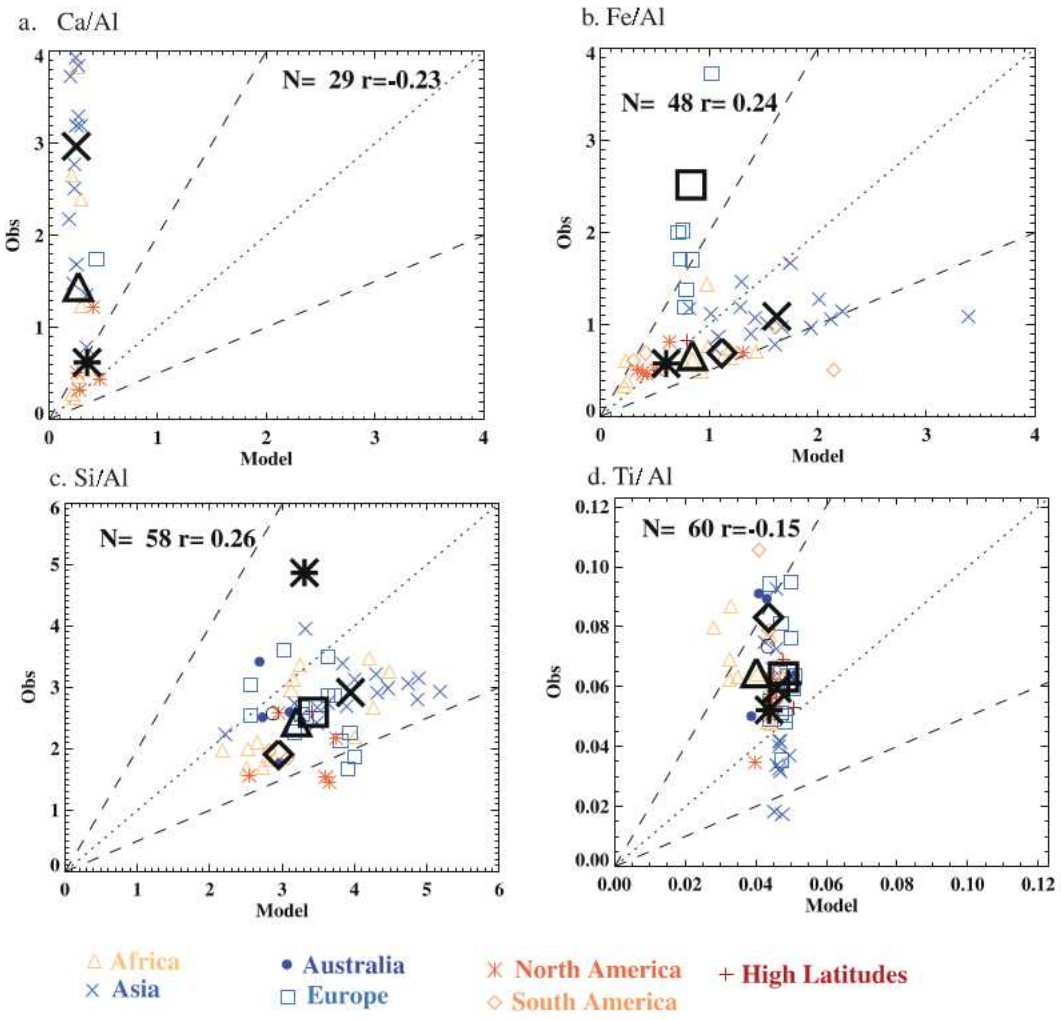

Figure 4. Scatter plot of the PM_{10} elemental ratios between model (*x*-axis) and observations (*y*-axis) for (a) Ca/Al, (b) Fe/Al, (c) Si/Al, and (d) Ti/Al where the ratios of concentrations are in ($\mu g/m^3$ divided by $\mu g/m^3$). In the scatter plots, the color and symbols indicate the regions, the bold black symbols are the average across each region (indicated by the symbol), the dotted line is the 1:1 line and the dashed lines are the factor of 2 uncertainties bound as described in the methods section. The spatial maps of the ratios are available in Figure S10 in Supporting Information S1.

worst in Asia and is seen to some extent in Africa. Improved methods to detect Ca derived minerals in EMIT are important to improve Ca simulations.

The cruise data suggest that the Ca in PM_{10} is similar for the model and the observations (Figure 3c; Table S8 in Supporting Information S1). Similarly, the limited $PM_{2.5}$ cruise data also suggests that the model is within the uncertainties of the model-data comparison for most of the observations (Figures S5c and S5d; Table S9 in Supporting Information S1).

3.1.3. Iron (Fe)

Simulated Fe was more highly correlated with available data compared to the other elements (Figure 5a vs. Figures 1a and 3a). This is consistent with its emissions inventory and transport modeling being much more mature than for other elements, and the emission data set we use here being focused on simulating Fe (Hand et al., 2004; Myriokefalitakis et al., 2018; Rathod et al., 2020, 2024; Scanza et al., 2018). The averages across the regions are within the 3× uncertainty, and the concentrations in non-natural dust dominated regions are similar between the model and observations (Figure 5). Studies have shown that the model is less able to simulate natural Fe derived from dust than anthropogenic sources of Fe (Rathod et al., 2020), but that anthropogenic sources are

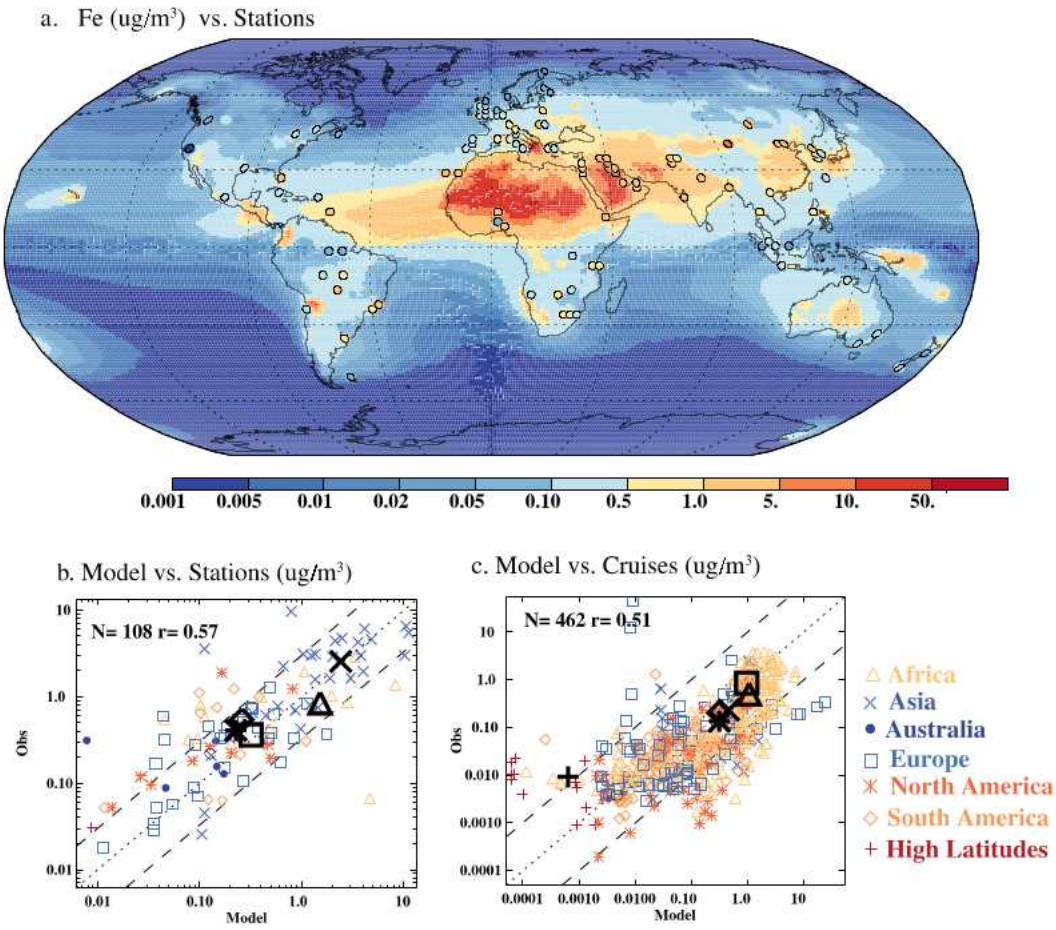

Figure 5. Same as Figure 1 but for Fe surface concentrations in the PM_{10} size fraction. Modeled values in μg/m^3 are shown in the background in (a), while the circles represent the observational measurements from land-based stations using the same color bar. A comparison of the model (*x*-axis) to the observations (*y*-axis) is shown for the station-based data (b) and the cruise data (c). The spatial comparison between the model and cruise data is shown in Figure S4c in Supporting Information S1. For clarity, all the observations are gridded to a 2° × 2° degrees. In the scatter plots, the color and symbols indicate the regions, the bold black symbols are the average across each region (indicated by the symbol), the dotted line is the 1:1 line and the dashed lines are the factor of 3 for land-based measurements (b) and 10 for ocean cruise data (c) uncertainty estimates. More statistics are shown in Table S6 in Supporting Information S1. More detailed views of the regions are shown in Figure S13 in Supporting Information S1. *N* and *r* represent the number of observations and correlation coefficient, respectively.

within a factor of 3 (Rathod et al., 2024). This suggests that difficulties in capturing the natural sources of dust derive from issues in simulating the elemental composition. The model suggests that the dominant dust sources of Fe are iron oxides (Figure S14 in Supporting Information S1) and of non-dust sources are volcanoes over the oceans, and fires and non-Al smelting over land regions (Figure S15 in Supporting Information S1). Comparisons of the Fe/Al ratios in dust dominated regions (Figure 4b) show that in most dust regions, the Fe/Al ratio is well simulated, except in Europe. The threshold used here (50% dust in the model) may not be strict enough to be able to filter out anthropogenic Fe sources (e.g., combustion).

Simulations of PM_{10} and $PM_{2.5}$ Fe are mostly within the uncertainties, especially for regional averages, although the results are a little high for South America (Figures S3e and S3f in Supporting Information S1). 37% and 24% of the PM_{10} and $PM_{2.5}$ model/data comparisons are outside 3× uncertainty (Tables S6 and S7 in Supporting Information S1).

Cruise data show that the average model results in different regions are close to averaged observations for PM_{10} (Figures S4c and 5c; Table S8 in Supporting Information S1) and $PM_{2.5}$ (Figures S5e and S5f; Table S9 in

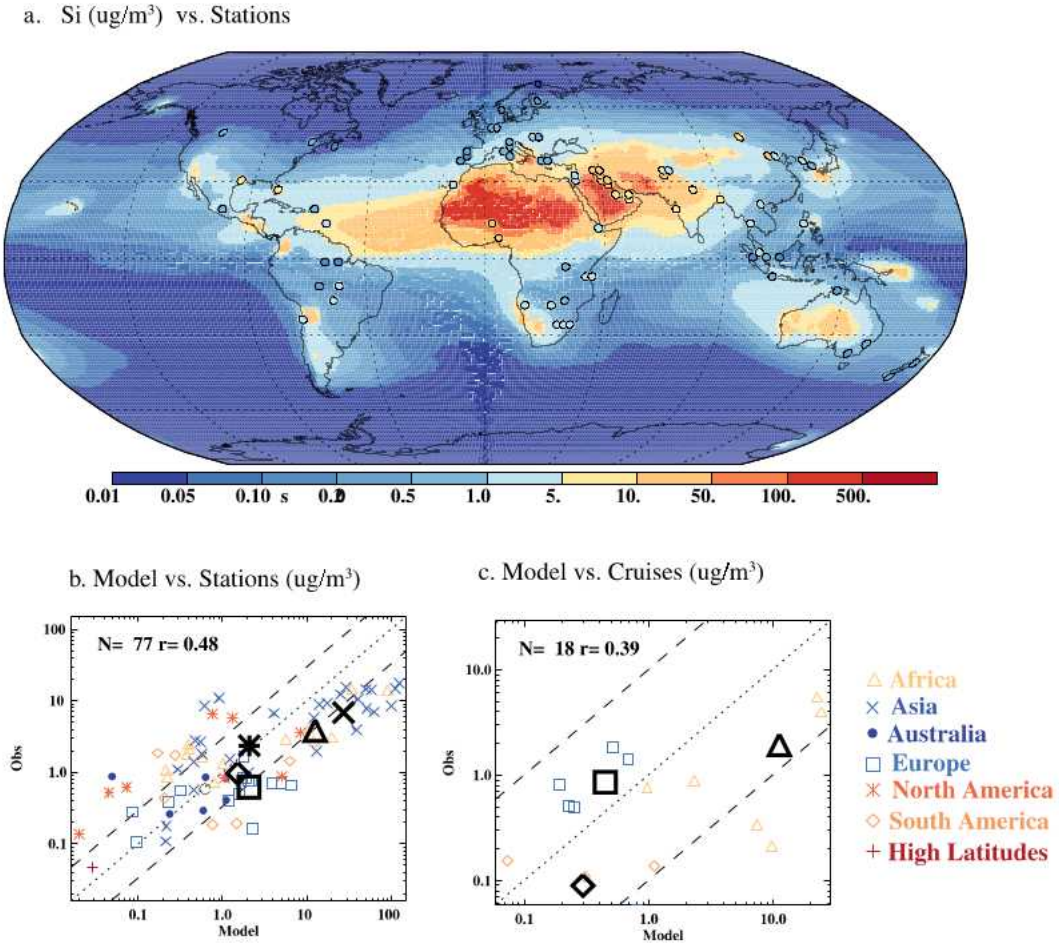

Figure 6. Same as Figure 1 but for Si surface concentrations in the PM_{10} size fraction. Modeled values in μg/m^3 are shown in the background in (a), while the circles represent the observational measurements from land-based stations using the same color bar. A comparison of the model (*x*-axis) to the observations (*y*-axis) is shown for the station-based data (b) and the cruise data (c). The spatial comparison between the model and cruise data is shown in Figure S4d in Supporting Information S1. For clarity, all the observations are gridded to a 2° × 2° degrees. In the scatter plots, the color and symbols indicate the regions, the bold black symbols are the average across each region (indicated by the symbol), the dotted line is the 1:1 line and the dashed lines are the factor of 3 for land-based measurements (b) and 10 for ocean cruise data (c) uncertainty estimates. More statistics are shown in Table S6 in Supporting Information S1. More detailed views of the regions are shown in Figure S17 in Supporting Information S1. *N* and *r* represent the number of observations and correlation coefficient, respectively.

Supporting Information S1), similar to previous results with a previous version of this model (Hamilton et al., 2019). For iron, there is another compilation of cruise data from Myriokefalitakis et al., 2018, and this model simulation gives a similar comparison to the cruise data as the previous study (Figure 5c; Figures S4c and S16 in Supporting Information S1). Further studies will consider in more detail the impact on soluble iron of the EMIT data set.

3.1.4. Silicon (Si)

Model simulations of Si show a maximum over desert regions, but also near volcanic regions (e.g., Sicily, Indonesia, and Japan) (Figure 6a). Model simulations of PM_{10} Si tend to be higher than the available station observations in the regional means, especially in Europe, Africa, and Asia (Figures 6a and 6b). This is consistent with Al, in suggesting dust sources are very high in Africa, but inconsistent with the results from Ca and Fe. The dominant dust source of Si is Quartz (Figure S18 in Supporting Information S1). The dominant non-dust source of Si in the model is volcanoes over the ocean with some contribution from coal over some land regions (Figure S19

in Supporting Information S1). In non-dust dominated regions (Figure 2d), such as parts of Europe or North America which have good data coverage, the model is similar to available observations, suggesting that the non-dust sources in the model are approximately correct. Volcanic sources of silicon may be poorly represented, as the model shows a maximum over Sicily from volcanoes (Figure 6a). The representation of volcanoes in these simulations is very simple and needs improvement, since it assumes constant outgassing, instead of intermittent ash generation. In dust-dominated regions, comparisons show a good correspondence of the ratios of Si/Al between model and data (Figure 4c).

Simulations of $PM_{2.5}$ Si over land tend to be within the 3× uncertainty bars, but slightly high (Figures S3g and S3h in Supporting Information S1). Approximately 51% and 22% of the Si observation-model comparisons for PM_{10} and $PM_{2.5}$, respectively, are outside the uncertainty bounds (Tables S6 and S7 in Supporting Information S1), suggesting that $PM_{2.5}$ is better simulated than PM_{10}.

Si data are sparse in cruises, and what little data there are displays some correspondence with the simulations for PM_{10} (Figure S4d in Supporting Information S1 and Figure 5c; Table S8 in Supporting Information S1; there are no Si cruise data in the $PM_{2.5}$ size fraction).

3.1.5. Titanium (Ti)

In the model simulations, the largest concentrations of Ti are near desert regions, or volcanoes, similar to Si and these are difficult to verify with the available observations (Figure 7). Over 4 orders of magnitude the model simulates much of the spatial variability (Figures 7a and 7c) with the regional averages all within the uncertainty bounds for PM_{10}. Ti is a trace amount in dust, and comes predominately associated with Illite and Kaolinite (Figure S21 in Supporting Information S1). The non-dust dominated sources of Ti over oceans (and some land regions) is volcanoes in the model, and over land, coal (Figure S22 in Supporting Information S1). In dust dominated regions, the Ti/Al ratio in the model is much less variable than in the observations (Figure 4d), but the model is just within the error bars in all regions.

For $PM_{2.5}$, the model tends to overpredict the regional averages in Europe and Asia (Figures S3i and S3j in Supporting Information S1). Approximately 41% and 27% of the observation-model comparisons for PM_{10} and $PM_{2.5}$, respectively, are within the uncertainty bounds (Tables S6 and S7 in Supporting Information S1), which suggests the PM_{10} simulations have more difficulty simulating the spatial spread in the values than the $PM_{2.5}$.

The cruise data suggests that the regional averages are similar between the model and observations, as the regional means are within the uncertainties in the PM_{10} size fraction (Figure 7c and Figure S4e; Table S8 in Supporting Information S1). This is not true in the high latitudes, as the Iceland volcano has been sampled in the observations but not in the model (Figure 7c and Figure S4e in Supporting Information S1). The limited $PM_{2.5}$ cruise data suggests the model is within the uncertainties (Figures S5g and 5h; Table S9 in Supporting Information S1).

3.2. Elemental Budgets

The overall emissions of each element in the atmospheric PM_{10} size fraction vary from almost 1,000 Tg/year for Si to ~10 Tg/year for Ti (Figure 8a). There are only a few literature values for the budgets of these elements, but a recent review tried to summarize our understanding of Al, Fe, and Ti (Mahowald et al., 2018) based on existing literature (Nriagu, 1989; Nriagu & Pacyna, 1988; Pacyna & Pacyna, 2001; Schlesinger, 1997). Previous studies did not compare to available surface concentrations, and thus were not shown to match observational estimates. Al, Fe, and Ti budgets are slightly higher in this study compared to the earlier work (Mahowald et al., 2018). For these three metals, the largest contribution comes from dust, which is much better resolved in this study, since we use mineralogy based on space-borne data and consider transport.

Within dust, the kaolinite fraction represents the most important sources for Al and Ti, while calcite is the most important for Ca (Figure 8b). Fe has roughly similar contributions from Fe oxides and illite, while Si comes mostly from quartz, but with significant contributions from illite (Figure 8b). Note that the observed Ca/Al ratios suggest the EMIT-based model is underestimating the Ca in dust (Figure 4a), and thus it is likely the global total from Calcite should be larger.

The contributions for all these elements are dominated by dust, as expected (Figure 8b: black and gray colors and patterns, Table 1). Contributions from anthropogenic sources tend to be small on a global average (pink and

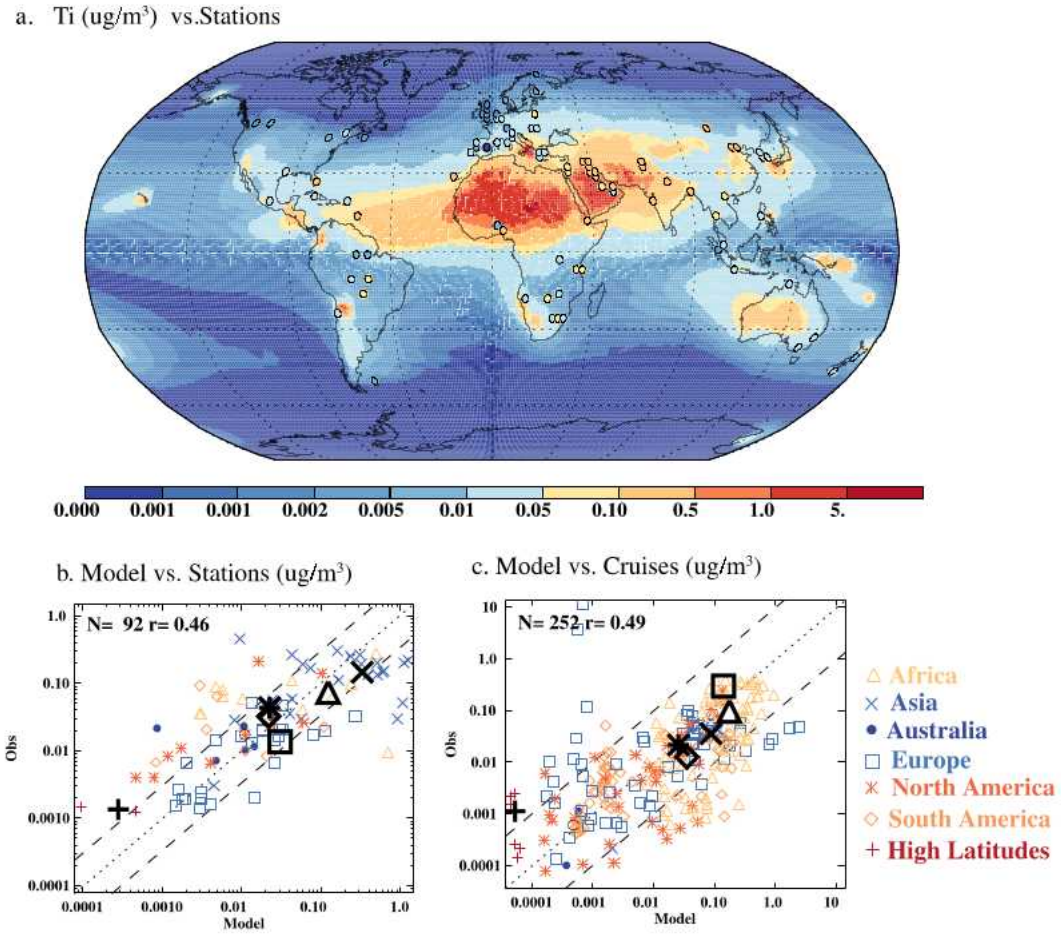

Figure 7. Same as Figure 1 but for Ti surface concentrations in the PM_{10} size fraction. Modeled values in $\mu g/m^3$ are shown in the background in (a), while the circles represent the observational measurements from land-based stations using the same color bar. A comparison of the model (*x*-axis) to the observations (*y*-axis) is shown for the station-based data (b) and the cruise data (c). The spatial comparison between the model and cruise data is shown in Figure S4e in Supporting Information S1. For clarity, all the observations are gridded to a 2° × 2°. In the scatter plots, the color and symbols indicate the regions, the bold black symbols are the average across each region (indicated by the symbol), the dotted line is the 1:1 line and the dashed lines are the factor of 3 for land-based measurements (b) and 10 for ocean cruise data (c) uncertainty estimates. More statistics are shown in Table S6 in Supporting Information S1. More detailed views of the regions are shown in Figure S20 in Supporting Information S1. *N* and *r* represent the number of observations and correlation coefficient, respectively.

purple colors in Figure 8b, Table 1). Some sources were not included in this study, including dust from agricultural tillage. Other non-dust sources can be important for some elements, especially Ca (sea salts) and volcanoes are important for several of these elements (Figure 8b; Table 1). The volcanic source included in this estimate is not well parameterized, as it uses a distribution of emissions estimated from continuous outgassing of SO_2, which is then scaled to obtain estimates similar to previous studies (see Section 2.3). Since outgassing distributions and processes are quite different to the explosive eruptions that are likely to produce the insoluble ash-based aerosol elements included in our model, these estimates are likely incorrect. This analysis suggests further work is justified on ash-based aerosol elements in order to understand the role of explosive volcanoes in their budgets.

The overall contribution from general categories show that dust is the dominant source of these elements (Table 1), while volcanoes are the next largest source. Some very small contributions from anthropogenic, fires, sea salts, and biogenics are also seen (Table 1). Comparison with the limited previous studies suggests a similar importance of different sources (Table S10 in Supporting Information S1) for most elements. The tiny amounts of Al and Fe from sea spray and biogenic particles is smaller in this study than one previous estimate (Mahowald, Li,

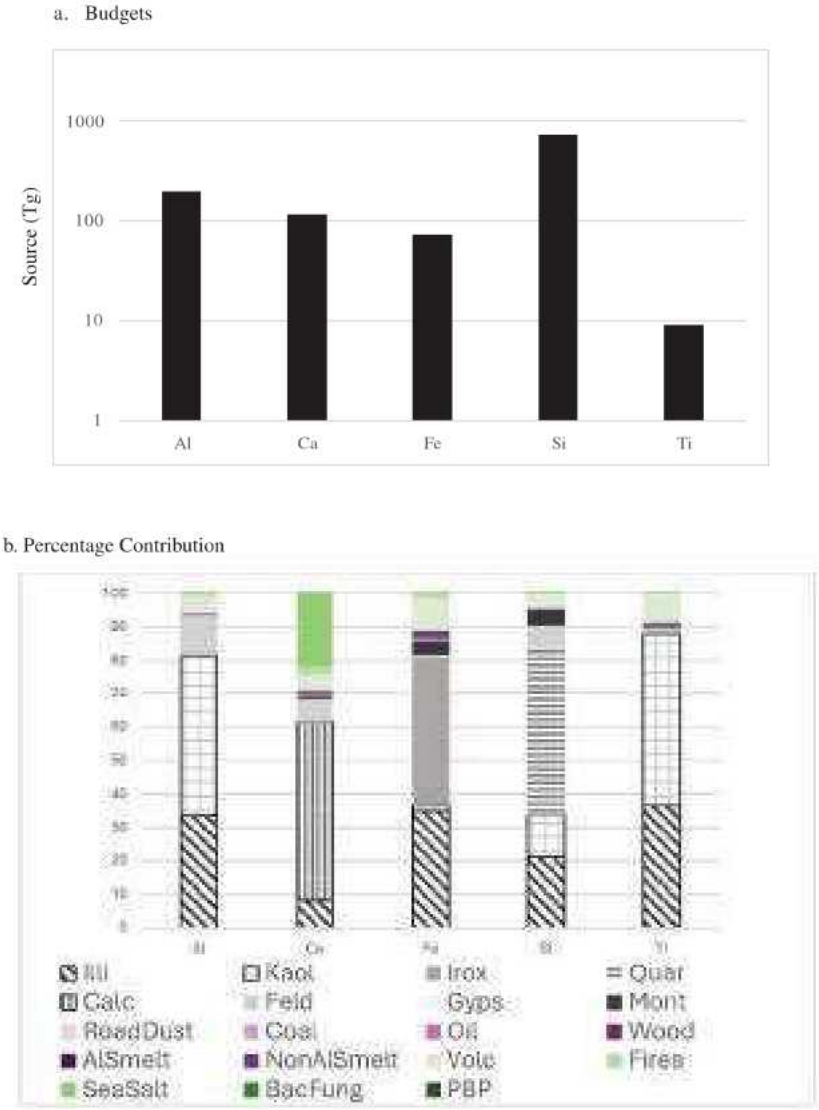

Figure 8. Elemental budgets. The atmospheric global total emissions (Tg/year) in the PM_{10} fraction is shown (a), with the contribution from each of the sources considered here in (b). The dust-based sources are in black and gray colors, while the pink and purple sources are anthropogenic and the green colors are non-dust natural aerosol sources. Emissions for each element for each source type is shown in Table S5 in Supporting Information S1. The abbreviations in the source contributions (b) are the following: Illi, Illite; Kaol, Kaolinite; Irox, Iron oxides; Quar, Quartz; Calc, Calcite; Feld, Feldspar; Gyps, Gypsum; Mont, Montmorillonite; RoadDust, Road dust; Coal, Coal burning; Oil, Oil burning; Wood, Wood burning; AlSmelt, Al smelting; NonAlSmelt, Non-Al smelting; Volc, Volcano; Fires, Open fires; SeaSalt, Sea Salts; BacFung, Bacteria and Fungi; PBP, other primary biogenic particles.

Vira, et al., 2025). Extraterrestrial sources of iron, from incoming meteorites for example, have been speculated to be important, but studies have shown their contribution is not significant even over remote ocean regions of soluble iron (Mahowald et al., 2009).

3.3. Deposition Changes Since Preindustrial Times

The extent of human modification of aerosol-induced deposition of important nutrients or pollutants is an important question for biogeochemists. Here we use the estimates from the model to look at the ratio of deposition for present day over preindustrial times, or how much deposition of each element is likely to have been changed. We assume that dust increased since preindustrial times, following the paleodata estimates in Kok et al. (2023), although these are uncertain, and based on limited data. These estimates suggest approximately a 55% increase in

Table 1
Elemental Budgets

	Al	Ca	Fe	Si	Ti
Total (Tg/year)	200	118	74	740	9
% Dust	93	69	86	95	91
% Anthropogenic	1	1	3	<1	1
% Fire	<1	2	1	<1	<1
% Biogenic	<1	<1	<1	<1	<1
% Sea Spray	<1	21	<1	<1	<1
% Volcanoes	6	5	10	5	8

global dust, which we implement on a regional basis, as deduced from the data (Kok et al., 2023). Since the elements we consider here are predominately from dust, we expect, and capture, an approximately 50% increase in these elements near dusty regions (Figure 9). Anthropogenic sources will have increased deposition in some regions as well, although their contribution is much smaller than the dust contributions, and volcanic sources globally (Figure 8b.). The smallest increases are seen in Ca away from the dust source areas, which have large non-dust natural sources; these are not thought to have changed as much since preindustrial times (Figure 9). The exact impact of these changes on deposition are not explored here explicitly, but the monthly mean gridded deposition fields are available for further study.

4. Summary and Conclusions

In this study we compiled available measurements of atmospheric surface concentrations of the dominant elements in dust (Al, Ca, Fe, Ti, and Si), and compared these against new model results focusing on these elements. For the first time, we looked at the non-dust atmospheric sources of Al, Ca, Ti, and Si and modeled their dispersion throughout the atmosphere from their source region to their site of deposition onto the surface. We focus here on the total elemental amounts, not the soluble fraction, because there is more data and knowledge of the total amounts. We acknowledge that soluble fractions can differ substantially from total concentrations, particularly for elements such as Fe, and are more directly relevant for biogeochemical impacts. Therefore, our results should be interpreted as constraints on total atmospheric elemental cycling, rather than bioavailable fluxes. Our goals were to better understand the atmospheric cycling (sources, distribution and deposition) of these elements, estimate where the non-dust sources were important, and consider how the deposition of these elements has changed compared to preindustrial times. We used new mineral estimates from EMIT derived from imaging

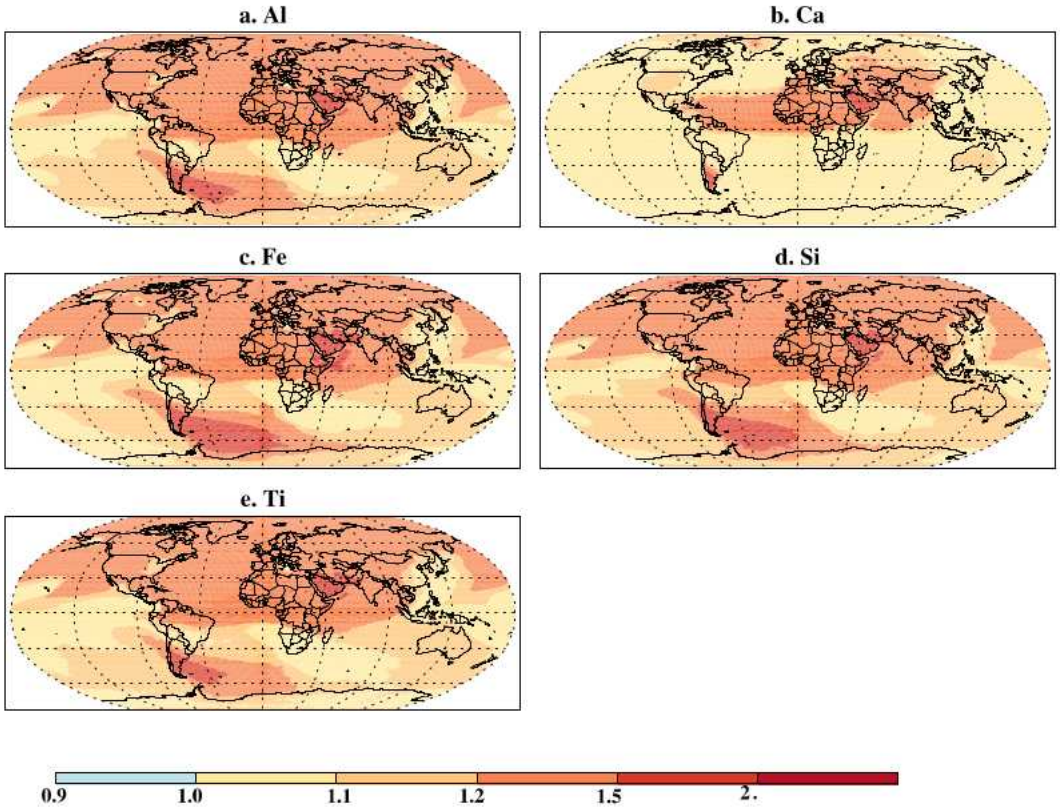

Figure 9. Increases in elemental deposition since preindustrial times. The ratio of present day to preindustrial annual averaged PM_{10} deposition at each grid point, as estimated in the model is shown for (a) Al, (b) Ca, (c) Fe, (d) Si, and (e) Ti.

Acknowledgments
NMM and LL would like to acknowledge the support of NASA Grant 80NSSC20K1674 and the EMIT project. EMIT is supported by the NASA Earth Venture Instrument program under the Earth Science Division of the Science Mission Directorate. NMM and LL would also like to acknowledge the support of the high-performance computing resources from Derecho provided by National Center for Atmospheric Research (NCAR)'s Computational and Information Systems Laboratory (CISL), sponsored by the National Science Foundation (NSF). We would also like to acknowledge the assistance of Paul Ekhart (EBAS), the many freely available air quality websites acknowledged in the paper: EBAS (https://ebas.nilu.no/)--including data affiliated with ACTRIS (Aerosol Clouds and Trace gas Research Infrastructure), EMEP (European Monitoring and Evaluation Programme), GAW-WDCA (Global Atmosphere Watch-World Data Centre for Aerosols), EANET Acid Deposition Monitoring Network in (East Asian)--All Indian Air Quality Management data (https://app.cpcbccr.com/ccr/#/caaqm-dashboard-all/caaqm-landing/data), US EPA CSN and IMPROVE, INDAAF ACTRIS-Fr (International Network to study Deposition and Atmospheric chemistry in Africa) (http://indaaf.obs-mip.fr). DDC would like to acknowledge the National Collaborative Research Infrastructure Scheme (NCRIS) for financial support. A portion of the research related to EMIT mission data products was carried out at the Jet Propulsion Laboratory, California Institute of Technology, under a contract with the National Aeronautics and Space Administration (80NM0018D0004). SC is grateful to the Gulf Research Program under the U.S. National Academies of Sciences, Engineering, and Medicine (Award No. SCON-10000653) for financial support. JPE acknowledges the support by the Department of Defence, of the Enhanced Particulate Matter Surveillance Program (EPMSP), contract number: W9124R-05-C-0135/SUBCLIN 000101-ACRN-AB, specifically for the aerosol data from the Middle East. M.G.A and C.P.G.P. acknowledge support from the Spanish Ministerio de Economía y Competitividad through the HEAVY and DUSTIMPACT project (Grants PID2022-140365OB-I00 and PID2024-157110OI-C21) and the BIOTA project (PID2022-139362OB-I00) funded by MCIN/AEI/10.13039/501100011033 and by ERDF/EU, the ERC under the Horizon 2020 research and innovation programme through the FRAGMENT project (Grant agreement no. 773051), the Horizon Europe programme under Grant Agreement No 101137680 via project CERTAINTY, and the AXA Research Fund through the AXA Chair on Sand and Dust Storms at BSC. RLM was

spectroscopy measurements from the International Space Station as well as elemental composition studies of the minerals to estimate elemental distributions for these dust-dominated elements. We included both natural and anthropogenic non-dust sources (e.g., Figure 8). Our model-data comparisons suggested that the model was able to capture much of the spatial variability seen in the observations, but there were still significant differences between the model and data that should be resolved in future studies, especially in dust-dominated areas, similar to previous studies (e.g., Rathod et al., 2024). Ca/Al in particular is underpredicting in desert regions, suggesting the under detection of Ca minerals in EMIT (Clark et al., 2024) is playing an important role and should be addressed in the future.

Because these elements originate predominantly from dust, and we followed recent studies that have suggested dust has increased by 55% since preindustrial times (Kok et al., 2023), we estimate a large increase in dust deposition over much of the globe for these elements (Figure 9). Increases were larger for Al, Fe, Si, and Ti, but smaller for Ca, which has more non-dust natural sources (Figure 8b).

For the first time, we estimate the non-dust sources of these elements and show that in many regions, the non-dust sources will dominate. These are sources from both other natural sources (e.g., volcanoes, sea spray, wildfires or primary biogenic particles) or from anthropogenic sources such as fuel combustion. Volcanic sources are estimated here to be the second largest sources, but are poorly represented here: future work should focus on improving the estimates of volcanic sources.

While the role of increased dust-borne Fe deposition to the oceans has been considered in substantial detail (e.g., Kok et a., 2023), changes in atmospheric concentrations and deposition of the other elements (e.g., Al, Ca, Si and Ti) have not yet been considered, although they could be important. In this study, we included a detailed study of both natural and anthropogenic, dust and non-dust sources of these elements which allows for future studies to look in more detail at the possible impacts using gridded monthly mean deposition data for preindustrial and present day.

While our study includes as much in situ concentration data as available, there are regions with little data, inhibiting our ability to verify model estimates against observations (e.g., Figure 1). More data outside North America, Europe, and Japan would enhance our understanding of the distribution of these important elements and their impact on ecosystems.

Conflict of Interest

The authors declare no conflicts of interest relevant to this study.

Availability Statement

The model output and observational compilation are Mahowald, Li, Gonçalves Ageitos et al. (2025). The supplemental information also includes the observational compilation and citations.

References

Aboagye-Okyere, A., Meidan, D., Hamilton, D. S., Hess, P., Kalashnikova, O., Garay, M., & Mahowald, N. M. (2025). The changing role of dust and open fires $PM_{2.5}$ on Africa's air quality and human health. *Environmental Research Letters*, *20*(9), 094013. https://doi.org/10.1088/1748-9326/adf07c

Achterberg, E. P., Steigenberger, S., Klar, J. K., Browning, T. J., Marsay, C. M., Painter, S. C., et al. (2021). Trace element biogeochemistry in the high latitude North Atlantic Ocean; seasonal variations and volcanic inputs. *Global Biogeochemical Cycles*, *34*(3), e2020GB006674. https://doi.org/10.1029/2020gb006674

Albani, S., Mahowald, N., Perry, A., Scanza, R., Zender, C., Flanner, M. G., et al. (2014). Improved representation of dust size and optics in the CESM. *Journal of Advances in Modeling Earth Systems*, *6*(3), 541–570. https://doi.org/10.1002/2013MS000279

Baker, A., Jickells, T., Biswas, K., Weston, K., & French, M. (2006). Nutrients in atmospheric aerosol particles along the Atlantic Meridional Transect. *Deep-Sea Research II*, *53*(14–16), 1706–1719. https://doi.org/10.1016/j.dsr2.2006.05.012

Baker, A. R., Adams, C., Bell, T. G., Jickells, T. D., & Ganzeveld, L. (2013). Estimation of atmospheric nutrient inputs to the Atlantic Ocean from 50°N to 50°S based on large-scale field sampling: Iron and other dust-associated elements. *Global Biogeochemical Cycles*, *27*(3), 755–767. https://doi.org/10.1002/gbc.20062

Baker, A. R., Kanakidou, M., Nenes, A., Myriokefalitakis, S., Croot, P. L., Duce, R. A., et al. (2021). Changing atmospheric acidity as a modulator of nutrient deposition and ocean biogeochemistry. *Science Advances*, *7*(28), eabd8800. https://doi.org/10.1126/sciadv.abd8800

Boyd, P., Ellwood, M., Tagliabue, A., & Twining, B. (2017). Biotic and abiotic retention, recycling and remineralization of metals in the ocean. *Nature Geoscience*, *10*(3), 167–173. https://doi.org/10.1038/ngeo2876

Boyd, P. W., Jickells, T., Law, C. S., Blain, S., Boyle, E. A., Buesseler, K. O., et al. (2007). Mesoscale iron enrichment experiments 1993 – 2005: Synthesis and future directions. *Science*, *315*(5812), 612–618. https://doi.org/10.1126/science.1131669

supported by the NASA Earth Mineral Dust Source Investigation (EMIT) and the NASA Modeling, Analysis and Prediction Program. PA acknowledge FAPESP - Fundação de Amparo à Pesquisa do Estado de São Paulo, Grant 2023/04358-9. FL acknowledges Chile's Sistema de Información Nacional de Calidad del Aire (https://sinca.mma.gob.cl/index.php/). H. M. was supported by the MEXT/JSPS KAKENHI Grants (JP23H00515, JP23K18519, JP23K24976, JP24H02225, JP26K00780, and JP26K03065), the MEXT Arctic Challenge for Sustainability II (ArCS II; JPMXD1420318865) and 3 (ArCS-3; JPMXD1720251001) Projects, and the Environment Research and Technology Development Fund 2–2301 (JPMEERF20232001) and 2–2602 (JPMEERF20262002) of the Environmental Restoration and Conservation Agency. SR acknowledge the support of the project AERO-EXTREME (PID2021-125669NB-I00) funded by the State Research Agency/ Agencia Estatal de Investigación of Spain and the European Regional Development Funds. GS and RUS acknowledge the GEOVIDE grant (ANR-13-B506-0014). The work of the University of Aveiro was partially supported by national funds through FCT – Fundação para a Ciência e a Tecnologia I.P., under the project CESAM-Centro de Estudos do Ambiente e do Mar, references UID/50017/2025 (https://doi.org/10.54499/UID/50017/2025) and LA/P/0094/2020 (https://doi.org/10.54499/LA/P/0094/2020). CSB acknowledges National Science Foundation support of GEOTRACES projects under awards OCE-1454368, OCE-1438047, and OCE-1756103. The Italian scientific activities at THAAO are partially founded by INGV and ENEA through support agreements with the National Science Foundation (USA) and Inussuk (DK). Long-term PM 10 measurements at Lampedusa have been carried out jointly by ENEA and University of Florence within several research projects funded by the Italian Ministry for University and Research and the Ministry of the Environment. Contributions at Lampedusa by Damiano Sferlazzo are gratefully acknowledged.

Brahney, J., Mahowald, N., Ward, D. S., Ballantyne, A. P., & Neff, J. C. (2015). Is atmospheric phosphorus pollution altering global alpine Lake stoichiometry? *Global Biogeochemical Cycles*, *29*(9), 1369–1383. https://doi.org/10.1002/2015GB005137

Brodrick, P., Okin, G., Ochoa, F., Thompson, D., Clark, R., Ehlmann, B., et al. (2025). *MIT L3 aggregated mineral spectral abundance and uncertainty 0.5 deg V002*. NASA Land Processes Distributed Active Archive Center. https://doi.org/10.5067/EMIT/EMITL3ASA.002

Burrows, S. M., Elbert, W., Lawrence, M. G., & Poschl, U. (2009). Bacteria in the global atmosphere--Part 1: Review and synthesis of literature for different ecosystems. *Atmospheric Chemistry and Physics*, *9*(23), 9263–9280. https://doi.org/10.5194/acp-9-9263-2009

Capone, D., Zehr, J., Paerl, H., Bergman, B., & Carpenter, E. (1997). Trichodesmium, a globally significant marine cyanobacterium. *Science*, *276*(5316), 1221–1229. https://doi.org/10.1126/science.276.5316.1221

Chapin, F. S., Vitusek, P. M., & Van Cleve, K. (1986). The nature of nutrient limitation in plant communities. *American Naturalist*, *127*, 48–58.

Chien, C.-T., Mackey, K. R. M., Dutkiewicz, S., Mahowald, N. M., Prospero, J. M., & Paytan, A. (2016). Effects of African dust deposition on phytoplankton in the western tropical Atlantic Ocean off Barbados. *Global Biogeochemical Cycles*, *30*(5), 716–734. https://doi.org/10.1002/2015GB005334

Claquin, T., Schulz, M., & Balkanski, Y. (1999). Modeling the mineralogy of atmospheric dust sources. *Journal of Geophysical Research*, *104*(D18), 22222–243256.

Clark, R. N., Swayze, G. A., Eric Livo, K., Brodrick, P. G., Dobrea, E. N., Vijayarangan, S., et al. (2024). Imaging spectroscopy: Earth and planetary remote sensing with the PSI Tetracorder and expert systems from rovers to EMIT and beyond. *Planetary Science Journal*, *5*(12), 276. https://doi.org/10.3847/PSJ/ad6c3a

Clark, R. N., Swayze, G. A., Livo, K. E., Kokaly, R. F., Sutley, S. J., Dalton, J. B., et al. (2003). Imaging spectroscopy: Earth and planetary remote sensing with the USGS Tetracorder and expert systems. *Journal of Geophysical Research*, *108*(12), 5131. https://doi.org/10.1029/2002jc001847

Coleman, R. W., Thompson, D. R., Brodrick, P. G., Dor, E. B., Cox, E., Pérez García-Pando, C., et al. (2024). An accuracy assessment of the surface reflectance product from the EMIT imaging spectrometer. *Remote Sensing of Environment*, *315*, 114450. https://doi.org/10.1016/j.rse.2024.114450

Computational and Information Systems Laboratory. (2019). *Cheyenne: HPE/SGI ICE XA System (NCAR Community Computing)*. National Center for Atmospheric Research. https://doi.org/10.5065/D6RX99HX

Desboeufs, K. V., Sofikitis, A., Losno, R., Colin, J. L., & Ausset, P. (2005). Dissolution and solubility of trace metals from natural and anthropogenic aerosol particulate matter. *Chemosphere*, *58*(2), 195–203. https://doi.org/10.1016/j.chemosphere.2004.02.025

Despres, V., Huffman, J., Burrows, S. M., Hoose, C., Safatov, A., Buryak, G., et al. (2012). Primary biological aerosol particles in the atmosphere: A review. *Tellus B*, *64*(15598), 15598. https://doi.org/10.3402/tellusb.v64i0.15598

Duce, R. A., LaRoche, J., Altieri, K., Arrigo, K. R., Baker, A. R., Capone, D. G., et al. (2008). Impacts of atmospheric anthropogenic nitrogen on the open ocean. *Science*, *320*(5878), 893–897. https://doi.org/10.1126/science.1150369

Duce, R. A., Liss, P. S., Merrill, J. T., Atlas, E. L., Buat-Menard, P., Hicks, B. B., et al. (1991). The atmospheric input of trace species to the world ocean. *Global Biogeochemical Cycles*, *5*(3), 193–259. https://doi.org/10.1029/91GB01778

Fantle, M. S., & Tipper, E. T. (2014). Calcium isotopes in the global biogeochemical Ca cycle: Implications for development of a Ca isotope proxy. *Earth-Science Reviews*, *129*, 148–177. https://doi.org/10.1016/j.earscirev.2013.10.004

Formenti, P., Caquineau, S., Chevaillier, S., Klaver, A., Desboeufs, K., Rajot, J. L., et al. (2014). Dominance of goethite over hematite in iron oxides of mineral dust from Western Africa: Quantitative partitioning by X-ray absorption spectroscopy. *Journal of Geophysical Research: Atmospheres*, *119*(22), 12740–12754. https://doi.org/10.1002/2014jd021668

Formenti, P., Nava, S., Prati, P., Chevaillier, S., Klaver, A., Lafon, S., et al. (2010). Self-attenuation artifacts and correction factors of light element measurements by X-ray analysis: Implication for mineral dust composition studies. *Journal of Geophysical Research*, *115*(D1), D01203. https://doi.org/10.1029/2009jd012701

Formenti, P., Rajot, J., Desboefs, K., Caquineau, S., Chevallier, S., Nava, S., et al. (2008). Regional variability of hte composition of mineral dust from Western Africa: Results from the AMMA SOP0/DABEX and DODO field campaigns. *Journal of Geophysical Research*, *113*(D23), D00C13. https://doi.org/10.1029/2008JD009903

Gelaro, R., McCarty, W., Suárez, M. J., Todling, R., Molod, A., Takacs, L., et al. (2017). The modern-era retrospective analysis for research and applications, version 2 (MERRA-2). *Journal of Climate*, *30*(14), 5419–5454. https://doi.org/10.1175/jcli-d-16-0758.1

Gidden, M. J., Riahi, K., Smith, S. J., Fujimori, S., Luderer, G., Kriegler, E., et al. (2019). Global emissions pathways under different socioeconomic scenarios for use in CMIP6: A dataset of harmonized emissions trajectories through the end of the century. *Geoscientific Model Development*, *12*(4), 1443–1475. https://doi.org/10.5194/gmd-12-1443-2019

Green, R. (2022). EMIT L2A estimated surface reflectance and uncertainty and masks 60 m V001 [Dataset]. *Land Processes DAAC (LP DAAC)*. https://doi.org/10.5067/EMIT/EMITL2ARFL.001

Green, R. O., Mahowald, N., Thompson, D. R., Ung, C., Brodrick, P., Pollock, R., et al. (2023). Performance and early results from the Earth surface mineral dust source investigation (EMIT) imaging spectroscopy mission. In *IEEE Aerospace Conference Proceedings* (Vol. 2023, pp. 1–10). IEEE Computer Society. https://doi.org/10.1109/AERO55745.2023.10115851

Green, R. O., Mahowald, N., Ung, C., Thompson, D. R., Bator, L., Bennet, M., et al. (2020). The Earth surface mineral dust source investigation: An Earth science imaging spectroscopy mission. *IEEE Transactions on Geoscience and Remote Sensing*. https://doi.org/10.1109/IGARSS39084.2020.9323741

Grousset, F., & Biscaye, P. (2005). Tracing dust sources and transport patterns using Sr, Nd and Pb isotopes. *Chemical Geology*, *222*(3–4), 149–167. https://doi.org/10.1016/j.chemgeo.2005.05.006

Hamilton, D. S., Hantson, S., Scott, C. E., Kaplan, J. O., Pringle, K. J., Nieradzik, L. P., et al. (2018). Reassessment of pre-industrial fire emissions strongly affects anthropogenic aerosol forcing. *Nature Communications*, *9*(1), 3182. https://doi.org/10.1038/s41467-018-05592-9

Hamilton, D. S., Perron, M. M. G., Bond, T. C., Bowie, A. R., Buchholz, R. R., Guieu, C., et al. (2021). Earth, wind, fire, and pollution: Aerosol nutrient sources and impacts on ocean biogeochemistry. *Annual Review of Marine Science*, *14*, 301–330. https://doi.org/10.1146/annurev-marine-031921

Hamilton, D. S., Scanza, R. A., Feng, Y., Guinness, J., Kok, J. F., Li, L., et al. (2019). Improved methodologies for Earth system modelling of atmospheric soluble iron and observation comparisons using the Mechanism of Intermediate complexity for Modelling Iron (MIMI v.1.0). *Geoscientific Model Development*, *12*(9), 3835–3862. https://doi.org/10.5194/gmd-12-3835-2019

Hand, J. L., Mahowald, N. M., Chen, Y., Siefert, R. L., Luo, C., Subramaniam, A., & Fung, I. (2004). Estimates of atmospheric-processed soluble iron from observations and a global mineral aerosol model: Biogeochemical implications. *Journal of Geophysical Research*, *109*(17), D17205. https://doi.org/10.1029/2004JD004574

Heald, C., & Spracklen, D. (2009). Atmospheric budget of primary biological aerosol particles from fungal sources. *Geophysical Research Letters*, *36*(9), L09806. https://doi.org/10.1029/2009GL037493

Hornby, A., Gazel, E., Bush, C., Dayton, K., & Mahowald, N. (2023). Phases in fine volcanic ash. *Scientific Reports*, *13*(1), 15728. https://doi.org/10.1038/s41598-023-41412-x

Huang, Y., Adebiyi, A. A., Formenti, P., & Kok, J. F. (2021). Linking the different diameter types of aspherical desert dust indicates that models underestimate coarse dust emission. *Geophysical Research Letters*, *48*(6), e2020GL092054. https://doi.org/10.1029/2020GL092054

Huneeus, N., Schulz, M., Balkanski, Y., Griesfeller, J., Prospero, J., Kinne, S., et al. (2011). Global dust model intercomparison in AeroCom phase I. *Atmospheric Chemistry and Physics*, *11*(15), 7781–7816. https://doi.org/10.5194/acp-11-7781-2011

Hurrell, J. W., Holland, M. M., Gent, P. R., Ghan, S., Kay, J. E., Kushner, P. J., et al. (2013). The Community Earth System Model: A framework for collaborative research. *Bulletin of the American Meteorological Society*, *94*(9), 1339–1360. https://doi.org/10.1175/BAMS-D-12-00121.1

Hyslop, N. P., Trzepla, K., & White, W. H. (2015). Assessing the suitability of historical $PM_{2.5}$ element measurements for trend analysis. *Environmental Science and Technology*, *49*(15), 9247–9255. https://doi.org/10.1021/acs.est.5b01572

Ito, A., Myriokefalitakis, S., Kanakidou, M., Mahowald, N. M., Scanza, R. A., Hamilton, D. S., et al. (2019). Pyrogenic iron: The missing link to high iron solubility in aerosols. *Science Advances*, *5*(5), 1–10. https://doi.org/10.1126/sciadv.aau7671

Jaenicke, R. (2005). Abundance of cellular material and proteins in the atmosphere. *Science*, *308*(5718), 73. https://doi.org/10.1126/science.1106335

Janssen, R., Heald, C., Steiner, A., Perring, A., Huffman, J. A., Robinson, E., et al. (2020). Drivers of the fungal spore bioaerosol budget: Observational analysis and global modelling. *Atmospheric Chemistry and Physics*, *21*(6), 4381–4401. https://doi.org/10.5194/acp-2020-569

Jickells, T., & Moore, C. M. (2015). The importance of atmospheric deposition for ocean productivity. *Annual Review of Ecology, Evolution, and Systematics*, *46*(1), 481–501. https://doi.org/10.1146/annurev-ecolsys-112414-054118

Jickells, T. D., An, Z. S., Andersen, K. K., Baker, A. R., Bergametti, C., Brooks, N., et al. (2005). Global iron connections between desert dust, ocean biogeochemistry, and climate. *Science*, *308*(5718), 67–71. https://doi.org/10.1126/science.1105959

Journet, E., Balkanski, Y., & Harrison, S. (2014). A new data set of soil mineralogy for dust-cycle modeling. *Atmospheric Chemistry and Physics*, *14*(8), 2014–3801. https://doi.org/10.5194/acp-14-3801-2014

Journet, E., Desboeufs, K. V., Caquineau, S., Colin, J.-L. J.-L., Desboufs, K., Caqineau, S., & Colin, J.-L. J.-L. (2008). Mineralogy as a critical factor of dust iron solubility. *Geophysical Research Letters*, *35*(7), L07805. https://doi.org/10.1029/2007GL031589

Klimont, Z., Kupiainen, K., Heyes, C., Purohit, P., Cofala, J., Rafaj, P., et al. (2017). Global anthropogenic emissions of particulate matter including black carbon. *Atmospheric Chemistry and Physics*, *17*(14), 8681–8723. https://doi.org/10.5194/acp-17-8681-2017

Kok, J. (2011). A scaling theory for the size distribution of emitted dust aerosols suggests climate models underestimate the size of the global dust cycle. *Proceedings of the National Academy of Science USA*, *108*(3), 1016–1021. https://doi.org/10.1073/pnas.1014798108

Kok, J. F., Mahowald, N. M., Fratini, G., Gillies, J. A., Ishizuka, M., Leys, J. F., et al. (2014). An improved dust emission model - Part 1: Model description and comparison against measurements. *Atmospheric Chemistry and Physics*, *14*(23), 13023–13041. https://doi.org/10.5194/acp-14-13023-2014

Kok, J. F., Ridley, D. A., Zhou, Q., Miller, R. L., Zhao, C., Heald, C. L., et al. (2017). Smaller desert dust cooling effect estimated from analysis of dust size and abundance. *Nature Geoscience*, *10*(4), 274–278. https://doi.org/10.1038/ngeo2912

Kok, J. F., Storelvmo, T., Karydis, V. A., Adebiyi, A. A., Mahowald, N. M., Evan, A. T., et al. (2023). Mineral dust aerosol impacts on global climate and climate change. *Nature Reviews Earth and Environment*, *4*(2), 71–86. https://doi.org/10.1038/s43017-022-00379-5

Li, L., Mahowald, N. M., Gonçalves Ageitos, M., Obiso, V., Miller, R. L., Pérez García-Pando, C., et al. (2024). Improved constraints on hematite refractive index for estimating climatic effects of dust aerosols. *Communications Earth & Environment*, *5*(1), 295. https://doi.org/10.1038/s43247-024-01441-4

Li, L., Mahowald, N. M., Kok, J. F., Liu, X., Wu, M., Leung, D. M., et al. (2022). Importance of different parameterization changes for the updated dust cycle modelling in the Community Atmosphere Model (version 6.1). *Geoscientific Model Development*, *15*(22), 8181–8219. https://doi.org/10.5194/gmd-15-8181-2022

Li, L., Mahowald, N. M., Liu, X., Gonçalves Ageitos, M., Ke, Z., Leung, D. M., et al. (2026). Modeling large dust aerosols in the Community Earth System Model Version 2 (CESM2). *Journal of Advances in Modeling Earth Systems*, *18*(4), e2025MS005420. https://doi.org/10.1029/2025MS005420

Li, L., Mahowald, N. M., Miller, R. L., Pérez Garciá-Pando, C., Klose, M., Hamilton, D. S., et al. (2021). Quantifying the range of the dust direct radiative effect due to source mineralogy uncertainty. *Atmospheric Chemistry and Physics*, *21*(5), 3973–4005. https://doi.org/10.5194/acp-21-3973-2021

Likens, G. E., Driscoll, C. T., & Buso, D. C. (1996). Long-term effects of acid rain: Response and recovery of a forest ecosystem. *Science*, *272*(5259), 244–246. https://doi.org/10.1126/science.272.5259.244

Liu, X., Easter, R. C., Ghan, S. J., Zaveri, R., Rasch, P., Shi, X., et al. (2011). Toward a minimal representation of aerosol direct and indirect effects: Model description and evaluation. *Geoscientific Model Development Discussions*, *4*(4), 3485–3598. https://doi.org/10.5194/gmdd-4-3485-2011

Liu, X., Ma, P. L., Wang, H., Tilmes, S., Singh, B., Easter, R. C., et al. (2016). Description and evaluation of a new four-mode version of the Modal Aerosol Module (MAM4) within version 5.3 of the Community Atmosphere Model. *Geoscientific Model Development*, *9*(2), 505–522. https://doi.org/10.5194/gmd-9-505-2016

Liu, X., Turner, J. R., Mitroo, D., Ren, Y., Oxford, C. R., Liu, W., & Martin, R. V. (2025). Assessing attenuation effects in X-ray fluorescence analysis of light elements in mineral dust. *ACS ES&T Air*, *3*(1), 175–185. https://doi.org/10.1021/acsestair.5c00295

López-Darias, J., Rodríguez, S., de la Rosa, J., Vilches, J., Boulesteix, T., Taquet, N., et al. (2025). Source apportionment of processes contributing to volcanic PM_{10} aerosols during the 2021 eruption of Tajogaite. *Science of the Total Environment*, *1000*, 180321. https://doi.org/10.1016/j.scitotenv.2025.180321

Lu, L., Li, L., Rathod, S., Hess, P., Martínez, C., Fernandez, N., et al. (2024). Characterizing the atmospheric Mn cycle and its impact on terrestrial biogeochemistry. *Global Biogeochemical Cycles*, *38*(4), e2023GB007967. https://doi.org/10.1029/2023GB007967

Lucarelli, F., Calzolai, G., Chiari, M., Nava, S., & Carraresi, L. (2018). Study of atmospheric aerosols by IBA techniques: The LABEC experience. *Nuclear Instruments and Methods in Physics Research, Section B: Beam Interactions with Materials and Atoms*, *417*, 121–127. https://doi.org/10.1016/j.nimb.2017.07.034

Mackey, K. R. M., Buck, K. N., Casey, J. R., Cid, A., Lomas, M. W., Sohrin, Y., & Paytan, A. (2012). Phytoplankton responses to atmospheric metal deposition in the coastal and open-ocean Sargasso Sea. *Frontiers in Microbiology*, *3*, 359. https://doi.org/10.3389/fmicb.2012.00359

Mahowald, N. (2011). Aerosol indirect effect on biogeochemical cycles and climate. *Science*, *334*(6057), 794–796. https://doi.org/10.1126/science.1207374

Mahowald, N., Jickells, T. D., Baker, A. R., Artaxo, P., Benitez-Nelson, C. R., Bergametti, G., et al. (2008). Global distribution of atmospheric phosphorus sources, concentrations and deposition rates, and anthropogenic impacts. *Global Biogeochemical Cycles*, *22*(4), GB4026. https://doi.org/10.1029/2008GB003240

Mahowald, N., Lindsay, K., Rothenberg, D., Doney, S. C., Moore, J. K., Thornton, P., et al. (2011). Desert dust and anthropogenic aerosol interactions in the Community Climate System Model coupled-carbon-climate model. *Biogeosciences*, *8*(2), 387–414. https://doi.org/10.5194/bg-8-387-2011

Mahowald, N. M., Engelstaedter, S., Luo, C., Sealy, A., Artaxo, P., Benitez-Nelson, C., et al. (2009). Atmospheric iron deposition: Global distribution, variability, and human perturbations. *Annual Review of Marine Science of Marine Science*, *1*, 245–278. https://doi.org/10.1146/annurev.marine.010908.163727

Mahowald, N. M., Hamilton, D. S., Mackey, K. R. M., Moore, J. K., Baker, A. R., Scanza, R., & Zhang, Y. (2018). Aerosol trace metal deposition dissolution and impacts on marine microorganisms and biogeochemistry. *Nature Communications*, *81*, 1–15. https://doi.org/10.1038/s41467-018-04970-7

Mahowald, N. M., Li, L., Gonçalves Ageitos, M., Miller, R., Pérez García-Pando, C., Ginoux, P., et al. (2025). Files for "Global Model Estimates of Atmospheric Al, Ca, Fe, Si, and Ti from Dust and Non-Dust Aerosols Informed by EMIT Surface Mineralogy and Evaluated Against Observations" [Dataset]. *Zenodo*. https://doi.org/10.5281/zenodo.17904049

Mahowald, N. M., Li, L., Vira, J., Prank, M., Hamilton, D. S., Matsui, H., et al. (2025). AERO-MAP: A data compilation and modeling approach to understand spatial variability in fine- and coarse-mode aerosol composition. *Atmospheric Chemistry and Physics*, *25*(9), 4665–4702. https://doi.org/10.5194/acp-25-4665-2025

Mahowald, N. M., Scanza, R., Brahney, J., Goodale, C. L., Hess, P. G., Moore, J. K., & Neff, J. (2017). Aerosol deposition impacts on land and ocean carbon cycles. *Current Climate Change Reports*, *3*(1), 16–31. https://doi.org/10.1007/s40641-017-0056-z

Marsay, C. M., Landing, W. M., Umstead, D., Till, C. P., Freiberger, R., Fitzsimmons, J. N., et al. (2022). Does sea spray aerosol contribute significantly to aerosol trace element loading? A case study from the U.S. GEOTRACES Pacific Meridional transect (GP15). *Global Biogeochemical Cycles*, *36*(8), e2022GB007416. https://doi.org/10.1029/2022GB007416

Martin, J. H. J. (1990). Glacial-interglacial CO_2 change: The iron hypothesis. *Paleoceanography*, *5*(1), 1–13. https://doi.org/10.1029/PA005i001p00001

Matsui, H., Mahowald, N. M., Moteki, N., Hamilton, D. S., Ohata, S., Yoshida, A., et al. (2018). Anthropogenic combustion iron as a complex climate forcer. *Nature Communications*, *9*(1), 1593. https://doi.org/10.1038/s41467-018-03997-0

Measures, C., & Vink, S. (2000). On the use of dissolved aluminum in surface waters to estimate dust deposition to the ocean. *Global Biogeochemical Cycles*, *14*(1), 317–327. https://doi.org/10.1029/1999gb001188

Menut, L., Siour, G., Bessagnet, B., Couvidat, F., Journet, E., Balkanski, Y., & Desboeufs, K. (2020). Modelling the mineralogical composition and solubility of mineral dust in the Mediterranean area with CHIMERE 2017r4. *Geoscientific Model Development*, *13*(4), 2051–2071. https://doi.org/10.5194/gmd-13-2051-2020

Moore, C. M., Mills, M. M., Arrigo, K. R., Berman-Frank, I., Bopp, L., Boyd, P. W., et al. (2013). Processes and patterns of oceanic nutrient limitation. *Nature Geoscience*, *6*(9), 701–710. https://doi.org/10.1038/ngeo1765

Moore, K., Doney, S. C., Lindsay, K., Mahowald, N., & Michaels, A. F. (2006). Nitrogen fixation amplifies the ocean biogeochemical response to decadal timescale variations in mineral dust deposition. *Tellus, Series B: Chemical and Physical Meteorology*, *58*(5), 560. https://doi.org/10.1111/j.1600-0889.2006.00209.x

Murray, R. W., Leinen, M., & Isern, A. R. (1993). Biogenic flux of Al to sediment in the central equatorial Pacific Ocean: Evidence for increased productivity during glacial periods. *Paleoceanography*, *8*(5), 651–670. https://doi.org/10.1029/93PA02195

Myriokefalitakis, S., Ito, A., Kanakidou, M., Nenes, A., Krol, M. C., Mahowald, N. M., et al. (2018). The GESAMP atmospheric iron deposition model intercomparison study. *Biogeosciences Discussions*, *1*, 1–50. https://doi.org/10.5194/bg-2018-285

Nriagu, J. (1989). A global assessment of natural sources of atmospheric trace metals. *Nature*, *338*(6210), 47–49. https://doi.org/10.1038/338047a0

Nriagu, J., & Pacyna, J. (1988). Quantitative assessment of worldwide contamination of air, water and soils by trace metals. *Nature*, *333*(6169), 134–139. https://doi.org/10.1038/333134a0

Okin, G. S., Mahowald, N., Chadwick, O. A., & Artaxo, P. (2004). Impact of desert dust on the biogeochemistry of phosphorus in terrestrial ecosystems. *Global Biogeochemical Cycles*, *18*(2), GB2005. https://doi.org/10.1029/2003GB002145

Okin, G. S., Ochoa, F., Brodrick, P. G., Thompson, D. R., Keebler, A., Ehlmann, B. L., et al. (2023). Earth Surface Mineral dust source InvesTigation (EMIT) EMIT L3 algorithm: Aggregated mineral spectral abundance theoretical basis. Retrieved from https://lpdaac.usgs.gov/documents/1801/EMIT_L3_ATBD_V1.pdf

Opazo, N., Cosentino, N. J., Ridgwell, A., & Lambert, F. (2025). Sensitivity of atmospheric carbon dioxide to dust iron solubility during the last glacial-interglacial cycle. *Paleoceanography and Paleoclimatology*, *40*(9), e2025PA005132. https://doi.org/10.1029/2025PA005132

Orians, K. J., Boyle, E. A., & Bruland, K. W. (1990). Dissolved titanium in the open ocean. *Nature*, *348*(6299), 322–324. https://doi.org/10.1038/348322a0

Orians, K. J., & Bruland, K. W. (1986). The biogeochemistry of aluminum in the Pacific Ocean. *Earth and Planetary Science Letters*, *78*(4), 397–410. https://doi.org/10.1016/0012-821X(86)90006-3

Pacyna, J. M., & Pacyna, E. G. (2001). An assessment of global and regional emissions of trace metals to the atmosphere from anthropogenic sources worldwide. *Environmental Reviews*, *9*(4), 269–298. https://doi.org/10.1139/er-9-4-269

Panta, A., Kandler, K., Alastuey, A., González-Flórez, C., González-Romero, A., Klose, M., et al. (2023). Insights into the single-particle composition, size, mixing state, and aspect ratio of freshly emitted mineral dust from field measurements in the Moroccan Sahara using electron microscopy. *Atmospheric Chemistry and Physics*, *23*(6), 3861–3885. https://doi.org/10.5194/acp-23-3861-2023

Paytan, A., Mackey, K. R. M. K. R. M., Chen, Y., Lima, I. D. I. D., Doney, S. C. S. C., Mahowald, N., et al. (2009). Toxicity of atmospheric aerosols on marine phytoplankton. *Proceedings of the National Academy of Sciences*, *106*(12), 4601–4605. https://doi.org/10.1073/pnas.0811486106

Philip, S., Martin, R. V., Snider, G., Weagle, C. L., Van Donkelaar, A., Brauer, M., et al. (2017). Anthropogenic fugitive, combustion and industrial dust is a significant, underrepresented fine particulate matter source in global atmospheric models. *Environmental Research Letters*, *12*(4), 044018. https://doi.org/10.1088/1748-9326/aa65a4

Rathod, S., Hamilton, D. S., Mahowald, N., Klimont, Z., Corbett, J. J., & Bond, T. (2020). A mineralogy-based anthropogenic combustion-iron emission inventory. *Journal of Geophysical Research: Atmospheres*, *125*(17), e2019JD032114. https://doi.org/10.1029/2019JD032114

Rathod, S. D., Hamilton, D. S., Nino, L., Kreidenweis, S. M., Bian, Q., Mahowald, N. M., et al. (2024). Constraining present-day anthropogenic total iron emissions using model and observations. *Journal of Geophysical Research: Atmospheres*, *129*(17), e2023JD040332. https://doi.org/10.1029/2023JD040332

Rauch, J. N., & Pacyna, J. M. (2009). Earth's global Ag, Al, Cr, Cu, Fe, Ni, Pb, and Zn cycles. *Global Biogeochemical Cycles*, *23*(2), GB2001. https://doi.org/10.1029/2008GB003376

Rodríguez, S., Calzolai, G., Chiari, M., Nava, S., García, M. I., López-Solano, J., et al. (2020). Rapid changes of dust geochemistry in the Saharan Air Layer linked to sources and meteorology. *Atmospheric Environment*, *223*, 117186. https://doi.org/10.1016/j.atmosenv.2019.117186

Rodríguez, S., Riera, R., Fonteneau, A., Alonso-Pérez, S., & López-Darias, J. (2023). African desert dust influences migrations and fisheries of the Atlantic skipjack-tuna. *Atmospheric Environment*, *312*, 120022. https://doi.org/10.1016/j.atmosenv.2023.120022

Scanza, R. A., Hamilton, D. S., Perez Garcia-Pando, C., Buck, C., Baker, A., & Mahowald, N. M. (2018). Atmospheric processing of iron in mineral and combustion aerosols: Development of an intermediate-complexity mechanism suitable for Earth system models. *Atmospheric Chemistry and Physics*, *18*, 14175–14196. https://doi.org/10.5194/acp-18-14175-80

Scanza, R. A., Mahowald, N., Ghan, S., Zender, C. S., Kok, J. F., Liu, X., et al. (2015). Modeling dust as component minerals in the Community Atmosphere Model: Development of framework and impact on radiative forcing. *Atmospheric Chemistry and Physics*, *15*(1), 537–561. https://doi.org/10.5194/acp-15-537-2015

Schlesinger, W. H. (1997). *Biogeochemistry: An analysis of global change* (2nd ed.). Academic Press.

Spiro, P., Jacob, D., & Logan, J. (1992). The global inventory of sulfur emissions with 1° x 1° resolution. *Journal of Geophysical Research*, *97*(D5), 6023–6036. https://doi.org/10.1029/91jd03139

Tagliabue, A., Bowie, A. R., Boyd, P. W., Buck, K. N., Johnson, K. S., & Saito, M. A. (2017). The integral role of iron in ocean biogeochemistry. *Nature*, *543*(7643), 51–59. https://doi.org/10.1038/nature21058

Thompson, D. R., Green, R. O., Bradley, C., Brodrick, P. G., Mahowald, N., Dor, E. B., et al. (2024). On-orbit calibration and performance of the EMIT imaging spectrometer. *Remote Sensing of Environment*, *303*, 113986. https://doi.org/10.1016/j.rse.2023.113986

Tomašek, I., Eychenne, J., Damby, D. E., Hornby, A. J., Romanias, M. N., Moune, S., et al. (2025). Physicochemical properties and bioreactivity of sub-10 μm geogenic particles: Comparison of volcanic ash and desert dust. *GeoHealth*, *9*(1), e2024GH001171. https://doi.org/10.1029/2024GH001171

Tréguer, P. J., Sutton, J. N., Brzezinski, M., Charette, M. A., Devries, T., Dutkiewicz, S., et al. (2021). Reviews and syntheses: The biogeochemical cycle of silicon in the modern ocean. *Biogeosciences*, *18*(4), 1269–1289. https://doi.org/10.5194/bg-18-1269-2021

van Hulten, M., Sterl, A., Middag, R., de Baar, H., Gehlen, M., Dutay, J.-C., & Tagliabue, A. (2014). On the effects of circulation, sediment resuspension and biological incorporation by diatoms in an ocean model of aluminum. *Biogeosciences*, *11*, 3757–3779.

Van Marle, M. J. E., Kloster, S., Magi, B. I., Marlon, J. R., Daniau, A. L., Field, R. D., et al. (2017). Historic global biomass burning emissions for CMIP6 (BB4CMIP) based on merging satellite observations with proxies and fire models (1750-2015). *Geoscientific Model Development*, *10*(9), 3329–3357. https://doi.org/10.5194/gmd-10-3329-2017

Vet, R., Artz, R. S. R. S., Carou, S., Shaw, M., Ro, C.-U. C.-U., Aas, W., et al. (2014). A global assessment of precipitation chemistry and deposition of sulfur, nitrogen, sea salt, base cations, organic acids, acidity and pH and phosphorus. *Atmospheric Environment*, *93*, 3–100. https://doi.org/10.1016/j.atmosenv.2013.11.013

Wiedinmyer, C., Linhavainen, H., Mahowald, N., Miller, R., Aguilar-islas, A., Batterman, S., et al. (2017). COARSE-MAP synthesis of observations and models for coarse-mode aerosols. In *Fall American Geophysical Union* (p. 3).

Wong, M. Y., Rathod, S. D., Marino, R., Li, L., Howarth, R. W., Alastuey, A., et al. (2021). Anthropogenic perturbations to the atmospheric molybdenum cycle. *Global Biogeochemical Cycles*, *35*(2), e2020GB006787. https://doi.org/10.1029/2020GB006787

Zender, C., Bian, H., & Newman, D. (2003). Mineral Dust Entrainment and Deposition (DEAD) model: Description and 1990s dust climatology. *Journal of Geophysical Research*, *108*(D14), 4416. https://doi.org/10.1029/2002JD002775

Zhang, Y., Mahowald, N., Scanza, R. A., Journet, E., Desboeufs, K., Albani, S., et al. (2015). Modeling the global emission, transport and deposition of trace elements associated with mineral dust. *Biogeosciences*, *12*(19), 5771–5792. https://doi.org/10.5194/bg-12-5771-2015

References From the Supporting Information

Aas, W., CAMP, EMEP, & NILU. (2015). PM mass at Birkenes. https://doi.org/10.48597/C8HZ-SJEZ

Adamides, A., & EMEP. (2016). OC/EC and inorganics in air and particle phase at Agia Marina Xyliatou/Cyprus Atmospheric Observatory. https://doi.org/10.48597/87AY-VFWR

Adamides, A., & EMEP. (2018). Aluminium and PM10_mass at Agia Marina Xyliatou/Cyprus atmospheric observatory. https://doi.org/10.48597/DWN4-T22K

Akpo, A., Ouafo-Leumbe, M.-R., Galy-Lacaux, C., Gardrat, E., Pont, V., Liousse, C., et al. (2023). $PM_{2.5}$ aerosol EC/OC, mineral and trace metals analysis, Djougou, Benin [Dataset]. *Aeris*. https://doi.org/10.25326/586

Akpo, A., Ouafo-Leumbe, M.-R., Galy-Lacaux, C., Gardrat, E., Pont, V., Liousse, C., et al. (2023). PM_{10} aerosol EC/OC, mineral and trace metals analysis, Djougou, Benin [Dataset]. *Aeris*. https://doi.org/10.25326/587

Alastuey, A., Areskoug, H., CAMPAIGN, & EMEP. (2016). Aluminium and inorganics in air and particle phase at Aspvreten. https://doi.org/10.48597/58V2-D24Y

Alastuey, A., Balan, V., CAMPAIGN, & EMEP. (2016). Aluminium and inorganics in air and particle phase at Leova II. https://doi.org/10.48597/6ZT9-3TYT

Alastuey, A., CAMPAIGN, & EMEP. (2010). Aluminium at Montseny. https://doi.org/10.48597/2M74-SR87

Alastuey, A., CAMPAIGN, & EMEP. (2010). Aluminium at Montseny. https://doi.org/10.48597/NYDQ-JH6X

Alastuey, A., CAMPAIGN, & EMEP. (2016). Aluminium and inorganics in air and particle phase at Montsec. https://doi.org/10.48597/SC76-NFZ5

Alastuey, A., CAMPAIGN, & EMEP. (2016). Aluminium and inorganics in air and particle phase at Montseny. https://doi.org/10.48597/34XW-TB8M

Alastuey, A., Cavalli, F., Putaud, J., CAMPAIGN, & EMEP. (2016). Aluminium and inorganics in air and particle phase at Ispra. https://doi.org/10.48597/GDE3-STEG

Alastuey, A., Ceburnis, D., O'Dowd, C., CAMPAIGN, & EMEP. (2016). Aluminium and inorganics in air and particle phase at Mace Head. https://doi.org/10.48597/Y252-B3Q5

Alastuey, A., Cerro, J., CAMPAIGN, & EMEP. (2016). Aluminium and inorganics in air and particle phase at Can Llompart. https://doi.org/10.48597/VXZR-Y654

Alastuey, A., Conil, S., CAMPAIGN, & EMEP. (2016). Aluminium and inorganics in air and particle phase at Observatoire Perenne de l'Environnement. https://doi.org/10.48597/XUMC-PA8H

Alastuey, A., & EMEP. (2010). Aluminium at Montseny. https://doi.org/10.48597/GEE9-X8KR

Alastuey, A., & EMEP. (2010). Aluminium at Montseny. https://doi.org/10.48597/SJ6Z-QBQK

Alastuey, A., & EMEP. (2010). OC/EC and inorganics in air and particle phase at Montseny. https://doi.org/10.48597/CB68-KCN3

Alastuey, A., & EMEP. (2010). OC/EC and inorganics in air and particle phase at Montseny. https://doi.org/10.48597/U9NW-GAXV
Alastuey, A., & EMEP. (2014). Aluminium and sulphate_corrected at Montseny. https://doi.org/10.48597/6QHC-4RJC
Alastuey, A., & EMEP. (2014). Aluminium and sulphate_corrected at Montseny. https://doi.org/10.48597/VZR6-7Q45
Alastuey, A., & EMEP. (2014). Inorganics in air and particle phase at Montseny. https://doi.org/10.48597/HV5A-AWC4
Alastuey, A., & EMEP. (2014). Inorganics in air and particle phase at Montseny. https://doi.org/10.48597/KUZD-FJED
Alastuey, A., Gevorgyan, L., CAMPAIGN, & EMEP. (2016). Aluminium and inorganics in air and particle phase at Amberd. https://doi.org/10.48597/45CD-EF6J
Alastuey, A., Hueglin, C., CAMPAIGN, & EMEP. (2016). Aluminium and inorganics in air and particle phase at Payerne. https://doi.org/10.48597/5HJC-TDEA
Alastuey, A., Jaffrezo, J., CAMPAIGN, & EMEP. (2016). Aluminium and inorganics in air and particle phase at SIRTA Atmospheric Research Observatory. https://doi.org/10.48597/FUE7-2728
Alastuey, A., Leeson, S., CAMPAIGN, & EMEP. (2016). Aluminium and inorganics in air and particle phase at Auchencorth Moss. https://doi.org/10.48597/8SW3-F363
Alastuey, A., Leeson, S., CAMPAIGN, & EMEP. (2016). Aluminium and inorganics in air and particle phase at Harwell. https://doi.org/10.48597/8NY5-2894
Alastuey, A., Mihalopoulos, N., CAMPAIGN, & EMEP. (2016). Aluminium and inorganics in air and particle phase at Finokalia. https://doi.org/10.48597/U6QZ-3JHV
Alastuey, A., Mitosinkova, M., CAMPAIGN, & EMEP. (2016). Aluminium and inorganics in air and particle phase at Starina. https://doi.org/10.48597/FDZ7-A6P9
Alastuey, A., Perez, N., ACTRIS, EMEP, & GAW-WDCA. (2018). OC/EC at Montseny. https://doi.org/10.48597/AWBN-GV54
Alastuey, A., Perez, N., ACTRIS, EMEP, & GAW-WDCA. (2020). OC/EC at Montsec. https://doi.org/10.48597/74YB-GWX6
Alastuey, A., Perez, N., ACTRIS, EMEP, & GAW-WDCA. (2021). OC/EC at Montseny. https://doi.org/10.48597/VJAT-QQ8W
Alastuey, A., Perez, N., ACTRIS, EMEP, & GAW-WDCA. (2023). OC/EC at Montseny. https://doi.org/10.48597/GR38-TKZM
Alastuey, A., Perez, N., ACTRIS, EMEP, & GAW-WDCA. (2023). OC/EC at Montseny. https://doi.org/10.48597/JMVU-WSUF
Alastuey, A., Perez, N., EMEP, EUSAAR, & GAW-WDCA. (2011). Organic_carbon at Montseny. https://doi.org/10.48597/PFWV-2V7Z
Alastuey, A., Querol, X., EUSAAR, & GAW-WDCA. (2010). PM mass at Montseny. https://doi.org/10.48597/35YJ-AHJ3
Alastuey, A., Querol, X., EUSAAR, & GAW-WDCA. (2010). PM_{25}_mass at Montseny. https://doi.org/10.48597/47P9-6P42
Alastuey, A., Riffault, V., CAMPAIGN, & EMEP. (2016). Aluminium and inorganics in air and particle phase at Revin. https://doi.org/10.48597/JC4A-D3ZS
Alastuey, A., Spindler, G., CAMPAIGN, & EMEP. (2016). Aluminium and inorganics in air and particle phase at Melpitz. https://doi.org/10.48597/SMP4-5YKT
Alves, G., Gonçalves, C., Fernandes, A. P., Tarelho, L., & Pio, C. (2011). Fireplace and woodstove emissions: A review of chemical composition of emission from combustion of western Mediterranean wood types. *Atmospheric Environment*, *45*(40), 7126–7135. https://doi.org/10.1016/j.atmosenv.2011.04.015
Amato, F., Alastuey, A., Karanasiou, A., Lucarelli, F., Nava, S., Calzolai, G., et al. (2016). AIRUSE-LIFE+: A harmonized PM speciation and source apportionment in five southern European cities. *Atmospheric Chemistry and Physics*, *16*(5), 3289–3309. https://doi.org/10.5194/acp-16-3289-2016
Andreae, T. W., Andreae, M. O., Ichoku, C., Maenhaut, W., Cafmeyer, J., Karnieli, A., & Orlovsky, L. (2002). Light scattering by dust and anthropogenic aerosol at a remote site in the Negev desert, Israel. *Journal of Geophysical Research*, *107*(D2), 4008. https://doi.org/10.1029/2001jd900252
Angelucci, M., & EMEP. (2019). Aluminium at Monte Martano. https://doi.org/10.48597/GYHN-3U45
Angelucci, M., & EMEP. (2023). Ammonium at Monte Martano. https://doi.org/10.48597/NPS5-YQ6Q
Angelucci, M., & EMEP. (2023). Inorganics in air and particle phase at Monte Martano. https://doi.org/10.48597/XBJW-CPMS
Angelucci, M., & EMEP. (2023). Nitrate at Monte Martano. https://doi.org/10.48597/QZBG-PBXP
Angelucci, M., & EMEP. (2023). PM10_mass at Monte Martano. https://doi.org/10.48597/QZG9-THDB
Angelucci, M., & EMEP. (2023). PM25_mass at Monte Martano. https://doi.org/10.48597/K8ZX-WENG
Angelucci, M., & EMEP. (2023). Sodium at Monte Martano. https://doi.org/10.48597/3KDJ-4VSX
Arimoto, R., Duce, R. A., Ray, B. J., & Tomza, U. (2003). Dry deposition of trace elements to the western North Atlantic. *Global Biogeochemical Cycles*, *17*(1), 1010. https://doi.org/10.1029/2001GB001406
Arimoto, R., Kim, Y. J., Kim, Y. P., Quinn, P. K., Bates, T. S., Anderson, T. L., et al. (2006). Characterization of Asian dust during ACE-Asia. *Global and Planetary Change*, *52*(1–4), 23–56. https://doi.org/10.1016/j.gloplacha.2006.02.013
Artaxo, P., Martins, J. V., Yamasoe, M. A., Procopio, A. S., Pauliquevis, T. M., Andrae, M. O., et al. (2002). Physical and chemical properties of aerosols in the wet and dry seasons in Rondonia, Amazonia. *Journal of Geophysical Research: Atmospheres*, *107*(D20), LBA 49-1–LBA 49-14. https://doi.org/10.1029/2001JD0000666
Atanacio, A. J., & Cohen, D. D. (2020). *The IAEA/RCA fine and coarse PMF receptor fingerprint database*. Australian Nuclear Science and Technology Organisation. Retrieved from http://www.ansto.gov.au/aspdatabases
Aurela, M., ACTRIS, CAMPAIGN, COLOSSAL, EMEP, & GAW-WDCA. (2018). OC/EC at Pallas (Matorova). https://doi.org/10.48597/CTJQ-83BT
Aurela, M., CAMPAIGN, & EMEP. (2004). OC/EC and PM10_mass at Virolahti II. https://doi.org/10.48597/HY6Q-CU7D
Baker, A. R., Li, M., & Chance, R. (2020). Trace metal fractional solubility in size-segregated aerosols from the tropical eastern Atlantic Ocean. *Global Biogeochemical Cycles*, *34*(6), e2019GB006510. https://doi.org/10.1029/2019GB006510
Balan, V., & EMEP. (2012). PM10_mass at Leova II. https://doi.org/10.48597/C5HP-ZST2
Balan, V., & EMEP. (2012). PM10_mass at Leova II. https://doi.org/10.48597/H7HD-BDRM
Balan, V., & EMEP. (2012). PM10_mass at Leova II. https://doi.org/10.48597/MJHN-GEY2
Balan, V., & EMEP. (2013). PM10_mass at Leova II. https://doi.org/10.48597/MJHN-GEY2
Balan, V., & EMEP. (2015). PM10_mass at Leova II. https://doi.org/10.48597/MJHN-GEY2
Balan, V., & EMEP. (2016). PM10_mass at Leova II. https://doi.org/10.48597/MJHN-GEY2
Barraza, F., Lambert, F., Jorquera, H., Villalobos, A. M., & Gallardo Klenner, L. (2017). Temporal evolution of main ambient $PM_{2.5}$ sources in Santiago, Chile, from 1998 to 2012. *Atmospheric Chemistry and Physics*, *17*(16), 10093–10107.
Becagli, S., Anello, F., Bommarito, C., Cassola, F., Calzolai, G., Di Iorio, T., et al. (2017). Constraining the ship contribution to the aerosol of the central Mediterranean. *Atmospheric Chemistry and Physics*, *17*(3), 2067–2084. https://doi.org/10.5194/acp-17-2067-2017

Becagli, S., Caiazzo, L., Di Iorio, T., di Sarra, A., Meloni, D., Muscari, G., et al. (2020). New insights on metals in the Arctic aerosol in a climate changing world. *Science of the Total Environment*, *741*, 140511. https://doi.org/10.1016/j.scitotenv.2020.140511
Becagli, S., Sferlazzo, D. M., Pace, G., Di Sarra, A., Bommarito, C., Calzolai, G., et al. (2012). Evidence for heavy fuel oil combustion aerosols from chemical analyses at the island of Lampedusa: A possible large role of ships emissions in the Mediterranean. *Atmospheric Chemistry and Physics*, *12*(7), 3479–3492. https://doi.org/10.5194/acp-12-3479-2012
Benson, S. L., Natusch, D. F. S., Wallace, J. R., & Evans, C. A. (1974). Trace elements in fly ash: Dependence of concentration on particle size. *Environmental Science & Technology*, *8*(10), 1107–1113. https://doi.org/10.1021/es60090a003
Bergametti, G., Gomes, L., Doude-Gaussen, G., Rognon, P., & Le Coustumer, M. N. (1989). African dust observed over the Canary Islands: Source-regions identification and the transport pattern for some summer situations. *Journal of Geophysical Research*, *94*, 14855–14864.
Birmili, W., & GAW-WDCA. (2018). Ammonium at Melpitz. https://doi.org/10.48597/466W-DX8G
Block, C. J., & Dams, R. (1976). Study of the arsenic emission during combustion of coal. *Environmental Science & Technology*, *10*(10), 1011–1017. https://doi.org/10.1021/es60118a021
Bolte, T., & EMEP. (2008). PM10_mass at Iskrba. https://doi.org/10.48597/M3PJ-ABKK
Bolte, T., & EMEP. (2012). PM10_mass at Iskrba. https://doi.org/10.48597/ARSX-NMZ7
Bolte, T., & EMEP. (2014). PM10_mass at Iskrba. https://doi.org/10.48597/M3PJ-ABKK
Bolte, T., & EMEP. (2014). PM25_mass at Iskrba. https://doi.org/10.48597/29GX-CSDS
Bourin, A., & EMEP. (2021). OC/EC at Revin. https://doi.org/10.48597/Q5X2-T4PH
Bourin, A., & EMEP. (2022). Inorganics in air and particle phase at Revin. https://doi.org/10.48597/KRR2-63E2
Bourin, A., & EMEP. (2022). PM10_mass at Revin. https://doi.org/10.48597/PSBV-D2TU
Bourin, A., & EMEP. (2022). PM25_mass at Revin. https://doi.org/10.48597/WMEG-BNXE
Bourin, A., & EMEP. (2023). Inorganics in air and particle phase at Revin. https://doi.org/10.48597/KRR2-63E2
Bourin, A., & EMEP. (2023). PM10_mass at Revin. https://doi.org/10.48597/PSBV-D2TU
Bourin, A., & EMEP. (2023). PM25_mass at Revin. https://doi.org/10.48597/WMEG-BNXE
Bourin, A., & EMEP. (2024). Inorganics in air and particle phase at Revin. https://doi.org/10.48597/KRR2-63E2
Bourin, A., & EMEP. (2024). PM mass at Revin. https://doi.org/10.48597/K39H-W2AG
Bozlaker, A., Buzcu-Güven, B., Fraser, M. P., & Chellam, S. (2013). Insights into PM10 sources in Houston, Texas: Role of petroleum refineries in enriching lanthanoid metals during episodic emission events. *Atmospheric Environment*, *69*, 109–117. https://doi.org/10.1016/j.atmosenv.2012.11.068
Bozlaker, A., Prospero, J. M., Price, J., & Chellam, S. (2019). Identifying and quantifying the impacts of advected North African dust on the concentration and composition of airborne fine particulate matter in Houston and Galveston, Texas. *Journal of Geophysical Research: Atmospheres*, *124*(22), 12282–12300. https://doi.org/10.1029/2019jd030792
Braban, C., CAMP, & EMEP. (2014). PM10_mass at Auchencorth Moss. https://doi.org/10.48597/SPHF-9C9V
Braban, C., CAMP, & EMEP. (2014). PM25_mass at Auchencorth Moss. https://doi.org/10.48597/JTEF-TC4B
Braban, C., & EMEP. (2013). Inorganics in air and particle phase at Auchencorth Moss. https://doi.org/10.48597/WRW5-BS4S
Braban, C., & EMEP. (2013). PM10_mass at Auchencorth Moss. https://doi.org/10.48597/UWQE-YHSE
Braban, C., & EMEP. (2013). PM25_mass at Auchencorth Moss. https://doi.org/10.48597/FVSU-DUEA
Braban, C., & EMEP. (2015). Inorganics in air and particle phase at Auchencorth Moss. https://doi.org/10.48597/8KH8-6WSE
Braban, C., & EMEP. (2015). PM mass at Auchencorth Moss. https://doi.org/10.48597/AF52-Q23C
Braban, C., & EMEP. (2015). PM mass at Auchencorth Moss. https://doi.org/10.48597/GWJD-BKDY
Braban, C., & EMEP. (2023). Inorganics in air and particle phase at Auchencorth Moss. https://doi.org/10.48597/KXN5-2P47
Buck, C. S., Aguilar-Islas, A., Marsay, C., Kadko, D., & Landing, W. M. (2019). Trace element concentrations, elemental ratios, and enrichment factors observed in aerosol samples collected during the US GEOTRACES eastern Pacific Ocean transect (GP16). *Chemical Geology*, *511*, 212–224. https://doi.org/10.1016/j.chemgeo.2019.01.002
Cape, J., & EMEP. (2012). Sulphate_corrected at Auchencorth Moss. https://doi.org/10.48597/6KN8-XPTM
Cape, J., & EMEP. (2012). PM10_mass at Auchencorth Moss. https://doi.org/10.48597/89MZ-JVCR
Cape, J., Telling, S., & EMEP. (2012). PM mass at Harwell. https://doi.org/10.48597/B6ZN-EREE
Cape, J., Telling, S., & EMEP. (2012). PM10_mass at Harwell. https://doi.org/10.48597/5XWE-N7CA
Cape, J., Telling, S., & EMEP. (2012). Sulphate_corrected at Harwell. https://doi.org/10.48597/9AYP-D33D
Cavalli, F., ACTRIS, CAMPAIGN, COLOSSAL, EMEP, & GAW-WDCA. (2023). OC/EC at Ispra. https://doi.org/10.48597/3TX4-UP28
Cavalli, F., Douglas, K., ACTRIS, EMEP, & GAW-WDCA. (2015). OC/EC at Ispra. https://doi.org/10.48597/CKHK-M6PR
Cavalli, F., Douglas, K., ACTRIS, EMEP, & GAW-WDCA. (2023). OC/EC at Ispra. https://doi.org/10.48597/VC4P-M5G6
Cavalli, F., & EMEP. (2012). Inorganics in air and particle phase at Ispra. https://doi.org/10.48597/V29Z-875S
Cavalli, F., & EMEP. (2012). PM25_mass at Ispra. https://doi.org/10.48597/49A3-ZDQU
Cavalli, F., & EMEP. (2013). OC/EC at Ispra. https://doi.org/10.48597/F2SX-YGW3
Cavalli, F., & EMEP. (2013). PM25_mass at Ispra. https://doi.org/10.48597/49A3-ZDQU
Cavalli, F., & EMEP. (2015). Elemental_carbon at Ispra. https://doi.org/10.48597/R37S-NWZE
Cavalli, F., & EMEP. (2015). Inorganics in air and particle phase at Ispra. https://doi.org/10.48597/N3ND-T8RG
Cavalli, F., & EMEP. (2015). Organic_carbon at Ispra. https://doi.org/10.48597/VD46-J7U7
Cavalli, F., & EMEP. (2018). Inorganics in air and particle phase at Ispra. https://doi.org/10.48597/3YJR-RZPS
Cavalli, F., EMEP, EUSAAR, & GAW-WDCA. (2013). OC/EC at Ispra. https://doi.org/10.48597/DFH3-7R4K
Cavalli, F., Passarella, R., & EMEP. (2015). Inorganics in air and particle phase at Ispra. https://doi.org/10.48597/JX4R-WSAT
Cavalli, F., Passarella, R., & EMEP. (2023). Inorganics in air and particle phase at Ispra. https://doi.org/10.48597/3MAQ-X9BY
Cavalli, F., Passarella, R., & EMEP. (2023). Inorganics in air and particle phase at Ispra. https://doi.org/10.48597/9W69-4YAT
Cavalli, F., Passarella, R., & EMEP. (2024). Inorganics in air and particle phase at Ispra. https://doi.org/10.48597/3MAQ-X9BY
Cavalli, F., Putaud, J., ACTRIS, EMEP, & GAW-WDCA. (2023). OC/EC at Ispra. https://doi.org/10.48597/JUES-KGVB
Cavalli, F., Putaud, J., ACTRIS, EMEP, & GAW-WDCA. (2023). OC/EC at Ispra. https://doi.org/10.48597/VC4P-M5G6
Ceburnis, D., CAMPAIGN, & EMEP. (2009). OC/EC at Mace Head. https://doi.org/10.48597/JFRX-DWUZ
Ceburnis, D., & EMEP. (2010). PM25_mass at Mace Head. https://doi.org/10.48597/C9J3-PBKQ
Chance, R., Shelley, R. U., & Baker, A. R. (2026). Southern South American dust inputs to the South Atlantic and Southern Oceans: Trace element solubility and deposition fluxes. *Global Biogeochemical Cycles*, *40*(2), e2025GB009011. https://doi.org/10.1029/2025GB009011
Chen, Y., & Siefert, R. (2003). Determination of various types of labile atmospheric iron over remote oceans. *Journal of Geophysical Research*, *108*(D24), 4774. https://doi.org/10.1029/2003jd003515

Chen, Y., & Siefert, R. L. (2004). Seasonal and spatial distributions and dry deposition fluxes of atmospheric total and labile iron over the tropical and subtropical North Atlantic Ocean. *Journal of Geophysical Research*, *109*(D9), D09305. https://doi.org/10.1029/2003JD003958
Chen, Y., Street, J., & Paytan, A. (2006). Comparison between pure-water- and seawater-soluble nutrient concentrations of aerosols from the Gulf of Aqaba. *Marine Chemistry*, *101*(1–2), 141–152. https://doi.org/10.1016/j.marchem.2006.02.002
Christopher, C., & EMEP. (2015). Inorganics in air and particle phase at Harwell. https://doi.org/10.48597/2B34-8T7T
Christopher, C., & EMEP. (2016). Inorganics in air and particle phase at Harwell.
Christopher, C., & EMEP. (2017). Inorganics in air and particle phase at Chilbolton Observatory. https://doi.org/10.48597/37CQ-SAZD
Chuang, P., Duvall, R., Shafer, M., & Schauer, J. (2005). The origin of water soluble particulate iron in the Asian atmospheric outflow. *Geophysical Research Letters*, *32*(7), L07813. https://doi.org/10.1029/2004GL021946
Cipoli, Y. A., Alves, C., Rapuano, M., Evtyugina, M., Rienda, I. C., Kováts, N., et al. (2023). Nighttime–daytime PM_{10} source apportionment and toxicity in a remoteness inland city of the Iberian Peninsula. *Atmospheric Environment*, *303*, 119771. https://doi.org/10.1016/j.atmosenv.2023.119771
Cohen, D., Garton, D., Stelcer, E., Hawas, O., Wang, T., Pon, S., et al. (2004). Multielemental analysis and characterization of fine aerosols at several key ACE-Asia sites. *Journal of Geophysical Research*, *109*(D19), D19S12. https://doi.org/10.1029/2003JD003569
Conil, S., & EMEP. (2021). PM10_mass at Observatoire Perenne de l'Environnement. https://doi.org/10.48597/A5BC-RQFZ
Conil, S., & EMEP. (2022). PM10_mass at Observatoire Perenne de l'Environnement. https://doi.org/10.48597/PF5C-DVNG
Conil, S., & EMEP. (2022). PM25_mass at Observatoire Perenne de l'Environnement. https://doi.org/10.48597/EK7Z-4X95
Conolly, C., CAMP, & EMEP. (2014). PM10_mass at Harwell. https://doi.org/10.48597/3V8A-NWQF
Conolly, C., CAMP, & EMEP. (2014). PM25_mass at Harwell. https://doi.org/10.48597/EE8D-EFP5
Conolly, C., CAMP, & EMEP. (2015). Inorganics in air and particle phase at Harwell. https://doi.org/10.48597/2B34-8T7T
da Silva, L. I. D., de Souza Sarkis, J. E., Zotin, F. M. Z., Carneiro, M. C., Neto, A. A., Cardoso, M. J. B., & Monteiro, M. I. C. (2008). Traffic and catalytic converter, Related atmospheric contamination in the metropolitan region of the city of Rio de Janeiro, Brazil. *Chemosphere*, *71*(4), 677–684. https://doi.org/10.1016/j.chemosphere.2007.10.057
Dongarra, G., Manno, E., Varrica, D., Lombardo, M., & Vultaggio, M. (2010). Study on ambient concentrations of PM_{10}, $PM_{2.5}$ and gaseous pollutants. Trace elements and chemical speciation of atmospheric particulates. *Atmospheric Environment*, *44*(39), 5244–5257. https://doi.org/10.1016/j.atmosenv.2010.08.041
Dongarra, G., Manno, E., Varrica, D., & Vultaggio, M. (2007). Mass levels, crustal component and trace elements in PM_{10} in Palermo, Italy. *Atmospheric Environment*, *41*(36), 7977–7986. https://doi.org/10.1016/j.atmosenv.2007.09.015
Dreher, K. L., Jaskot, R. H., Lehmann, J. R., Richards, J. H., McGee, J. K., Ghio, A. J., & Costa, D. L. (1997). Soluble transition metals mediate residual oil fly ash-induced acute lung injury. *Journal of Toxicology and Environmental Health*, *50*(3), 285–305. https://doi.org/10.1080/00981097160492
Eiko, N., CAMPAIGN, & EMEP. (2007). Inorganics in air and particle phase at Harwell. https://doi.org/10.48597/GK55-7JGP
Eiko, N., CAMPAIGN, & EMEP. (2007). Nitrate at Harwell. https://doi.org/10.48597/8SVH-X2RC
Eiko, N., CAMPAIGN, & EMEP. (2008). Inorganics in air and particle phase at Auchencorth Moss. https://doi.org/10.48597/BB8C-5EF2
Engelbrecht, J. P., McDonald, E. V., Gillies, J. A., Jayanty, R. K. M., Casuccio, G., & Gertler, A. W. (2009). Characterizing mineral dusts and other aerosols from the Middle East—Part 1: Ambient sampling. *Inhalation Toxicology*, *21*(4), 297–326. https://doi.org/10.1080/08958370802464273
Ferreira, C. A. C., Machado, A. T., Lima, L. R. P. D. A., & Cardoso, R. J. C. (2011). Stabilization of electric-arc furnace dust in concrete. *Materials Research*, *14*(3), 513–519. https://doi.org/10.1590/S1516-14392011000400014
Furu, E., Angyal, A., Szoboszlai, Z., Papp, E., Török, Z., & Kertész, Z. (2022). Characterization of aerosol pollution in two Hungarian cities in winter 2009, 2010. *Atmosphere*, *13*(4), 554. https://doi.org/10.3390/atmos13040554
Furu, E., Katona-Szabo, I., Angyal, A., Szoboszlai, Z., Török, Z., & Kertész, Z. (2015). The effect of the tramway track construction on the aerosol pollution in Debrecen, Hungary. *Nuclear Instruments and Methods in Physics Research Section B: Beam Interactions with Materials and Atoms*, *363*, 124–130. https://doi.org/10.1016/j.nimb.2015.08.014
Fuzzi, S., Decesari, S., Facchini, M. C., Cavalli, F., Emblico, L., Mircea, M., et al. (2007). Overview of the inorganic and organic composition of size-segregated aerosol in Rondonia, Brazil, from the biomass-burning period to the onset of the wet season. *Journal of Geophysical Research*, *112*(D1), D01201. https://doi.org/10.1029/2005jd006741
Gehrig, R., CAMPAIGN, & EMEP. (2007). OC/EC at Payerne. https://doi.org/10.48597/F6WK-E9XB
Gehrig, R., CAMPAIGN, & EMEP. (2009). Sodium at Payerne. https://doi.org/10.48597/ETYT-63PV
Gehrig, R., CAMPAIGN, & EMEP. (2015). Inorganics in air and particle phase at Payerne. https://doi.org/10.48597/Z52G-GY5Z
Gehrig, R., & EMEP. (2009). PM mass at Payerne. https://doi.org/10.48597/63GE-2K4K
Gehrig, R., & EMEP. (2009). PM10_mass at Payerne. https://doi.org/10.48597/63GE-2K4K
Gehrig, R., & EMEP. (2009). PM25_mass at Payerne. https://doi.org/10.48597/6FWT-3VZ5
Gehrig, R., & EMEP. (2012). PM10_mass at Payerne. https://doi.org/10.48597/HNK4-24Z9
Gehrig, R., & EMEP. (2014). PM10_mass at Payerne. https://doi.org/10.48597/63GE-2K4K
Gehrig, R., & EMEP. (2014). PM25_mass at Payerne. https://doi.org/10.48597/6FWT-3VZ5
GEOTRACES Intermediate Data Product Group. (2023). The GEOTRACES Intermediate Data Product 2021 version 2 (IDP2021v2).
Gianini, M. F. D., Fischer, A., Gehrig, R., Ulrich, A., Wichser, A., Piot, C., et al. (2012). Comparative source apportionment of PM_{10} in Switzerland for 2008/2009 and 1998/1999 by Positive Matrix Factorisation. *Atmospheric Environment*, *54*, 149–158. https://doi.org/10.1016/j.atmosenv.2012.02.036
Gianini, M. F. D., Gehrig, R., Fischer, A., Ulrich, A., Wichser, A., & Hueglin, C. (2012). Chemical composition of PM_{10} in Switzerland: An analysis for 2008/2009 and changes since 1998/1999. *Atmospheric Environment*, *54*, 97–106. https://doi.org/10.1016/j.atmosenv.2012.02.037
Gomez, D., & Smichowski, P. (2024). Multielemental profile of PM10 of Buenos Aires, Argentina [Dataset]. *Zenodo*. https://zenodo.org/records/10926019
Gonzalez, A., CAMPAIGN, & EMEP. (2007). PM10_mass at Montseny. https://doi.org/10.48597/KDTJ-VVW7
Gonzalez, A., CAMPAIGN, & EMEP. (2007). PM10_mass at Montseny. https://doi.org/10.48597/8YA7-CQ69
Gonzalez, A., CREATE, EMEP, EUSAAR, & GAW-WDCA. (2007). Inorganics in air and particle phase at Montseny. https://doi.org/10.48597/27FC-BC7B
Gonzalez, A., & EMEP. (2008). Aluminium and inorganics in air and particle phase at Montseny. https://doi.org/10.48597/RMJR-PBBX
Gonzalez, A., & EMEP. (2008). OC/EC and aluminium at Montseny. https://doi.org/10.48597/4QXR-FGFC
Gonzalez, A., & EMEP. (2008). OC/EC, aluminium and inorganics in air and particle phase at Montseny. https://doi.org/10.48597/RMJR-PBBX
Gonzalez, A., & EMEP. (2008). OC/EC at Montseny. https://doi.org/10.48597/QMBY-8CRE

Gonzalez, A., EMEP, EUSAAR, & GAW-WDCA. (2008). Inorganics in air and particle phase at Montseny. https://doi.org/10.48597/97Y3-H69V
Gruening, C., CAMPAIGN, & EMEP. (2008). Inorganics in air and particle phase at Ispra. https://doi.org/10.48597/GB8M-HJPY
Gruening, C., & EMEP. (2007). Elemental_carbon at Ispra. https://doi.org/10.48597/FM4Q-XKPG
Gruening, C., & EMEP. (2007). Organic_carbon at Ispra. https://doi.org/10.48597/SC55-A3YE
Gruening, C., & EMEP. (2008). Inorganics in air and particle phase at Ispra. https://doi.org/10.48597/JPZR-BNK9
Gruening, C., & EMEP. (2010). Ammonium at Ispra. https://doi.org/10.48597/ZJFH-9F5Z
Gruening, C., & EMEP. (2014). Organic_carbon at Ispra. https://doi.org/10.48597/SC55-A3YE
Gruening, C., & EMEP. (2014). Sulphate_total at Ispra. https://doi.org/10.48597/6W6S-GZVB
Hakola, H., AMAP, & EMEP. (2016). PM25_mass at Pallas (Matorova). https://doi.org/10.48597/Z3FP-X7NF
Hakola, H., & EMEP. (2012). PM10_mass at Virolahti II. https://doi.org/10.48597/CGC8-98AP
Hakola, H., & EMEP. (2012). PM25_mass at Uto. https://doi.org/10.48597/PF6R-WYHC
Hakola, H., & EMEP. (2013). Organic_carbon at Uto. https://doi.org/10.48597/3FM8-4SXP
Hakola, H., & EMEP. (2013). Organic_carbon at Virolahti II. https://doi.org/10.48597/K6E4-UH3U
Hakola, H., & EMEP. (2016). PM10_mass at Virolahti II. https://doi.org/10.48597/CGC8-98AP
Hakola, H., & EMEP. (2016). PM25_mass at virolahti II. https://doi.org/10.48597/92MR-ZGJT
Hand, J. L., Gill, T. E., & Schichtel, B. A. (2017). Spatial and seasonal variability in $PM_{2.5}$ mineral dust and PM10-$PM_{2.5}$ aerosol mass at remote sites across the United States. *Journal of Geophysical Research: Atmospheres*, *122*(5), 3080–3097. https://doi.org/10.1002/2016jd026290
Hanssen, J., CAMP, CREATE, EMEP, GAW-WDCA, & NILU. (2004). Ammonium at birkenes. https://doi.org/10.48597/47Y8-Q7GQ
Hanssen, J., CAMPAIGN, EMEP, & NILU. (2014). Inorganics in air and particle phase at Birkenes. https://doi.org/10.48597/323F-J8N3
Hanssen, J., EMEP, & NILU. (2024). PM mass at Birkenes. https://doi.org/10.48597/DYKJ-TNKF
Hansson, H., CAMPAIGN, & EMEP. (2004). OC/EC and PM10_mass at Aspvreten. https://doi.org/10.48597/PZQS-99BP
Harrison, R., EMEP, EUSAAR, & GAW-WDCA. (2009). Nitrate at Harwell. https://doi.org/10.48597/TTDP-7Z4J
Harrison, R., EMEP, EUSAAR, & GAW-WDCA. (2010). Sulphate_total at Harwell. https://doi.org/10.48597/RKYA-RXAS
Harrison, R., EMEP, EUSAAR, & GAW-WDCA. (2012). OC/EC at Harwell. https://doi.org/10.48597/74CC-J55K
Harrison, R., EMEP, EUSAAR, & GAW-WDCA. (2014). OC/EC at Harwell. https://doi.org/10.48597/XQVD-9CZ2
Hellen, H., AMAP, & EMEP. (2020). PM25_mass at Pallas (Matorova). https://doi.org/10.48597/CK8K-R5RJ
Hellen, H., AMAP, & EMEP. (2021). PM25_mass at Pallas (Matorova). https://doi.org/10.48597/CK8K-R5RJ
Hellen, H., AMAP, & EMEP. (2022). PM25_mass at Pallas (Matorova). https://doi.org/10.48597/X3TP-83TT
Hellen, H., AMAP, & EMEP. (2023). PM mass at Pallas (Matorova). https://doi.org/10.48597/NCHF-8P4J
Hellen, H., & EMEP. (2020). PM25_mass at Uto. https://doi.org/10.48597/5MRK-D98F
Hellen, H., & EMEP. (2023). PM mass at Uto. https://doi.org/10.48597/NJFV-P6MR
Hellen, H., & EMEP. (2023). PM25_mass at Uto. https://doi.org/10.48597/V96A-YKXX
Herut, B. (2024). Particulate atmospheric concentrations of trace metals and leachable nutrients in air at the Southeastern Mediterranean Sea (1994–1999) [Dataset]. *Zenodo*. https://zenodo.org/records/11004473
Herut, B., & Krom, M. (1996). Atmospheric input of nutrients and dust to the SE Mediterranean. In S. Guerzoni & R. Chester (Eds.), *The impact of desert dust across the Mediterranean* (pp. 349–360).
Hopke, P. K. (2024). Complete PM compositional data set from Kevo, Finland [Dataset]. *Zenodo*. https://doi.org/10.5281/zenodo.10882915
Hsu, C. Y., Chiang, H. C., Lin, S. L., Chen, M. J., Lin, T. Y., & Chen, Y. C. (2016). Elemental characterization and source apportionment of PM_{10} and $PM_{2.5}$ in the western coastal area of central Taiwan. *Science of the Total Environment*, *541*, 1139–1150. https://doi.org/10.1016/j.scitotenv.2015.09.122
Hueglin, C., ACTRIS, & EMEP. (2023). OC/EC at Payerne. https://doi.org/10.48597/J4TE-JCAE
Hueglin, C., CAMPAIGN, & EMEP. (2009). OC/EC at Payerne. https://doi.org/10.48597/J8WX-R5G6
Hueglin, C., & EMEP. (2012). OC/EC at Payerne. https://doi.org/10.48597/P94N-RVYE
Hueglin, C., & EMEP. (2013). OC/EC and PM25_mass at Payerne. https://doi.org/10.48597/ZJFD-EH72
Hueglin, C., & EMEP. (2013). PM10_mass at Payerne. https://doi.org/10.48597/FWVZ-5DNK
Hueglin, C., & EMEP. (2015). OC/EC and PM25_mass at Payerne. https://doi.org/10.48597/RVKY-VFF5
Hueglin, C., & EMEP. (2015). PM10_mass at Payerne. https://doi.org/10.48597/VSK5-C2U3
Hueglin, C., & EMEP. (2023). OC/EC at Payerne. https://doi.org/10.48597/J4TE-JCAE
Hueglin, C., & EMEP. (2023). OC/EC and PM25_mass at Payerne. https://doi.org/10.48597/RVKY-VFF5
Hueglin, C., & EMEP. (2023). PM10_mass at Payerne. https://doi.org/10.48597/VSK5-C2U3
Hueglin, C., & EMEP. (2023). PM25_mass at Payerne. https://doi.org/10.48597/YV3Q-GQJJ
Hueglin, C., Gehrig, R., Baltensperger, U., Gysel, M., Monn, C., & Vonmont, H. (2005). Chemical characterisation of $PM_{2.5}$, PM_{10} and coarse particles at urban, near-city and rural sites in Switzerland. *Atmospheric Environment*, *39*(4), 637–651. https://doi.org/10.1016/j.atmosenv.2004.10.027
Huggins, F. E., & Dunmyre, G. R. (1981). Investigation of the high-temperature behavior of coal ash in reducing and oxidizing atmospheres. *Fuel*, *60*(7), 585–597. https://doi.org/10.1016/0016-2361(81)90158-7
Jaffrezo, J., Conil, S., Elazzouzi, R., ACTRIS, EMEP, & GAW-WDCA. (2022). OC/EC at Observatoire Perenne de l'Environnement. https://doi.org/10.48597/77QC-RW4Q
Jaffrezo, J., Conil, S., Elazzouzi, R., ACTRIS, EMEP, & GAW-WDCA. (2022). OC/EC at Observatoire Perenne de l'Environnement. https://doi.org/10.48597/N5XS-K2TD
Jaffrezo, J., Conil, S., Vella, A., ACTRIS, EMEP, & GAW-WDCA. (2021). OC/EC at Observatoire Perenne de l'Environnement. https://doi.org/10.48597/3NWK-K6S4
Jaffrezo, J., Conil, S., Vella, A., ACTRIS, EMEP, & GAW-WDCA. (2021). OC/EC at Observatoire Perenne de l'Environnement. https://doi.org/10.48597/597D-98KD
Jaffrezo, J., Conil, S., Vella, A., ACTRIS, EMEP, & GAW-WDCA. (2021). OC/EC at Observatoire Perenne de l'Environnement. https://doi.org/10.48597/A6N3-Y8EA
Jaffrezo, J., Conil, S., Vella, A., ACTRIS, EMEP, & GAW-WDCA. (2021). OC/EC at Observatoire Perenne de l'Environnement. https://doi.org/10.48597/HWQ3-8WE4
Jaffrezo, J., Conil, S., Vella, A., ACTRIS, EMEP, & GAW-WDCA. (2021). OC/EC at Observatoire Perenne de l'Environnement. https://doi.org/10.48597/MKN2-JF5R
Jaffrezo, J., Conil, S., Vella, A., ACTRIS, EMEP, & GAW-WDCA. (2021). OC/EC at Observatoire Perenne de l'Environnement. https://doi.org/10.48597/U632-CZ2G

Jickells, T. D., Baker, A. R., & Chance, R. (2016). Atmospheric transport of trace elements and nutrients to the oceans. *Philosophical Transactions of the Royal Society A: Mathematical, Physical and Engineering Sciences*, *374*(2081), 20150286. https://doi.org/10.1098/rsta.2015.0286
Johansen, A., & Hoffmann, M. (2003). Chemical characterization of ambient aerosol collected during the northeast monsoon season over the Arabian Sea: Labile-Fe(II) and other trace metals. *Journal of Geophysical Research*, *108*(D14), 408. https://doi.org/10.1029/2002jd003280
Johansen, A. M., Siefert, R. L., & Hoffmann, M. R. (2000). Chemical composition of aerosols collected over the tropical North Atlantic Ocean. *Journal of Geophysical Research*, *105*(D12), 15277–15312. https://doi.org/10.1029/2000jd900024
Kertész, Z., Aljboor, S., Angyal, A., Papp, E., Furu, E., Szarka, M., et al. (2024). Characterization of urban aerosol pollution before and during the COVID-19 crisis in a central-eastern European urban environment. *Atmospheric Environment*, *318*, 120267. https://doi.org/10.1016/j.atmosenv.2023.120267
Kido, K., & Nishimura, M. (1975). *Silica in the sea-its forms and dissolution rate* (pp. 323–338). Pergamon Press.
Kleanthous, S., & EMEP. (2008). PM10_mass at Agia Marina Xyliatou/Cyprus Atmospheric Observatory. https://doi.org/10.48597/A32B-WNTR
Kleanthous, S., & EMEP. (2008). PM25_mass at Agia Marina Xyliatou/Cyprus Atmospheric Observatory. https://doi.org/10.48597/K58S-B9SZ
Kleanthous, S., & EMEP. (2012). OC/EC and inorganics in air and particle phase at Agia Marina Xyliatou/Cyprus Atmospheric Observatory. https://doi.org/10.48597/P25Y-E8H2
Kleanthous, S., & EMEP. (2013). OC/EC and inorganics in air and particle phase at Agia Marina Xyliatou/Cyprus Atmospheric Observatory. https://doi.org/10.48597/P25Y-E8H2
Kleanthous, S., & EMEP. (2015). OC/EC and inorganics in air and particle phase at Agia Marina Xyliatou/Cyprus Atmospheric Observatory. https://doi.org/10.48597/H4F9-6D76
Kleanthous, S., & EMEP. (2016). Aluminium at Agia Marina Xyliatou/Cyprus Atmospheric Observatory. https://doi.org/10.48597/RK6J-F7DB
Kleanthous, S., & EMEP. (2017). Aluminium at Agia Marina Xyliatou/Cyprus Atmospheric Observatory. https://doi.org/10.48597/FBCK-8B3D
Kleanthous, S., & EMEP. (2017). Aluminium at Agia Marina Xyliatou/Cyprus Atmospheric Observatory. https://doi.org/10.48597/RK6J-F7DB
Kleanthous, S., & EMEP. (2018). Ammonium at Agia Marina Xyliatou/Cyprus Atmospheric Observatory. https://doi.org/10.48597/CYCA-H6UX
Kleanthous, S., & EMEP. (2018). Aluminium at Agia Marina Xyliatou/Cyprus Atmospheric Observatory. https://doi.org/10.48597/HVSC-5TJP
Kleanthous, S., & EMEP. (2018). Aluminium at Agia Marina Xyliatou/Cyprus Atmospheric Observatory. https://doi.org/10.48597/RK6J-F7DB
Kleanthous, S., & EMEP. (2018). Inorganics in air and particle phase at Agia Marina Xyliatou/Cyprus Atmospheric Observatory. https://doi.org/10.48597/4RG4-97YH
Kleanthous, S., & EMEP. (2018). Inorganics in air and particle phase at Agia Marina Xyliatou/Cyprus Atmospheric Observatory. https://doi.org/10.48597/S7DS-GG2N
Kleanthous, S., & EMEP. (2018). PM10_mass at Agia Marina Xyliatou/Cyprus Atmospheric Observatory. https://doi.org/10.48597/DWN4-T22
Kolesa, T., & EMEP. (2010). Aluminium at Iskrba. https://doi.org/10.48597/A4PZ-GEF3
Kolesa, T., & EMEP. (2011). Aluminium at Iskrba. https://doi.org/10.48597/P43T-3WNG
Kolesa, T., & EMEP. (2011). Aluminium at Iskrba. https://doi.org/10.48597/TQJR-2VTS
Kolesa, T., & EMEP. (2014). Aluminium at Iskrba. https://doi.org/10.48597/A4PZ-GEF3
Kolesa, T., & EMEP. (2014). OC/EC at Iskrba. https://doi.org/10.48597/5CMN-EMPA
Kolesa, T., & EMEP. (2017). OC/EC at Iskrba. https://doi.org/10.48597/QRUZ-AW9N
Kolesa, T., Kranjc, I., & EMEP. (2017). PM mass at Iskrba. https://doi.org/10.48597/FGC4-MH9K
Kolesa, T., Kranjc, I., & EMEP. (2017). PM10_mass at Iskrba. https://doi.org/10.48597/G5Q7-TDZR
Kolesa, T., Kranjc, I., & EMEP. (2018). PM10_mass at Iskrba. https://doi.org/10.48597/G5Q7-TDZR
Kolesa, T., Kranjc, I., & EMEP. (2018). PM25_mass at Iskrba. https://doi.org/10.48597/YM4V-M4FG
Kolesa, T., Kranjc, I., & EMEP. (2019). Inorganics in air and particle phase at Iskrba. https://doi.org/10.48597/HDJE-R459
Kolesa, T., Kranjc, I., & EMEP. (2019). Inorganics in air and particle phase at Iskrba. https://doi.org/10.48597/TDE3-9G63
Kolesa, T., Kranjc, I., & EMEP. (2019). PM10_mass at Iskrba. https://doi.org/10.48597/G5Q7-TDZR
Kolesa, T., Kranjc, I., & EMEP. (2019). PM25_mass at Iskrba. https://doi.org/10.48597/YM4V-M4FG
Kolesa, T., Kranjc, I., & EMEP. (2020). Inorganics in air and particle phase at Iskrba. https://doi.org/10.48597/TDE3-9G63
Kolesa, T., Kranjc, I., & EMEP. (2020). OC/EC at Iskrba. https://doi.org/10.48597/TQMP-Y3CQ
Kolesa, T., Kranjc, I., & EMEP. (2020). PM10_mass at Iskrba. https://doi.org/10.48597/G5Q7-TDZR
Kolesa, T., Kranjc, I., & EMEP. (2020). PM25_mass at Iskrba.
Kolesa, T., Kranjc, I., & EMEP. (2021). Inorganics in air and particle phase at Iskrba. https://doi.org/10.48597/HDJE-R459
Kolesa, T., Kranjc, I., & EMEP. (2021). OC/EC at Iskrba. https://doi.org/10.48597/58C7-DKYF
Kolesa, T., Kranjc, I., & EMEP. (2021). OC/EC at Iskrba. https://doi.org/10.48597/QRUZ-AW9N
Kolesa, T., Kranjc, I., & EMEP. (2021). OC/EC at Iskrba. https://doi.org/10.48597/TQMP-Y3CQ
Kolesa, T., Kranjc, I., & EMEP. (2023). Inorganics in air and particle phase at Iskrba. https://doi.org/10.48597/TDE3-9G63
Kolesa, T., Kranjc, I., & EMEP. (2023). OC/EC at Iskrba. https://doi.org/10.48597/3JJU-Q7D3
Kolesa, T., Kranjc, I., & EMEP. (2023). PM10_mass at Iskrba. https://doi.org/10.48597/G5Q7-TDZR
Kolesa, T., Kranjc, I., & EMEP. (2023). PM25_mass at Iskrba. https://doi.org/10.48597/YM4V-M4FG
Kolesa, T., Kranjc, I., & EMEP. (2024). Inorganics in air and particle phase at Iskrba. https://doi.org/10.48597/TDE3-9G63
Kranjc, I., Kolesa, T., & EMEP. (2019). PM25_mass at Iskrba. https://doi.org/10.48597/YM4V-M4FG
Kranjc, I., Kolesa, T., & EMEP. (2021). OC/EC at Iskrba. https://doi.org/10.48597/QRUZ-AW9N
Krognes, T., EMEP, & NILU. (2000). PM10_mass at Birkenes. https://doi.org/10.48597/BKNJ-AXFH
Krognes, T., EMEP, & NILU. (2014). PM10_mass at Birkenes. https://doi.org/10.48597/BKNJ-AXFH
Kubilay, N., Nickovic, S., Moulin, C., & Dulac, F. (2000). An illustration of the transport and deposition of mineral dust onto the eastern Mediterranean. *Atmospheric Environment*, *34*(8), 1293–1303. https://doi.org/10.1016/s1352-2310(99)00179-x
Kulmala, M., EMEP, EUSAAR, & GAW-WDCA. (2012). PM mass at Hyytiala. https://doi.org/10.48597/WK4E-86CP
Kulmala, M., Petaja, T., EMEP, & GAW-WDCA. (2017). PM mass at Hyytiala. https://doi.org/10.48597/ZKK3-ZBCF
Kulmala, M., Petaja, T., & GAW-WDCA. (2023). PM10_mass at Hyytiala. https://doi.org/10.48597/XCMY-8P6J
Kulmala, M., Petaja, T., Virkkula, A., Luoma, K., ACTRIS, CAMPAIGN, et al. (2021). OC/EC at hyytiala. https://doi.org/10.48597/45DE-MZNZ
Kyllönen, K., AMAP, & EMEP. (2013). Aluminium at Pallas (Matorova). https://doi.org/10.48597/42NT-7AJG
Kyllönen, K., & EMEP. (2013). Aluminium at Ahtari II. https://doi.org/10.48597/E2AN-MPCC
Kyllönen, K., EMEP, & HELCOM. (2012). Aluminium at Virolahti II. https://doi.org/10.48597/KA4S-56QT

Kyllönen, K., Vestenius, M., Anttila, P., Makkonen, U., Aurela, M., Waengberg, I., et al. (2020). Trends and source apportionment of atmospheric heavy metals at a subarctic site during 1996–2018. *Atmospheric Environment*, *236*, 117644. https://doi.org/10.1016/j.atmosenv.2020.117644

Laing, J. R., Hopke, P. K., Hopke, E. F., Husain, L., Dutkiewicz, V. A., Paatero, J., & Viisanen, Y. (2014). Long-term particle measurements in Finnish Arctic: Part I, Chemical composition and trace metal solubility. *Atmospheric Environment*, *88*, 275–284. https://doi.org/10.1016/j.atmosenv.2014.03.002

Laing, J. R., Hopke, P. K., Hopke, E. F., Husain, L., Dutkiewicz, V. A., Paatero, J., & Viisanen, Y. (2014). Long-term particle measurements in Finnish Arctic: Part II, Trend analysis and source location identification. *Atmospheric Environment*, *88*, 285–296. https://doi.org/10.1016/j.atmosenv.2014.01.015

Losno, R., Bergametti, G., & Carlier, P. (1992). Origins of atmospheric particulate matter over the North Sea and the Atlantic Ocean. *Journal of Atmospheric Chemistry*, *15*(3–4), 333–352. https://doi.org/10.1007/bf00115403

Lucarelli, F., Barrera, V., Becagli, S., Chiari, M., Giannoni, M., Nava, S., et al. (2019). Combined use of daily and hourly data sets for the source apportionment of particulate matter near a waste incinerator plant. *Environmental Pollution*, *247*, 802–811. https://doi.org/10.1016/j.envpol.2018.11.107

Lungu, M., & EMEP. (2019). PM10_mass at Leova II. https://doi.org/10.48597/MJHN-GEY2

Lungu, M., & EMEP. (2020). PM10_mass at Leova II. https://doi.org/10.48597/MJHN-GEY2

Lungu, M., & EMEP. (2023). PM10_mass at Leova II. https://doi.org/10.48597/4WZZ-YCUA

Lyu, S., Wei, X., Chen, J., Wang, C., Wang, X., & Pan, D. (2017). Titanium as a beneficial element for crop production. *Frontiers in Plant Science*, *8*, 597. https://doi.org/10.3389/fpls.2017.00597

Machado, J., Brehm, F., Moraes, C., Santos, R. C., Vilela, A. C. F., & da Cunha, C. (2006). Chemical, physical, structural and morphological characterization of the electric arc furnace dust. *Journal of Hazardous Materials*, *136*(3), 953–960. https://doi.org/10.1016/j.jhazmat.2006.01.044

Mackey, K. R. M., Hunter, D., Fischer, E. V., Jiang, Y., Allen, B., Chen, Y., et al. (2013). Aerosol-nutrient-induced picoplankton growth in Lake Tahoe. *Journal of Geophysical Research: Biogeosciences*, *118*(3), 1054–1067. https://doi.org/10.1002/jgrg.20084

Maenhaut, W., & Cafmeyer, J. (1998). Long-term atmospheric aerosol study at urban and rural sites in Belgium using multi-elemental analysis by particle-induced X-ray emission spectrometry and short-irradiation instrumental neutron activation analysis. *X-Ray Spectrometry*, *27*(4), 236–246. https://doi.org/10.1002/(sici)1097-4539(199807/08)27:4<236::aid-xrs292>3.0.co;2-f

Maenhaut, W., Cafmeyer, J., Ptasinski, J., Andreae, M. O., Andreae, T. W., Elbert, W., et al. (1997). Chemical composition and light scattering of the atmospheric aerosol at a remote site in the Negev desert, Israel. *Journal of Aerosol Science*, *28*(Suppl. 1), S73–S74. https://doi.org/10.1016/s0021-8502(97)85037-9

Maenhaut, W., De Ridder, D. J., Fernandez-Jimenez, M. T., Hooper, M. A., Hooper, B., & Nurhayati, M. (2002). Long-term observations of regional aerosol composition at two sites in Indonesia. *Nuclear Instruments and Methods in Physics Research Section B: Beam Interactions with Materials and Atoms*, *189*(1–4), 259–265. https://doi.org/10.1016/s0168-583x(01)01054-0

Maenhaut, W., Fernandez-Jimenez, M. T., & Artaxo, P. (1999). Long-term study of atmospheric aerosols in Cuiabo, Brazil: Multielemental composition, sources and source apportionment. *Journal of Aerosol Science*, *30*, S259–S260. https://doi.org/10.1016/s0021-8502(99)80141-4

Maenhaut, W., Fernandez-Jimenez, M. T., Rajta, I., Dubtsov, S., Meixner, F. X., Andreae, M., et al. (2000). Long-term aerosol composition measurements and source apportionment at Rukomechi, Zimbabwe. *Journal of Aerosol Science*, *31*(Suppl. 1), S228–S229. https://doi.org/10.1016/s0021-8502(00)90237-4

Maenhaut, W., Francois, F., Cafmeyer, J., Gilot, C., & Hanssen, J. (1997). Long-term aerosol study in southern Norway, and the relationship of aerosol components to source regions. In *EUROTRAC Symposium 96: Transport and transformation of pollutants in the troposphere* (pp. 277–280). Computational Mechanics.

Maenhaut, W., Koppen, G., & Artaxo, P. (1996). Long-term atmospheric aerosol study in Cuiaba, Brazil: Multielemental composition, sources, and impact of biomass burning. *Biomass Burning and Global Change*, *2*, 637–652.

Maenhaut, W., Raes, N., Chi, X., Cafmeyer, J., & Wang, W. (2008). Chemical composition and mass closure for $PM_{2.5}$ and PM_{10} aerosols at K-puszta, Hungary, in summer 2006. *X-Ray Spectrometry*, *37*(2), 193–197. https://doi.org/10.1002/xrs.1062

Maenhaut, W., Raes, N., Chi, X., Cafmeyer, J., Wang, W., & Salma, I. (2005). Chemical composition and mass closure for fine and coarse aerosols at a kerbside in Budapest, Hungary, in spring 2002. *X-Ray Spectrometry*, *34*(4), 290–296. https://doi.org/10.1002/xrs.820

Maenhaut, W., Salma, I., Cafmeyer, J., Annegarn, H. J., & Andreae, M. O. (1996). Regional atmospheric aerosol composition and sources in the eastern Transvaal, South Africa, and impact of biomass burning. *Journal of Geophysical Research*, *101*(D19), 23631–23650. https://doi.org/10.1029/95jd02930

Maenhaut, W., Salomonovic, R., Cafmeyer, J., Ichoku, C., Karnieli, A., & Andreae, M. O. (1996). Anthropogenic and natural radiatively active aerosol types at Sede Boker, Israel. *Journal of Aerosol Science*, *27*(Suppl. 1), S47–S48. https://doi.org/10.1016/0021-8502(96)00096-1

Makkonen, U., AMAP, & EMEP. (2015). Aluminium at Pallas (Matorova). https://doi.org/10.48597/AAF3-U34J

Makkonen, U., AMAP, & EMEP. (2019). Aluminium at Pallas (Matorova). https://doi.org/10.48597/XDM4-YJ7E

Makkonen, U., AMAP, & EMEP. (2020). Aluminium at Pallas (Matorova). https://doi.org/10.48597/5BHQ-KFX8

Makkonen, U., AMAP, & EMEP. (2021). Aluminium at Pallas (Matorova). https://doi.org/10.48597/5BHQ-KFX8

Makkonen, U., & EMEP. (2013). Inorganics in air and particle phase at Uto. https://doi.org/10.48597/AEDE-DCAJ

Makkonen, U., & EMEP. (2013). Inorganics in air and particle phase at Uto. https://doi.org/10.48597/KFMD-MGR5

Makkonen, U., & EMEP. (2013). Inorganics in air and particle phase at Virolahti II. https://doi.org/10.48597/MHT7-PUZC

Makkonen, U., & EMEP. (2013). Inorganics in air and particle phase at Virolahti II. https://doi.org/10.48597/ZCF4-WCCR

Makkonen, U., & EMEP. (2013). Inorganics in air and particle phase at Pallas (Matorova). https://doi.org/10.48597/5ZEK-ZRY4

Makkonen, U., & EMEP. (2013). Inorganics in air and particle phase at Pallas (Matorova). https://doi.org/10.48597/NM3J-XX7R

Makkonen, U., & EMEP. (2015). Aluminium at Ahtari II. https://doi.org/10.48597/7BEP-GZD4

Makkonen, U., & EMEP. (2015). Aluminium at Virolahti II. https://doi.org/10.48597/AFYH-ERAQ

Makkonen, U., & EMEP. (2021). Aluminium at Hyytiala. https://doi.org/10.48597/D4V8-EFK7

Mamane, Y., Miller, J. L., & Dzubay, T. G. (1987). Characterization of individual fly ash particles from coal- and oil-fired power plants. *Atmospheric Environment*, *21*(12), 2737–2749. https://doi.org/10.1016/0004-6981(87)90211-3

Marconi, M., Sferlazzo, D. M., Becagli, S., Bommarito, C., Calzolai, G., Chiari, M., et al. (2014). Saharan dust aerosol over the central Mediterranean Sea: PM_{10} chemical composition and concentration versus optical columnar measurements. *Atmospheric Chemistry and Physics*, *14*(4), 2039–2054. https://doi.org/10.5194/acp-14-2039-2014

Marsay, C. M., Kadko, D., Landing, W. M., & Buck, C. S. (2022). Bulk aerosol trace element concentrations and deposition fluxes during the U.S. GEOTRACES GP15 Pacific Meridional Transect. *Global Biogeochemical Cycles*, *36*(2), e2021GB007122. https://doi.org/10.1029/2021GB007122

Marsay, C. M., Kadko, D., Landing, W. M., Morton, P. L., Summers, B. A., & Buck, C. S. (2018). Concentrations, provenance and flux of aerosol trace elements during US GEOTRACES Western Arctic cruise GN01. *Chemical Geology*, *502*, 1–14. https://doi.org/10.1016/j.chemgeo.2018.06.007

Martinez-Tarazona, M. R., & Spears, D. A. (1996). The fate of trace elements and bulk minerals in pulverized coal combustion in a power station. *Fuel Processing Technology*, *47*(1), 79–92. https://doi.org/10.1016/0378-3820(96)01001-6

Martins Dos Santos, S., & EMEP. (2023). PM25_mass at Ispra. https://doi.org/10.48597/TUVA-W8RZ

McGhee, E., CAMPAIGN, & EMEP. (2022). OC/EC at Auchencorth Moss. https://doi.org/10.48597/267N-USEU

McGhee, E., CAMPAIGN, & EMEP. (2022). OC/EC at Chilbolton Observatory. https://doi.org/10.48597/N47M-HAQP

McNeill, J., Snider, G., Weagle, C. L., Walsh, B., Bissonnette, P., Stone, E., et al. (2020). Large global variations in measured airborne metal concentrations driven by anthropogenic sources. *Scientific Reports*, *10*(1), 21817. https://doi.org/10.1038/s41598-020-78789-y

Menut, L., Siour, G., Bessagnet, B., Couvidat, F., Journet, E., Balkanski, Y., & Desboeufs, K. (2020). Modelling the mineralogical composition and solubility of mineral dust in the Mediterranean area with CHIMERE 2017r4. *Geoscientific Model Development*, *13*(4), 2051–2071. https://doi.org/10.5194/gmd-13-2051-2020

Mihalopoulos, N., Kouvarakis, G., AMAP, EUSAAR, & GAW-WDCA. (2010). PM10_mass at Finokalia. https://doi.org/10.48597/JX65-9QB8

Mihalopoulos, N., Kouvarakis, G., Kalivitis, N., ACTRIS, EMEP, & GAW-WDCA. (2015). Equivalent_black_carbon at Finokalia. https://doi.org/10.48597/AGY9-QWTB

Mihalopoulos, N., Kouvarakis, G., Kalivitis, N., ACTRIS, EMEP, & GAW-WDCA. (2017). Equivalent_black_carbon at Finokalia. https://doi.org/10.48597/3237-HVFZ

Mihalopoulos, N., Kouvarakis, G., Kalivitis, N., & GAW-WDCA. (2013). PM10_mass at Finokalia. https://doi.org/10.48597/Z66M-9GD7

Mihalopoulos, N., Kouvarakis, G., Theodosi, C., ACTRIS, EMEP, & GAW-WDCA. (2015). OC/EC at Finokalia. https://doi.org/10.48597/STDG-8XZP

Mihalopoulos, N., Theodosi, C., Kouvarakis, G., ACTRIS, EMEP, & GAW-WDCA. (2016). OC/EC at Finokalia. https://doi.org/10.48597/AHTY-W5R7

Mihalopoulos, N., Tsagaraki, M., Kouvarakis, G., ACTRIS, CAMPAIGN, COLOSSAL, & GAW-WDCA. (2019). OC/EC at Finokalia. https://doi.org/10.48597/AHTY-W5R7

Minarikova, V., & EMEP. (2021). PM10_mass at Starina. https://doi.org/10.48597/9Q25-H98X

Mirante, F., Alves, C., Pio, C., Pindado, O., Perez, R., Revuelta, M. A., & Artiñano, B. (2013). Organic composition of size segregated atmospheric particulate matter, during summer and winter sampling campaigns at representative sites in Madrid, Spain. *Atmospheric Research*, *132–133*, 345–361. https://doi.org/10.1016/j.atmosres.2013.07.005

Mitosinkova, M., & EMEP. (2008). PM10_mass at Starina. https://doi.org/10.48597/E4AS-N3G9

Mitosinkova, M., & EMEP. (2016). PM10_mass at Starina. https://doi.org/10.48597/5EEA-5DG3

Mitosinkova, M., & EMEP. (2016). PM10_mass at Starina. https://doi.org/10.48597/E4AS-N3G9

Mitosinkova, M., & EMEP. (2017). PM10_mass at Starina. https://doi.org/10.48597/SY9N-3RB4

Mkoma, S. L. (2008). *Physico-chemical characterisation of atmospheric aerosols in Tanzania, with emphasis on the carbonaceous aerosol components and on chemical mass closure*. Ph.D. Thesis (p. 162). Ghent University.

Mkoma, S. L., Maenhaut, W., Chi, X., Wang, W., & Raes, N. (2009). Characterisation of PM_{10} atmospheric aerosols for the wet season 2005 at two sites in East Africa. *Atmospheric Environment*, *43*(3), 631–639. https://doi.org/10.1016/j.atmosenv.2008.10.008

Morera-Gómez, Y., Elustondo, D., Lasheras, E., Alonso-Hernández, C. M., & Santamaría, J. M. (2018). Chemical characterization of PM10 samples collected simultaneously at a rural and an urban site in the Caribbean coast: Local and long-range source apportionment. *Atmospheric Environment*, *192*, 182–192. https://doi.org/10.1016/j.atmosenv.2018.08.058

Mueller, K., & EMEP. (2014). Equivalent_black_carbon at Melpitz. https://doi.org/10.48597/9X5B-KR3N

Mueller, K., & GAW-WDCA. (2018). Inorganics in air and particle phase at Melpitz. https://doi.org/10.48597/VPEK-MKEF

Nava, S., Calzolai, G., Chiari, M., Giannoni, M., Giardi, F., Becagli, S., et al. (2020). Source apportionment of $PM_{2.5}$ in Florence (Italy) by PMF analysis of aerosol composition records. *Atmosphere*, *11*(5), 484. https://doi.org/10.3390/atmos11050484

Nava, S., Lucarelli, F., Amato, F., Becagli, S., Calzolai, G., Chiari, M., et al. (2015). Biomass burning contributions estimated by synergistic coupling of daily and hourly aerosol composition records. *Science of the Total Environment*, *511*, 11–20. https://doi.org/10.1016/j.scitotenv.2014.11.034

Nyanganyura, D., Maenhaut, W., Mathuthu, M., Makarau, A., & Meixner, F. X. (2007). The chemical composition of tropospheric aerosols and their contributing sources to a continental background site in northern Zimbabwe from 1994 to 2000. *Atmospheric Environment*, *41*(12), 2644–2659. https://doi.org/10.1016/j.atmosenv.2006.11.015

O'Dowd, C., Ceburnis, D., & GAW-WDCA. (2023). PM mass at Mace Head. https://doi.org/10.48597/7XDZ-XKK9

O'Dowd, C., Ceburnis, D., & GAW-WDCA. (2023). PM25_mass at Mace Head. https://doi.org/10.48597/5FAR-4R97

Oliveira, C., & PAHLIS Team. (2009). Atmospheric pollution in Lisbon urban atmosphere. In *European Geosciences Union General Assembly, 19–24 April, Vienna, Austria*.

Ostrowska, A., & Porębska, G. (2017). The content of calcium and magnesium and the Ca:Mg ratio in cultivated plants in the context of human and animal demand for nutrients. *Journal of Elementology*, *22*(3/2017), 995–1004. https://doi.org/10.5601/jelem.2016.21.4.1246

Ouafo-Leumbe, M.-R., Galy-Lacaux, C., Liousse, C., Pont, V., Akpo, A., Doumbia, T., et al. (2018). Chemical composition and sources of atmospheric aerosols at Djougou (Benin). *Meteorology and Atmospheric Physics*, *130*(5), 591–609. https://doi.org/10.1007/s00703-017-0538-5

Paul, W., & EMEP. (2015). PM mass at Harwell. https://doi.org/10.48597/5XWE-N7CA

Paul, W., & EMEP. (2015). PM mass at Harwell. https://doi.org/10.48597/X8V4-MAZV

Paul, W., & EMEP. (2016). PM mass at Harwell. https://doi.org/10.48597/5XWE-N7CA

Paul, W., & EMEP. (2016). PM mass at Harwell. https://doi.org/10.48597/X8V4-MAZV

Paul, W., & EMEP. (2017). PM mass at Chilbolton Observatory. https://doi.org/10.48597/AUQF-4ZQA

Paul, W., & EMEP. (2023). PM mass at Chilbolton Observatory. https://doi.org/10.48597/DDF6-D6SR

Pedroni, V., & EMEP. (2023). PM25_mass at Ispra. https://doi.org/10.48597/X37R-JBYN

Pedroni, V., Martins Dos Santos, S., & EMEP. (2023). PM25_mass at Ispra. https://doi.org/10.48597/TUVA-W8RZ

Pedroni, V., Martins Dos Santos, S., & EMEP. (2023). PM25_mass at Ispra. https://doi.org/10.48597/X37R-JBYN

Perez, N., Alastuey, A., ACTRIS, & EMEP. (2015). Aluminium and inorganics in air and particle phase at Montseny. https://doi.org/10.48597/JYYP-PUJT

Perez, N., Alastuey, A., ACTRIS, & EMEP. (2015). Aluminium and inorganics in air and particle phase at Montseny. https://doi.org/10.48597/XHT4-C8NV

Perez, N., Alastuey, A., ACTRIS, EMEP, & GAW-WDCA. (2021). Aluminium and inorganics in air and particle phase at Montseny. https://doi.org/10.48597/4KEY-TWBM
Perez, N., Alastuey, A., ACTRIS, EMEP, & GAW-WDCA. (2021). Aluminium and inorganics in air and particle phase at Montseny. https://doi.org/10.48597/GHW4-977V
Perez, N., Alastuey, A., ACTRIS, EMEP, & GAW-WDCA. (2021). Aluminium and inorganics in air and particle phase at Montseny. https://doi.org/10.48597/T5QK-MV5M
Perez, N., Alastuey, A., ACTRIS, EMEP, & GAW-WDCA. (2021). Aluminium and inorganics in air and particle phase at Montseny. https://doi.org/10.48597/XKAP-FB34
Perez, N., Alastuey, A., ACTRIS, EMEP, & GAW-WDCA. (2022). Aluminium and inorganics in air and particle phase at Montseny. https://doi.org/10.48597/UWR3-UDDG
Perez, N., Alastuey, A., ACTRIS, EMEP, & GAW-WDCA. (2022). Aluminium and inorganics in air and particle phase at Montseny. https://doi.org/10.48597/YHGD-YGMT
Perez, N., Alastuey, A., ACTRIS, EMEP, & GAW-WDCA. (2023). Aluminium and inorganics in air and particle phase at Montseny. https://doi.org/10.48597/UWR3-UDDG
Perez, N., Alastuey, A., ACTRIS, EMEP, & GAW-WDCA. (2023). Aluminium and inorganics in air and particle phase at Montseny. https://doi.org/10.48597/YHGD-YGMT
Perez, N., Alastuey, A., & EMEP. (2014). PM25_mass at Montseny. https://doi.org/10.48597/KASD-BMQV
Perez, N., Alastuey, A., & EMEP. (2014). PM10_mass at Montseny. https://doi.org/10.48597/UBW2-UHTM
Perez, N., Alastuey, A., & EMEP. (2021). PM10_mass at Montseny. https://doi.org/10.48597/B8H7-SJMR
Perez, N., Alastuey, A., & EMEP. (2021). PM25_mass at Montseny. https://doi.org/10.48597/R8BV-EVJJ
Perez, N., & EMEP. (2012). Aluminium at Montseny. https://doi.org/10.48597/4GX6-ZV9F
Perez, N., & EMEP. (2012). Aluminium at Montseny. https://doi.org/10.48597/RRQP-MCJJ
Perez, N., & EMEP. (2012). Inorganics in air and particle phase at Montseny. https://doi.org/10.48597/3XUW-KFBA
Perez, N., & EMEP. (2012). Inorganics in air and particle phase at Montseny. https://doi.org/10.48597/6YQB-2MEN
Perez, N., & EMEP. (2013). Aluminium and inorganics in air and particle phase at Montseny. https://doi.org/10.48597/2TTG-DXVD
Perez, N., & EMEP. (2013). Aluminium and inorganics in air and particle phase at Montseny. https://doi.org/10.48597/Y99M-J8K9
Perez, N., & EMEP. (2014). Inorganics in air and particle phase at Montseny. https://doi.org/10.48597/TQBT-3WGJ
Perez, N., & EMEP. (2014). Inorganics in air and particle phase at Montseny. https://doi.org/10.48597/VAWC-SARQ
Perez, N., Pey, J., Querol, X., Alastuey, A., Lopez, J. M., & Viana, M. (2008). Partitioning of major and trace components in PM_{10}, $PM_{2.5}$, PM_1 at an urban site in Southern Europe. *Atmospheric Environment*, *42*(8), 1677–1691. https://doi.org/10.1016/j.atmosenv.2007.11.034
Perrino, C., CAMPAIGN, & EMEP. (2007). Aluminium and inorganics in air and particle phase at Montelibretti. https://doi.org/10.48597/H223-WFQE
Perrino, C., CAMPAIGN, & EMEP. (2007). Aluminium at Montelibretti. https://doi.org/10.48597/E5TP-PNQK
Perrino, C., CAMPAIGN, & EMEP. (2007). Ammonium at Montelibretti. https://doi.org/10.48597/ASHJ-BSWX
Perrino, C., CAMPAIGN, & EMEP. (2007). Inorganics in air and particle phase at Montelibretti. https://doi.org/10.48597/6BDY-Q342
Perrino, C., CAMPAIGN, & EMEP. (2007). Inorganics in air and particle phase at Montelibretti. https://doi.org/10.48597/W67T-KUF6
Perrino, C., CAMPAIGN, & EMEP. (2007). OC/EC, aluminium and sodium at Montelibretti. https://doi.org/10.48597/GYJH-629M
Perrino, C., CAMPAIGN, & EMEP. (2007). OC/EC and inorganics in air and particle phase at Montelibretti. https://doi.org/10.48597/894S-ZEFR
Perrino, C., CAMPAIGN, & EMEP. (2009). OC/EC at Montelibretti. https://doi.org/10.48597/PNAD-M9HK
Perrino, C., CAMPAIGN, & EMEP. (2014). Sodium at Ispra. https://doi.org/10.48597/WF9F-G6VB
Perrino, C., & EMEP. (2003). PM10_mass at Montelibretti. https://doi.org/10.48597/3FWF-GQVS
Perrino, C., & EMEP. (2003). Sulphate_total at Montelibretti. https://doi.org/10.48597/DQ2B-FCH6
Perrino, C., & EMEP. (2006). PM10_mass at Montelibretti. https://doi.org/10.48597/THQB-2GNS
Perrino, C., & EMEP. (2007). Inorganics in air and particle phase at Montelibretti. https://doi.org/10.48597/44SM-2Z3Q
Perrino, C., & EMEP. (2007). Inorganics in air and particle phase at Montelibretti. https://doi.org/10.48597/JSAW-KPJN
Perrino, C., & EMEP. (2007). Inorganics in air and particle phase at Montelibretti. https://doi.org/10.48597/STK9-AW9E
Perrino, C., & EMEP. (2007). Nitrate at Montelibretti. https://doi.org/10.48597/BKZK-3BQ6
Perrino, C., & EMEP. (2007). PM10_mass at Montelibretti. https://doi.org/10.48597/R35B-YSQN
Perrino, C., & EMEP. (2008). Inorganics in air and particle phase at Montelibretti. https://doi.org/10.48597/YUVF-GYZQ
Perrino, C., & EMEP. (2008). PM10_mass at Montelibretti. https://doi.org/10.48597/F5ZR-3W5K
Perrino, C., & EMEP. (2008). PM25_mass at Montelibretti. https://doi.org/10.48597/KZVG-NC7E
Perrino, C., & EMEP. (2012). PM10_mass at Montelibretti. https://doi.org/10.48597/F5ZR-3W5K
Perrino, C., & EMEP. (2014). Inorganics in air and particle phase at Montelibretti. https://doi.org/10.48597/HEXA-54E2
Perrino, C., & EMEP. (2014). Inorganics in air and particle phase at Montelibretti. https://doi.org/10.48597/HQDM-CJ5M
Perrino, C., & EMEP. (2014). PM10_mass at Montelibretti. https://doi.org/10.48597/3FWF-GQVS
Perrino, C., & EMEP. (2014). PM10_mass at Montelibretti. https://doi.org/10.48597/F5ZR-3W5K
Perrino, C., & EMEP. (2014). PM25_mass at Montelibretti. https://doi.org/10.48597/KZVG-NC7E
Perrino, C., & EMEP. (2014). Sulphate_total at Montelibretti. https://doi.org/10.48597/C6A8-FGHU
Perrino, C., & EMEP. (2015). Inorganics in air and particle phase at Montelibretti. https://doi.org/10.48597/8E8J-GBM2
Petit, J., Truong, F., Bonnaire, N., ACTRIS, EMEP, & GAW-WDCA. (2021). OC/EC at SIRTA Atmospheric Research Observatory. https://doi.org/10.48597/CFQC-TZXU
Petit, J., Truong, F., Bonnaire, N., ACTRIS, EMEP, & GAW-WDCA. (2021). OC/EC at SIRTA Atmospheric Research Observatory. https://doi.org/10.48597/TYJ5-W35G
Petit, J., Truong, F., Bonnaire, N., ACTRIS, EMEP, & GAW-WDCA. (2021). OC/EC at SIRTA Atmospheric Research Observatory. https://doi.org/10.48597/FC4B-MHNZ
Pio, C., Casotti, R. I., Nunes, T., Gonçalves, C., Tchepel, O., Pina, N. K., et al. (2022). Impact of biomass burning and non-exhaust vehicle emissions on PM10 levels in a mid-size non-industrial western Iberian city. *Atmospheric Environment*, *289*, 119293. https://doi.org/10.1016/j.atmosenv.2022.119293
Poulain, L., Fuchs, S., ACTRIS, & EMEP. (2021). Inorganics in air and particle phase at Melpitz. https://doi.org/10.48597/4UJ2-NH8A
Poulain, L., Fuchs, S., ACTRIS, & EMEP. (2021). Sulphate_corrected at Melpitz. https://doi.org/10.48597/ZSMW-GWHY
Poulain, L., Fuchs, S., ACTRIS, & EMEP. (2022). Sulphate_corrected at Melpitz. https://doi.org/10.48597/ZSMW-GWHY

Poulain, L., Roedger, A., ACTRIS, & EMEP. (2021). OC/EC at Melpitz. https://doi.org/10.48597/UEB8-XKV9
Poulain, L., Roedger, A., ACTRIS, & EMEP. (2023). OC/EC and PM25_mass at Melpitz. https://doi.org/10.48597/S64J-Q3J3
Poulain, L., Roedger, A., ACTRIS, & EMEP. (2023). OC/EC at Melpitz. https://doi.org/10.48597/RJU6-3SH8
Poulain, L., Roedger, A., & EMEP. (2021). PM mass at Melpitz. https://doi.org/10.48597/JA9D-4YHY
Poulain, L., Roedger, A., & EMEP. (2023). PM10_mass at Melpitz. https://doi.org/10.48597/JA9D-4YHY
Presicci, A., EMEP, EUSAAR, & GAW-WDCA. (2008). Nitrate at Harwell. https://doi.org/10.48597/APDS-UJX3
Presicci, A., EMEP, EUSAAR, & GAW-WDCA. (2008). OC/EC at Harwell. https://doi.org/10.48597/B22N-H6YY
Prospero, J. (1996). The atmospheric transport of particles to the ocean. In I. Ittekkot, P. Schaffer, S. Honjo, & P. J. Depetris (Eds.), *Particle flux in the ocean*. John Wiley.
Prospero, J. M., Uematsu, M., & Savoie, D. L. (1989). Mineral aerosol transport to the Pacific Ocean. In *Chemical Oceanography* (Vol. 10, pp. 187–218). Academic Press Limited.
Putaud, J., CAMPAIGN, & EMEP. (2004). OC/EC and PM10_mass at Ispra. https://doi.org/10.48597/N5BR-C3PE
Putaud, J., CAMPAIGN, & EMEP. (2009). OC/EC at Ispra. https://doi.org/10.48597/K3BK-YK27
Putaud, J., & EMEP. (2003). PM mass at Ispra. https://doi.org/10.48597/8VEK-XDTH
Putaud, J., & EMEP. (2005). Elemental_carbon at Ispra. https://doi.org/10.48597/F2VH-Q56U
Putaud, J., & EMEP. (2005). Organic_carbon at Ispra. https://doi.org/10.48597/GR72-8SKR
Putaud, J., & EMEP. (2007). Inorganics in air and particle phase at Ispra. https://doi.org/10.48597/JA26-324T
Putaud, J., & EMEP. (2009). Ammonium at Ispra. https://doi.org/10.48597/3YJR-RZPS
Putaud, J., & EMEP. (2009). Ammonium at Ispra. https://doi.org/10.48597/99UY-S3XA
Putaud, J., & EMEP. (2009). Nitrate at Ispra. https://doi.org/10.48597/YU8D-CCB8
Putaud, J., & EMEP. (2013). Elemental_carbon at Ispra. https://doi.org/10.48597/4BUG-EY9J
Putaud, J., & EMEP. (2013). OC/EC at Ispra. https://doi.org/10.48597/4BUG-EY9J
Putaud, J., & EMEP. (2014). Elemental_carbon and inorganics in air and particle phase at Ispra. https://doi.org/10.48597/NHTW-ZYCK
Putaud, J., & EMEP. (2014). Elemental_carbon and inorganics in air and particle phase at Ispra. https://doi.org/10.48597/QTPE-Y9AQ
Putaud, J., & EMEP. (2014). Inorganics in air and particle phase at Ispra. https://doi.org/10.48597/BBED-UXQU
Putaud, J., & EMEP. (2014). Inorganics in air and particle phase at Ispra. https://doi.org/10.48597/WX9T-HNUA
Putaud, J., & EMEP. (2014). Nitrate at Ispra. https://doi.org/10.48597/YU8D-CCB8
Putaud, J., & EMEP. (2014). PM25_mass at Ispra. https://doi.org/10.48597/49A3-ZDQU
Putaud, J., EMEP, EUSAAR, & GAW-WDCA. (2009). OC/EC at ispra. https://doi.org/10.48597/SAN6-WCBP
Putaud, J., EMEP, EUSAAR, & GAW-WDCA. (2014). OC/EC at ispra. https://doi.org/10.48597/SAN6-WCBP
Putaud, J. P., Raes, F., Van Dingenen, R., Brueggemann, E., Facchini, M. C., Decesari, S., et al. (2004). A European aerosol phenomenology - 2: Chemical characteristics of particulate matter at kerbside, urban, rural and background sites in Europe. *Atmospheric Environment*, *38*(16), 2579–2595. https://doi.org/10.1016/j.atmosenv.2004.01.041
Putaud, J. P., Van Dingenen, R., Alastuey, A., Bauer, H., Birmili, W., Cyrys, J., et al. (2010). A European aerosol phenomenology - 3: Physical and chemical characteristics of particulate matter from 60 rural, urban, and kerbside sites across Europe. *Atmospheric Environment*, *44*(10), 1308–1320. https://doi.org/10.1016/j.atmosenv.2009.12.011
Querol, X., Alastuey, A., ACTRIS, EMEP, & GAW-WDCA. (2014). OC/EC at Montseny. https://doi.org/10.48597/J356-MMR6
Querol, X., Alastuey, A., ACTRIS, EMEP, & GAW-WDCA. (2014). OC/EC at Montseny. https://doi.org/10.48597/Q6P6-43W6
Querol, X., Alastuey, A., ACTRIS, EMEP, & GAW-WDCA. (2015). OC/EC at Montseny. https://doi.org/10.48597/2X7A-HWD5
Querol, X., Alastuey, A., ACTRIS, EMEP, & GAW-WDCA. (2015). OC/EC at Montseny. https://doi.org/10.48597/ZMZZ-H2CE
Querol, X., Alastuey, A., EMEP, EUSAAR, & GAW-WDCA. (2013). OC/EC at Montseny. https://doi.org/10.48597/348U-SDNA
Querol, X., Alastuey, A., EMEP, EUSAAR, & GAW-WDCA. (2013). OC/EC at Montseny. https://doi.org/10.48597/ARCK-RFU6
Querol, X., Alastuey, A., EMEP, EUSAAR, & GAW-WDCA. (2013). OC/EC at Montseny. https://doi.org/10.48597/ZE95-UXAF
Querol, X., CAMPAIGN, & EMEP. (2007). PM25_mass at Montseny. https://doi.org/10.48597/ED6Q-HSPZ
Querol, X., CAMPAIGN, & EMEP. (2007). PM25_mass at Montseny. https://doi.org/10.48597/XK2C-X4DZ
Querol, X., Cusack, M., EMEP, EUSAAR, & GAW-WDCA. (2010). Aluminium and inorganics in air and particle phase at Montseny. https://doi.org/10.48597/HGDD-KZPD
Querol, X., Cusack, M., EMEP, EUSAAR, & GAW-WDCA. (2010). Inorganics in air and particle phase at Montseny. https://doi.org/10.48597/7DD7-HK28
Querol, X., Fernandez-Turiel, J. L., & López-Soler, A. (1995). Trace elements in coal and their behavior during combustion in a large power station. *Fuel*, *74*(3), 331–343. https://doi.org/10.1016/0016-2361(95)93464-0
Querol, X., Perez, N., EMEP, EUSAAR, & GAW-WDCA. (2010). Aluminium and inorganics in air and particle phase at Montseny. https://doi.org/10.48597/5SUH-APJB
Querol, X., Perez, N., EMEP, EUSAAR, & GAW-WDCA. (2010). Aluminium at Montseny. https://doi.org/10.48597/6Z5D-9ACJ
Rathod, S., Hamilton, D. S. D. S., Mahowald, N., Klimont, Z., Corbett, J. J., & Bond, T. C. (2020). A mineralogy-based anthropogenic combustion-iron emission inventory. *Journal of Geophysical Research: Atmospheres*, *125*(17), e2019JD032114. https://doi.org/10.1029/2019JD032114
Rodriguez, S., Cuevas, E., Prospero, J. M., Alastuey, A., Querol, X., Lopez-Solano, J., et al. (2015). Modulation of Saharan dust export by the North African dipole. *Atmospheric Chemistry and Physics*, *15*(13), 7471–7486. https://doi.org/10.5194/acp-15-7471-2015
Rodriguez Gonzalez, S., Alastuey, A., Alonso-Perez, S., Querol, X., Cuevas Agullo, E., Abreu Afonso, J., et al. (2011). Transport of desert dust mixed with North African industrial pollutants in the subtropical Saharan Air Layer. *Atmospheric Chemistry and Physics*, *11*(13), 6663–6685. https://doi.org/10.5194/acp-11-6663-2011
Salma, I., Maenhaut, W., Annegarn, H. J., Andreae, M. O., Meixner, F. X., & Garstang, M. (1997). Combined application of INAA and PIXE for studying the regional aerosol composition in southern Africa. *Journal of Radioanalytical and Nuclear Chemistry*, *216*(1), 143–148. https://doi.org/10.1007/bf02034512
Salmi, T., AMAP, & EMEP. (2014). Aluminium at Pallas (Matorova). https://doi.org/10.48597/TAZH-AC6C
Salmi, T., CAMPAIGN, & EMEP. (2007). Inorganics in air and particle phase at Virolahti II. https://doi.org/10.48597/868Y-J2CF
Salmi, T., CAMPAIGN, & EMEP. (2007). Inorganics in air and particle phase at Virolahti II. https://doi.org/10.48597/CCUU-C434
Salmi, T., CAMPAIGN, & EMEP. (2007). Inorganics in air and particle phase at Virolahti II. https://doi.org/10.48597/XYVX-A6WT
Salmi, T., CAMPAIGN, & EMEP. (2007). PM mass at Virolahti II. https://doi.org/10.48597/ZNKY-2GXF
Salmi, T., EMEP, & HELCOM. (2010). Aluminium at Virolahti II. https://doi.org/10.48597/DP6G-WM9N
Salmi, T., EMEP, & HELCOM. (2018). Aluminium at Virolahti II. https://doi.org/10.48597/27YH-SRTJ

Sauvage, S., CAMPAIGN, COLOSSAL, & EMEP. (2018). OC/EC at Revin. https://doi.org/10.48597/V3DH-CJYK
Sauvage, S., & EMEP. (2009). PM10_mass at Revin. https://doi.org/10.48597/D6Q2-95A8
Sauvage, S., & EMEP. (2009). PM10_mass at Revin. https://doi.org/10.48597/GJWS-8R4H
Sauvage, S., & EMEP. (2014). OC/EC and inorganics in air and particle phase at Revin. https://doi.org/10.48597/RPNE-T3MW
Sauvage, S., & EMEP. (2014). PM10_mass at Revin. https://doi.org/10.48597/D6Q2-95A8
Sauvage, S., & EMEP. (2014). PM25_mass at Revin. https://doi.org/10.48597/4GF3-97G5
Sauvage, S., & EMEP. (2016). OC/EC and inorganics in air and particle phase at Revin. https://doi.org/10.48597/QP7A-8UAF
Sauvage, S., & EMEP. (2017). Inorganics in air and particle phase at Revin. https://doi.org/10.48597/7A6U-QREQ
Sauvage, S., & EMEP. (2017). PM25_mass at Revin. https://doi.org/10.48597/4GF3-97G5
Sauvage, S., & EMEP. (2018). OC/EC at Revin. https://doi.org/10.48597/YTEN-WCAM
Sauvage, S., & EMEP. (2019). OC/EC at Revin. https://doi.org/10.48597/Q5X2-T4PH
Sauvage, S., & EMEP. (2020). PM25_mass at Revin. https://doi.org/10.48597/WMEG-BNXE
Sauvage, S., & EMEP. (2021). Inorganics in air and particle phase at Revin. https://doi.org/10.48597/47CV-6AV6
Sauvage, S., & EMEP. (2023). PM10_mass at Revin. https://doi.org/10.48597/PSBV-D2TU
Savoie, D. L., Prospero, J. M., Larsen, R. J., Huang, R., Izaguirre, M. A., Huang, T., et al. (1993). Nitrogen and sulfur species in Antarctic aerosols at Mawson, Palmer Station, and Marsh (King George Island). *Journal of Atmospheric Chemistry*, *17*(2), 95–122. https://doi.org/10.1007/bf00702821
Savvides, C., & EMEP. (2024). Aluminium and inorganics in air and particle phase at Agia Marina Xyliatou/Cyprus Atmospheric Observatory. https://doi.org/10.48597/3D23-MMN6
Savvides, C., & EMEP. (2024). Aluminium and inorganics in air and particle phase at Agia Marina Xyliatou/Cyprus Atmospheric Observatory. https://doi.org/10.48597/DWN4-T22K
Savvides, C., & EMEP. (2024). Aluminium and inorganics in air and particle phase at Agia Marina Xyliatou/Cyprus Atmospheric Observatory. https://doi.org/10.48597/JFF9-GMTV
Savvides, C., & EMEP. (2024). Aluminium and inorganics in air and particle phase at Agia Marina Xyliatou/Cyprus Atmospheric Observatory. https://doi.org/10.48597/MAQS-NCGB
Savvides, C., & EMEP. (2024). Aluminium and PM10_mass at Agia Marina Xyliatou/Cyprus Atmospheric Observatory. https://doi.org/10.48597/DWN4-T22K
Savvides, C., & EMEP. (2024). Aluminium at Agia Marina Xyliatou/Cyprus Atmospheric Observatory. https://doi.org/10.48597/HVSC-5TJP
Savvides, C., & EMEP. (2024). OC/EC and inorganics in air and particle phase at Agia Marina Xyliatou/Cyprus Atmospheric Observatory. https://doi.org/10.48597/DWN4-T22K
Savvides, C., & EMEP. (2024). OC/EC and inorganics in air and particle phase at Agia Marina Xyliatou/Cyprus Atmospheric Observatory. https://doi.org/10.48597/MAQS-NCGB
Savvides, C., & EMEP. (2024). PM25_mass at Agia Marina Xyliatou/Cyprus Atmospheric Observatory. https://doi.org/10.48597/K58S-B9SZ
Schlesinger, W. H. (1997). *Biogeochemistry: An analysis of global change* (2nd ed., p. 588). Academic Press.
Schmidl, C., Marr, I. L., Caseiro, A., Kotianová, P., Berner, A., Bauer, H., et al. (2008). Chemical characterisation of fine particle emissions from wood stove combustion of common woods growing in mid-European Alpine regions. *Atmospheric Environment*, *42*(1), 126–141. https://doi.org/10.1016/j.atmosenv.2007.09.028
Sciare, J., Crenn, V., Petit, J., & GAW-WDCA. (2013). PM10_mass at SIRTA Atmospheric Research Observatory. https://doi.org/10.48597/YER7-CKFQ
Sellegri, K., ACTRIS, EMEP, EUSAAR, & GAW-WDCA. (2016). OC/EC at Puy de Dome. https://doi.org/10.48597/USYK-S69Z
Sellegri, K., ACTRIS, EMEP, & GAW-WDCA. (2015). OC/EC at Puy de Dome. https://doi.org/10.48597/ZG79-TSBG
Sellegri, K., EMEP, EUSAAR, & GAW-WDCA. (2008). OC/EC at Puy de Dome. https://doi.org/10.48597/D3Z5-ZFRP
Sellegri, K., EMEP, EUSAAR, & GAW-WDCA. (2010). OC/EC at Puy de Dome. https://doi.org/10.48597/MY4X-QQFB
Sellegri, K., EMEP, EUSAAR, & GAW-WDCA. (2015). OC/EC at Puy de Dome. https://doi.org/10.48597/63B3-EU6K
Sellegri, K., EMEP, EUSAAR, & GAW-WDCA. (2016). OC/EC at Puy de Dome. https://doi.org/10.48597/25WG-HVUC
Sellegri, K., EMEP, EUSAAR, & GAW-WDCA. (2016). OC/EC at Puy de Dome. https://doi.org/10.48597/GE5T-58D4
Sellegri, K., EMEP, EUSAAR, & GAW-WDCA. (2016). OC/EC at Puy de Dome. https://doi.org/10.48597/KCFG-VHEZ
Shelley, R. U., Landing, W. M., Ussher, S. J., Planquette, H., & Sarthou, G. (2018). Regional trends in the fractional solubility of Fe and other metals from North Atlantic aerosols (GEOTRACES cruises GA01 and GA03) following a two-stage leach. *Biogeosciences*, *15*(8), 2271–2288. https://doi.org/10.5194/bg-15-2271-2018
Siefert, R. L., Johansen, A. M., & Hoffmann, M. R. (1999). Chemical characterization of ambient aerosol collected during the southwest monsoon and intermonsoon seasons over the Arabian Sea: Labile-Fe(II) and other trace metals. *Journal of Geophysical Research*, *104*(D3), 3511–3526. https://doi.org/10.1029/1998JD100067
Silva, H. F., Matos, M. J., Oliveira, C., Ferreira, A. F., Oliveira, J. C., Cantinho, P., et al. (2010). Effect of climate on PM concentration and size distribution in two sites in the city of Lisbon, Encontro de Jovens Químicos Portugueses, Aveiro, 21 to 23 of April.
Sjoberg, K., & EMEP. (2006). PM mass at Aspvreten. https://doi.org/10.48597/PYMH-YKVX
Sjoberg, K., & EMEP. (2009). PM mass at Aspvreten. https://doi.org/10.48597/39BV-5QYM
Sjoberg, K., & EMEP. (2011). PM10_mass at Aspvreten. https://doi.org/10.48597/UGGB-PXC7
Sjoberg, K., & EMEP. (2013). PM10_mass at Aspvreten. https://doi.org/10.48597/W6XF-FPSJ
Sjoberg, K., & EMEP. (2014). PM25_mass at Aspvreten. https://doi.org/10.48597/Z82G-42SR
Sjoberg, K., & EMEP. (2015). PM mass at Aspvreten. https://doi.org/10.48597/FANR-XNAY
Sjoberg, K., & EMEP. (2015). PM10_mass at Aspvreten. https://doi.org/10.48597/W6XF-FPSJ
Sjoberg, K., & EMEP. (2015). PM25_mass at Aspvreten. https://doi.org/10.48597/2Y8P-ZCUQ
Sjoberg, K., & EMEP. (2015). PM25_mass at Aspvreten. https://doi.org/10.48597/M7TU-9695
Sjoberg, K., & EMEP. (2016). PM mass at Aspvreten. https://doi.org/10.48597/FANR-XNAY
Sjoberg, K., & EMEP. (2016). PM10_mass at Aspvreten. https://doi.org/10.48597/FANR-XNAY
Sjoberg, K., & EMEP. (2016). PM10_mass at Aspvreten. https://doi.org/10.48597/HQ55-J2VA
Smichowski, P., Gomez, D. R., Dawidowski, L. E., Gine, M. F., Bellato, A. C. S., & Reich, S. L. (2004). Monitoring trace metals in urban aerosols from Buenos Aires city. Determination by plasma-based techniques. *Journal of Environmental Monitoring*, *6*(4), 286–294. https://doi.org/10.1039/b312446k
Smis, A., Ancin Murguzur, F. J., Struyf, E., Soininen, E. M., Herranz Jusdado, J. G., Meire, P., & Bråthen, K. A. (2014). Determination of plant silicon content with near infrared reflectance spectroscopy. *Frontiers in Plant Science*, *5*. https://doi.org/10.3389/fpls.2014.00496

Smith, R. D., Campbell, J. A., & Nielson, K. K. (1979). Characterization and formation of submicron particles in coal-fired plants. *Atmospheric Environment*, *13*(5), 607–617. https://doi.org/10.1016/0004-6981(79)90189-6
Spindler, G., ACTRIS, & EMEP. (2014). OC/EC at Melpitz. https://doi.org/10.48597/K22R-NWZW
Spindler, G., ACTRIS, & EMEP. (2016). OC/EC at Melpitz. https://doi.org/10.48597/MNCP-5QRJ
Spindler, G., ACTRIS, EMEP, & GAW-WDCA. (2017). OC/EC at Melpitz. https://doi.org/10.48597/R9PQ-ZUP5
Spindler, G., CAMPAIGN, & EMEP. (2009). OC/EC at Melpitz. https://doi.org/10.48597/S45P-4UGX
Spindler, G., & EMEP. (2011). Inorganics in air and particle phase at Melpitz. https://doi.org/10.48597/YHHP-83DG
Spindler, G., & EMEP. (2011). OC/EC and inorganics in air and particle phase at Melpitz. https://doi.org/10.48597/5745-N9JS
Spindler, G., & EMEP. (2011). OC/EC and inorganics in air and particle phase at Melpitz. https://doi.org/10.48597/7JJQ-VQPT
Spindler, G., & EMEP. (2011). OC/EC and inorganics in air and particle phase at Melpitz. https://doi.org/10.48597/PMQ3-SYAZ
Spindler, G., & EMEP. (2012). OC/EC and inorganics in air and particle phase at Melpitz. https://doi.org/10.48597/JQV2-HKFY
Spindler, G., & EMEP. (2012). Sulphate_corrected at Melpitz. https://doi.org/10.48597/ZHYH-9HCU
Spindler, G., & EMEP. (2014). OC/EC and inorganics in air and particle phase at Melpitz. https://doi.org/10.48597/5U4T-APJN
Spindler, G., & EMEP. (2015). Inorganics in air and particle phase at Melpitz. https://doi.org/10.48597/GNWC-PTY3
Spindler, G., & EMEP. (2015). Inorganics in air and particle phase at Melpitz. https://doi.org/10.48597/N5JP-JCTN
Spindler, G., & EMEP. (2015). Inorganics in air and particle phase at Melpitz. https://doi.org/10.48597/RDZ8-324F
Spindler, G., & EMEP. (2015). PM mass at Melpitz. https://doi.org/10.48597/EPQZ-MESE
Spindler, G., & EMEP. (2016). Inorganics in air and particle phase at Melpitz. https://doi.org/10.48597/AAF3-U34J
Spindler, G., & EMEP. (2016). PM mass at Melpitz. https://doi.org/10.48597/EPQZ-MESE
Spindler, G., & EMEP. (2018). OC/EC and inorganics in air and particle phase at Melpitz. https://doi.org/10.48597/6E66-9VEY
Spindler, G., & EMEP. (2022). Inorganics in air and particle phase at Melpitz. https://doi.org/10.48597/RXQV-SQGV
Spindler, G., & EMEP. (2022). OC/EC and inorganics in air and particle phase at Melpitz. https://doi.org/10.48597/6E66-9VEY
Spindler, G., Roedger, A., ACTRIS, & EMEP. (2018). OC/EC at Melpitz. https://doi.org/10.48597/RJU6-3SH8
Spindler, G., Roedger, A., ACTRIS, & EMEP. (2023). OC/EC at Melpitz. https://doi.org/10.48597/RJU6-3SH8
Steenari, B. M., Schelander, S., & Lindqvist, O. (1999). Chemical and leaching characteristics of ash from combustion of coal, peat and wood in a 12 MW CFB—A comparative study. *Fuel*, *78*(2), 249–258. https://doi.org/10.1016/S0016-2361(98)00137-9
Swap, R. J., Annegarn, H. J., Suttles, J. T., Haywood, J., Helmlinger, M. C., Hely, C., et al. (2002). The Southern African Regional Science Initiative (SAFARI 2000): Overview of the dry season field campaign. *South African Journal of Science*, *98*(3–4), 125–130.
Telling, S., & EMEP. (2013). Inorganics in air and particle phase at Harwell. https://doi.org/10.48597/AWZH-349S
Telling, S., & EMEP. (2013). Inorganics in air and particle phase at Harwell. https://doi.org/10.48597/RC72-84U3
Telling, S., & EMEP. (2013). PM10_mass at Harwell. https://doi.org/10.48597/3V8A-NWQF
Telling, S., & EMEP. (2013). PM25_mass at Harwell. https://doi.org/10.48597/EE8D-EFP5
Tsai, S. L., & Tsai, M. S. (1998). A study of the extraction of vanadium and nickel in oil-fired fly ash. *Resources, Conservation and Recycling*, *22*(3–4), 163–176. https://doi.org/10.1016/S0921-3449(98)00007-X
Tunved, P., ACTRIS, EMEP, EUSAAR, & GAW-WDCA. (2013). OC/EC at Aspvreten. https://doi.org/10.48597/T8X5-2789
Tunved, P., ACTRIS, EMEP, & GAW-WDCA. (2015). OC/EC at Aspvreten. https://doi.org/10.48597/2FWN-S9JX
Tunved, P., ACTRIS, EMEP, & GAW-WDCA. (2014). OC/EC at Aspvreten. https://doi.org/10.48597/KEJJ-3S34
Uematsu, M., Duce, R. A., Prospero, J. M., Chen, L., Merrill, J. T., & McDonald, R. L. (1983). Transport of mineral aerosol from Asia over the North Pacific Ocean. *Journal of Geophysical Research*, *88*(C9), 5343–5352. https://doi.org/10.1029/jc088ic09p05343
Vincent, K., & EMEP. (2011). PM mass at Harwell. https://doi.org/10.48597/MCBQ-KWJK
Vincent, K., & EMEP. (2011). PM10_mass at Harwell. https://doi.org/10.48597/QQKZ-A9TW
Vincent, K., & EMEP. (2011). PM25_mass at Harwell. https://doi.org/10.48597/EUKJ-T9DR
Vincent, K., & EMEP. (2013). PM mass at Auchencorth Moss. https://doi.org/10.48597/4SDR-74Z5
Vincent, K., & EMEP. (2013). PM mass at Harwell. https://doi.org/10.48597/4DU3-65BS
Vincent, K., & EMEP. (2014). PM mass at Auchencorth Moss. https://doi.org/10.48597/6FDK-GNRE
Vincent, K., & EMEP. (2014). PM mass at Harwell. https://doi.org/10.48597/MP3N-P3X3
Vincent, K., & EMEP. (2014). PM25_mass at Auchencorth Moss. https://doi.org/10.48597/8FF6-7BX8
Vincent, K., & EMEP. (2014). PM25_mass at Harwell. https://doi.org/10.48597/JPZD-EV8M
Vincent, K., & EMEP. (2015). PM mass at Harwell. https://doi.org/10.48597/5XWE-N7CA
Virkkula, A., Aurela, M., Hillamo, R., Maekelae, T., Pakkanen, T., Kerminen, V. M., et al. (1999). Chemical composition of atmospheric aerosol in the European subarctic: Contribution of the Kola Peninsula smelter areas, central Europe, and the Arctic Ocean. *Journal of Geophysical Research*, *104*(D19), 23681–23696. https://doi.org/10.1029/1999jd900426
Watson, J. G., Chow, J. C., & Houck, J. E. (2001). $PM_{2.5}$ chemical source profiles for vehicle exhaust, vegetative burning, geological material, and coal burning in Northwestern Colorado during 1995. *Chemosphere*, *43*(8), 1141–1151. https://doi.org/10.1016/S0045-6535(00)00171-5
Xiao, Y. H., Liu, S. R., Tong, F. C., Kuang, Y. W., Chen, B. F., & Guo, Y. D. (2014). Characteristics and sources of metals in TSP and $PM_{2.5}$ in an urban forest park at Guangzhou. *Atmosphere*, *5*(4), 775–787. https://doi.org/10.3390/atmos5040775
Young, M., CAMPAIGN, & EMEP. (2004). OC/EC and PM10_mass at Mace Head. https://doi.org/10.48597/WJ8Z-AYRB
Yttri, K., Aas, W., EMEP, & GAW-WDCA. (2016). OC/EC at Leova II. https://doi.org/10.48597/M7UM-T4CX
Yttri, K., CAMPAIGN, EMEP, & NILU. (2009). OC/EC at Birkenes. https://doi.org/10.48597/4ZZA-9PJE
Yttri, K., CREATE, EMEP, GAW-WDCA, & NILU. (2010). OC/EC at Birkenes. https://doi.org/10.48597/DP9X-WQPT
Yttri, K., CREATE, EMEP, GAW-WDCA, & NILU. (2010). OC/EC at Birkenes. https://doi.org/10.48597/QC2T-UT7A
Yttri, K., EMEP, EUSAAR, GAW-WDCA, & NILU. (2010). OC/EC at Birkenes. https://doi.org/10.48597/9DKT-K7SY
Yttri, K., EMEP, EUSAAR, GAW-WDCA, & NILU. (2010). OC/EC at Birkenes. https://doi.org/10.48597/DP9X-WQPT
Yttri, K., EMEP, EUSAAR, GAW-WDCA, & NILU. (2010). Organic_carbon at Birkenes. https://doi.org/10.48597/GXM6-6CRY
Yttri, K., EMEP, & NILU. (2010). OC/EC at Birkenes. https://doi.org/10.48597/DP9X-WQPT
Yttri, K., EMEP, & NILU. (2010). OC/EC at Birkenes. https://doi.org/10.48597/QC2T-UT7A
Zhang, H., Wang, S., Hao, J., Wan, L., Jiang, J., Zhang, M., et al. (2012b). Chemical and size characterization of particles emitted from the burning of coal and wood in rural households in Guizhou, China. *Atmospheric Environment*, *51*, 94–99. https://doi.org/10.1016/j.atmosenv.2012.01.042